Sensitivity control of optical fiber biosensors utilizing turnaround point long period gratings with self-assembled polymer coatings

Erika L. Gifford

Dissertation submitted to the faculty of the Virginia Polytechnic Institute and State University in partial fulfillment of the requirements for the degree of

Doctor of Philosophy
In
Physics

Dr. James R. Heflin
Dr. Alfred L. Ritter
Dr. Hans D. Robinson
Dr. Richey M. Davis

June 26, 2008
Blacksburg, Va

Keywords: Ionic Self-Assembled Multilayers, Long Period Fiber Grating, Biosensor, Fiber Optics, Nanometer-thick Thin Films, Optical Sensors

Sensitivity control of optical fiber biosensors utilizing turnaround point long period gratings with self-assembled polymer coatings

Erika L. Gifford

ABSTRACT

Biosensors have a multitude of important applications in basic research, environmental monitoring, biodefense, and medicine. This research aims to show that Ionic Self-Assembled Multilayers (ISAMs) adsorbed on Long Period Gratings (LPGs) can serve as a highly sensitive, robust, inexpensive optical-based biosensor platform. The ISAM technique is a layer-by-layer deposition method that builds nanometer-thick films based on the principle of Coulomb attraction between oppositely charged polyelectrolyte solutions while LPGs cause strong attenuation bands that enable an optical fiber to be extremely sensitive to changes in the surrounding environment. LPGs have been shown to be highly sensitive to the adsorption of nanoscale self-assembled films on the optical fiber cladding surface. In this work, we utilize Turnaround Point (TAP) LPGs, which possess even greater sensitivity than standard LPGs. This thesis focuses on evaluation of approaches to increasing the sensitivity of the sensor platfom, implementation of a biosensor for detection of several biomolecules, and preliminary evaluation of the potential for pH sensing.

For a thin-film coated TAP LPG, we have demonstrated that shifts in the transmitted light intensity at the resonant wavelength of the LPG can result from the variation in film thickness and/or refractive index. We have observed decreases in intensity as large a 7 dB for one bilayer of ISAM film (~1 nm), which corresponds to an 80% decrease in the transmitted light intensity at the resonant wavelength. We have also shown that the sensitivity of the TAP LPG sensor can be increased by implementing nm-

thick ISAM films that have a refractive index greater than silica. Furthermore, it is shown that incorporation of silica nanoparticles into the ISAM films significantly increases sensitivity through increased surface area and thickness.

The biotin-streptavidin system was used as a model for implementaion and optimization of the ISAM-coated TAP LPG biosensor platform. Through evaluation of various biotin derivatives to maximize the amount functionalized onto the ISAM film, optimization of the ISAM film properties, and use of LPGs designed for higher sensitivity, the minimum detectable concentration of streptavidin was decreased from 0.0125 mg/ml to 12.0 ng/ml. The biosensor platform was then tested on prostate specific antigen (PSA), which is used as a clinical marker for early diagnosis of potential prostate cancer. Using a direct crosslinking approach of the monoclonal antibody to PSA into the ISAM film, a sensitivity level of 11.64 ng/ml PSA was obtained through combined optimization of the ISAM film and antibody surface coverage. Finally, the potential of ISAM TAP LPGs as pH sensors was examined based on the pH dependent swelling of ISAM films.

Acknowledgements

I have so many influential people that I would like to thank for helping me to reach all of my academic goals. I will begin by extending my sincere gratitude to my wonderful advisor, Dr. Heflin, for all of his patience, encouragement, guidance, and support. I am so grateful to him for giving me the opportunity to take this project to a higher level and complete my Ph.D.

I also want to thank the people at Prime Photonics, especially Tipper Rumpf and Chris Wescott, for helping me with several projects, giving me the chance to foster a new application of my research, and allowing me to use their lab facilities whenever I needed. Special thanks should go to Dr. Wang because this project began as his creative, innovative idea. Without his idea and his teachings, I would not be here. My sincere gratitude also extends to Dr. Rik Obiso who helped me tremendously to understand the biology and chemistry in my research. Without his excellent advice and guidance I would not have been as successful in my experimentation.

I need to thank my committee members: Dr. Richey Davis, Dr. Hans Robinson, and Dr. Alfred Ritter for all of their support and insightful suggestions along the way. I am also very grateful to Christa Thomas for all of the help and encouragement she gave me from the moment I got here.

Lastly, I want to thank my husband, Andrew, for all of his encouragement, love, support, and understanding through this long journey in our lives. My parents, family, and wonderful friends also deserve all my gratitude for always having faith in me and never letting me give up. Without all of them, I know I would not have made it this far.

Table of Contents

List of Figures

List of Tables

Chapter 1. Introduction

1.1 Motivation

Biological sensors (or biosensors) are devices used for the detection of an analyte; they convert a biochemical signal into a quantifiable physical signal such as light or an electric pulse. The goal of this research is to develop a highly sensitive biosensor platform that exhibits simplicity and versatility in wide range of applications including basic research, environmental monitoring, biodefense, and medicine. In the environment, these sensors can be used to sense harmful and hazardous environmental pollutants in the air, ground, water, etc. In the military, they can detect deadly chemicals used in biological warfare. Biosensors can be used in the health industry to monitor a diabetic patient's glucose levels, determine the efficiency of cancer treatment, and for a vast array of other applications. In the food industry, biosensors can determine if harmful bacteria are growing in or on food items. Rapid assay biosensors can speed the progress of drug discovery. The biosensors investigated in this thesis are based on self-assembled organic films on optical fibers with Long Period Gratings (LPGs) and they demonstrate exceptional sensitivity, even for films less than 1 nm thick.

The sensor works by depositing thin films on the LPG, which causes a change in the effective refractive index of the cladding mode. This allows light to couple from the core of the optical fiber into a cladding mode, which leads to a detectable decrease in transmission at the attenuation wavelength. Different biological and chemical sensing materials can be easily functionalized in various ways to bind with the thin self-assembled films on the fiber, which yield a highly versatile sensor platform. The binding

events further alter the effective refractive index of the cladding mode, which is observed as a further decrease in transmitted light intensity at the attenuation wavelength. This is the mechanism by which thin-film coated LPGs can be used as sensors. Some potential advantages of thin film-coated LPGs as biosensors are that they can be robust, reusable, easy to use, cost-effective, and generate high sensitivity.

Increasing the sensitivity of thin film-coated LPG biosensors has been thoroughly explored in this thesis by implementing turnaround point (TAP) LPGs, which are specially designed to allow the strongest possible coupling between the core and the cladding. This allows small changes in thickness and refractive index of films absorbed on the TAP LPGs to have much larger effects, which leads to increased sensitivity. Further, different film materials with different refractive indices were examined in order to determine which films allowed optimal sensitivity on the TAP LPG.

The implementation of thin film-coated TAP LPG biosensors for the detection of streptavidin, the anthracis protective antigen, and the prostate specific antigen were examined in great detail and numerous approaches to increasing the sensitivity were developed. Preliminary studies to evaluate the possibility of pH sensing capabilities of thin film-coated TAP LPGs were also performed.

1.2 Ionic Self-Assembled Multilayers (ISAMs)

Ionic Self-Assembled Multilayers (ISAMs) are created by a layer-by-layer deposition technique and these layers display excellent reliability, stability, and film quality. They are built on a substrate at the nanoscale level by subsequent immersions in oppositely charged polyelectrolyte solutions. They are held together by Coulomb

attraction between the oppositely charged layers. This technique allows for precise control over the thickness and refractive index of the ISAM films deposited on a substrate. These films can be deposited on any surface with a minimum charge density. The ISAMs can be adjusted to incorporate a variety of materials such as proteins, ligands, bacteria, etc. The ISAM technique is very beneficial because it enables films to be built on a very wide variety of substrates.

1.3 Thin Films Adsorbed on LPGs

LPGs embedded in optical fibers are like spectral filters. They allow only certain wavelengths of light to pass through, while others are coupled out of the fiber. ISAMs can be absorbed onto optical fibers with internal LPGs in the same way as discussed previously. This process creates the biosensor platform upon which different biological and chemical sensing agents can be deposited and detected. The addition of thin films on LPGs changes the effective refractive index of the lossy cladding modes of the fiber which leads to either a detectable decrease in transmission or a detectable shift in resonant wavelength. Antibodies or other biological sensing elements can be functionalized in various ways to enable them to bind with the ISAM films on an LPG. This binding of additional material further changes the effective refractive index of the cladding mode. This leads to a further detectable decrease in transmission or a shift in resonant wavelength. This is the mechanism by which thin film coated LPGs can be used as sensors.

1.4 Outline

This dissertation is arranged in the following manner. Chapter 2 gives a brief history of biosensors and different biosensor approaches, along with some types of transducers used in sensing. Optical biosensors are also discussed in detail here.

Chapter 3 provides background on ISAMs, LPGs, and turnaround point LPGs. It has been previously shown that the film thickness and refractive index of ISAM films can be very precisely controlled by altering the pH of the polyelectrolyte solutions used to build the films. Also discussed is how ISAMs deposited on LPGs generate notable shifts in resonant wavelength, even for films less than 1 nm thick. This allows them to be used as sensors. Furthermore, turnaround point LPGs are introduced as much more sensitive to the addition of thin films on the fiber than conventional LPGs.

Chapter 4 discusses the experimental results of ISAM sensitivity studies on TAP LPGs. It is shown that the sensitivity of the TAP LPG to the thickness of the ISAM film increases with increased film thickness. Also, it is shown that the sensitivity of the TAP LPG is significantly increased when ISAMs with higher refractive indices are implemented in the platform. Furthermore, it is shown that silica nanoparticles, which provide increased film thickness and surface area, significantly increase sensitivity. Lastly, new specially designed TAP LPGs are also shown to drastically increase sensitivity.

Chapter 5 focuses on implementation of the ISAM TAP LPG biosensor, the optimization processes, and sensitivity improvements. Preliminary data on a biosensor for the detection of the anthracis protective antigen was obtained. The detection limit for the antigen was 0.1 mg/ml. This is higher than desired for environmental monitoring

applications. However, the experiment was performed early on in the course of this thesis before the more sensitive LPGs were obtained, before the new-more powerful broadband light source was implemented, and before the biosensor system was optimized. In spite of all this, the results do verify the concept of an optical fiber-based biosensor that implements ISAM-coated TAP LPGs.

Biotin-streptavidin was next used as a model biological system. Through a series of improvements on the biotin derivative employed and approaches to increase the amount of biotin attached to the ISAM film, an ultimate sensitivity level of 12.0 ng/ml of streptavidin was achieved. Furthermore, through many optimization procedures including: 1) directly crosslinking the antibody to the prostate specific antigen (PSA); 2) depositing more ISAM films on the fiber to push the LPG spectra closer to the TAP; and 3) increasing both the concentration and amount of antibody used; a sensitivity level of 11.64 ng/ml of PSA was achieved for a prostate cancer biosensor.

Chapter 6 examines the possibility of developing the optical fiber sensor into a pH sensor by observing how ISAMs coated on TAP LPGs change with respect to pH. In prior publications, poly(allylamine hydrochloride) (PAH) and poly(acrylic acid) (PAA) pH detection was claimed based on LPGs that had PAH/PAA films adsorbed on their surface such that the polymeric matrix adjusted its optical thickness when the pH was changed. They stated that when the sensor was placed in the buffer solutions of higher pH, the thickness of the ISAM layers should decrease, yielding shifts in the attenuation wavelength. Numerous studies of PAH/PAA ISAM films on TAP LPGs were conducted. From the results, we concluded that the prior work must have been sensing the concentration of salt ions in the buffer, and not the concentration of hydrogen ions.

Consequently, our focus switched to reports of discontinuous pH-induced swelling in PAH and poly(styrene sulfonate) (PSS) ISAM films made from pHs greater than 9.0. The reversible discontinuous transitions were attributed to discontinuous changes in the degree of ionization of free amine groups of PAH and a significant shift in the pK_a value of PAH from its local environment within the multilayers. This created a history-dependent swelling behavior of the multilayers. Tests were conducted using PAH/PSS ISAM films fabricated at pH 9.3 on TAP LPGs. Some systematic differences were observed in the LPG spectrum when it was exposed to DI water with pHs of 4.0, 5.4, and 7.0. It was found that the spectra were more repeatable when each measurement was preceded by a 3 minute DI soak of pH 2.0 to "reset" the film to a swollen state. This study demonstrates a potential for pH measurement using ISAM TAP LPGs, but significant improvement is required in order to create stable, reproducible measurements at any pH.

Chapter 2. Biosensor Background

2.1 Brief History of Biosensors

Professor Leland C. Clark, Jr. was born in 1918 and received his Ph.D. in physiology and biochemistry from the University of Rochester School of Medicine.[1] He was responsible for the invention of the oxygen electrode and its modification with enzymes. Because of this invention, he is often identified as the father of the biosensor concept.[2] Clark published his paper on the oxygen electrode in 1956. However, he had a strong desire to expand the range of analytes that could be measured in the body. Thus, at a New York Academy of Sciences symposium he discussed "how to make electrochemical sensors (pH, potentiometric, polarographic, or conductometric) more intelligent" by adding "enzyme transducers as membrane enclosed sandwiches."[2] He later verified this idea with a glucose experiment.

Clark invented such a sensor and it became the basis for multiple variations of the initial design and, as a result, several other oxidase enzymes were immobilized by other research scientists. Clark's sensor had such a large impact in the science world that his basic concept of oxygen measurement is still used commercially. Today, though, it is more common to measure hydrogen peroxide.

The idea of thermal transducers for biosensors was brought forth in 1974, and they were called thermal enzyme probes and enzyme thermistors. In 1975 Yellow Springs Instrument Company (YSI) successfully introduced their glucose biosensor that focuses on amperometric detection of hydrogen peroxide. This particular biosensor was the stepping stone for many more to come. A potentiometric enzyme electrode was

initially developed by Montalvo and Guilbault. They created a urea sensor based on urease immobilized at an ammonium-selective liquid membrane electrode.

Also, in 1975 N. Opitz and DW Lubbers from Max-Planck-Institut für Molekulare Physiologie, Dortmund, Germany developed the term optode, which characterizes a fiber optic sensor with an immobilized indicator to measure oxygen or carbon dioxide.[3] They also made an optical biosensor for alcohol by immobilizing alcohol oxidase on the end of a fiber optic oxygen sensor. Furthermore, in 1975, Divie said that bacteria could be used as the biological element in microbial electrodes for the measurement of alcohol.[3] Divie's paper stimulated the minds of researchers in Japan and around the world to really examine the environmental and biotechnological applications of biosensors.

An electrochemical glucose biosensor was implemented in an artificial pancreas in 1976 by Clemens *et al*. It was marketed by Miles (Elkhart) as the Biostator. The Biostator is no longer sold because VIA Medical (San Diego) developed a semi-continuous catheter-based blood glucose analyzer. Also, in 1976, the Lactate Analyzer LA 640 was developed by La Roche (Switzerland). This analyzer functions by transferring electrons from lactate dehydrogenase to an electrode. This led to applications in sports and medicine.

A paper written by B. Liedberg *et al*. was ground breaking for using direct immunosensors by attaching antibodies to a potentiometric or piezoelectric transducer.[4] In their work they discuss implementing surface plasmon resonance to monitor affinity reactions in real time. The BIAcore (Pharmacia, Sweden) initiated in 1990 utilizes this technique.

Finally, in the 1980s, commercial success for biosensors was obtained on a much larger scale. A highly cited paper was published in 1984 on the use of ferrocene and its derivatives as an immobilized mediator for use with oxidoredutases.[2] This led to the development of inexpensive enzyme electrodes, consequently creating the basis for the screen-printed enzyme electrodes initiated by MediSense (Cambridge, USA) in 1987, which resulted in a home blood-glucose monitor that was the size of a pen. Since then, technology has continued to advance and much better devices have been created. By 1996 MediSense's sales reached $175 million per annum when they were bought by Abbott. Bayer, Boehringer Mannheim (now Roche Diagnostics), and LifeScan all now have competing biosensors. They control a large fraction of the biosensor market.

Today there are many devices utilizing enzymes, cell receptors, nucleic acids, antibodies, and intact cells in conjunction with optical, electrochemical, thermometric, and piezoelectric transducers. In each of these areas, there are many different paths that can be taken that lead to applications in medicine, food safety, environmental monitoring, and biodefense.

In the history of biosensors, it can be said that the 1980s was the era of invention, while in the 1990s, commercialization was at the forefront. The market for biosensors is ever-growing and developing.

2.2 Biosensor Approaches

Biosensors are devices that convert a biological response into some sort of measurable signal. Oftentimes biosensors are used to determine the concentration of a particular substance or to detect the presence of a certain analyte in question. They have

the ability to connect high specificity with a variety of processing techniques to obtain ultra sensitive biological detection systems.[5] The biosensor field is ever-growing and expanding with new, innovative and advanced technology. The field has an estimated 60% annual growth rate. The main areas of interest are the health-care industry, food safety, and environmental monitoring. The field of biosensors is highly multidisciplinary, incorporating such areas as chemistry, physics, biology, software engineering, and electronics.

Biosensors are generally separated into two categories: biocatalysis-based and bio-affinity based. Biocatalysis-based biosensors make use of enzymes as their biological sensing elements. The specificity of an enzyme-based biosensor is based upon the specificity of the enzymatic action.[5] For example, if an enzyme that has a certain reaction with glucose is integrated into a biosensor, that particular sensor will only have the basis for glucose and will not detect any other substance that is closely related chemically. Then, there will be a signal from the change in the transducer initiated by the interaction between the glucose and glucose-reactive enzyme.

2.2.1 Biocatalysis Sensors

Biocatalytic-based biosensors implement two mechanisms. The first uses the catalytic transformation of a pollutant. The second utilizes detection that mediates or alters the enzyme's activity. The first mechanism has environmental applications with both advantages and limitations. Some advantages include: easy to create and operate, can be designed to work continuously and reversibly, can also be engineered so the only required reagent is the analyte in question. The limitations come from the inherent

characteristics of the enzyme and involve a small number of environmental pollutants, which are substrates for the enzyme, and the moderately high detection limits for environmental pollutants.[7] However, there have been biosensor formats developed which significantly decrease the aforementioned limitations.

In biocatalytic biosensors used for environmental applications, the other crucial mechanism is hindrance of the enzyme caused by the pollutant. These formats have intrinsic benefits, which encompass the larger number of environmental pollutants that impede the enzyme and the low concentrations necessary to influence the enzyme activity.

Enzyme inhibition is the basis for a number of intrinsic limitations for biosensors. These assay formats necessitate the use of substrates, and sometimes mediators and cofactors, as well as the analyte of interest. The pollutants need to be chemically oxidized to metabolic intermediates to display the highest sensitivities for several of these assays. Due to the irreversibility of a number of analyte-enzyme interactions which yield increased sensitivity, the biosensor may become inactive after just one measurement.

2.2.2 Bioaffinity Sensors

Bioaffinity-based biosensors used for environmental applications generally implement proteins, dyes, lectins, antibodies, antibody-related substances, etc. as their biological sensing elements.[5] These sensors detect the binding events themselves. They use antibodies/antibody-related substances because there is an abundance of monoclonal and polyclonal antibodies directed toward a large variety of environmental pollutants as well as the relatively high selectivity and affinity of recognition proteins for a certain

compound or closely related groups of compounds.[6] Besides the large range of antibodies directed towards different environmental pollutants, a range of assay formats has also been established with essentially every type of known signal transducer.

Another type of bioaffinity-based biosensor is an immunosensor. They use antibodies and antibody-related substances as their biological sensing elements. Antibodies are proteins created in the immune system of animals as a response to a "foreign material" (the antigen) entering into their system. Generally, antibodies do not catalyze chemical transformations. Instead, they go through a physical transformation where they tightly bind to the antigen that generated the response and mark it for other elements in the immune system.[5] In general, for a biosensor the antibodies directed against the material being studied are immobilized on the biosensor's transducer. Next, the sensor is exposed to that material. If the antigen being sought out is in that material, it will bind to the immobilized antibody to create an antibody-antigen complex. As a result, a physical property of the environment being monitored will be altered at the surface of the transducer. Consequently, this alteration will be signaled by the transducer. There are a number of different ways to classify immunosensors based on format considerations or the signal transducers. One helpful differentiator involves grouping based on disposable or reusable/regenerable format configurations. Immunosensors with disposable formats are associated with immunoassay test kits. Thus, properties that are significant for this comparison are more practical in nature and include the potential for multi-analyte capability, assay time, system cost, format versatility, reproducibility, assay cost, assay sensitivity, shelf life, ruggedness, etc.[6] There are also multiple-use immunosensors. These can be regenerated or recharged and

can be rather advantageous, for example for use as detectors for flow injection analysis and chromatographic systems. Fiber optic and continuous flow immunosensors have been used to detect explosive residues in ground water.

2.2.3 Microorganism Sensors

One other type of sensor is a microorganism-based biosensor. They are used for environmental monitoring applications. There are three main techniques/systems which these sensors utilize. The first being one in which the pollutant is a respiratory substrate. This is the most commonly used mechanism. These biosensors detect biodegradable organic compounds measured as biological oxygen demand (BOD).[6] BOD is generally used to detect how much biodegradable organic compounds exist in industrial waste water. There is another microorganism-based biosensor technique where the analyte being studied inhibits respiration. In general, microorganism-based biosensors are fairly simple to create and they have the ability to function over a large range of temperature and pH. They do have their disadvantages, though. One being the long assay times involving the initial response and return to the baseline. Due to this fact, these sensors might be best-suited for toxicity screenings, or circumstances with well defined toxic compounds, or measuring total toxicity.

2.3 Biosensor Transducers

2.3.1 Potentiometric Transducers

There are five main categories of transducers used in biosensors. The first to be

discussed are potentiometric transducers. Their underlying principle is the charge development related to the activity of the analyte that is in the sample through the Nernst relation.

$$E = E_0 \pm \frac{RT}{nF} \ln a_1 \tag{2.1}$$

where R is the gas constant, E_0 is the standard potential for a_1 = 1 mol l^{-1}, T is the temperature in Kelvin, F is the Faraday constant, n is the number of total charges on an ion, and +/- denote cations/anions.[6] In general, two electrodes must be in contact with the sample: one reference electrode and one working electrode. Utilizing these ion-selective membranes enable the transducers to become sensitive to numerous ions and gases. The pH electrodes can measure the enzymes activities. Such enzymes as urease, penicillinase, glucose oxidase, and acetylcholinesterase have been monitored. These particular enzymes consume or produce protons due to catalysis. This mechanism does have its limitations. First, the enzymes alter the pH. This change in pH is necessary for the detection of activity. However, it affects the enzyme catalysis. Consequently, the dynamic range of the assay is limited. Moreover, the buffer capacity of the assay solution significantly influences the analyte response curve, and the assay solution needs to be fixed to match the reference standards. These difficulties can be remedied by implementing a pH-stat configuration that makes up for the enzyme-catalyzed pH change or by obtaining the starting rates prior to changing the pH of the substance. A pH-stat analyzer calculates the optimal pH value for the reaction being examined.[7] It helps maintain a steady pH during chemical or biological reactions by adding OH^- or H_3O^+ reagents. The analyzer also outputs a real-time reading of the amount of added reagent and variation of pH over time. Furthermore, it calculates the kinetics of the reaction

being examined based on the amount of reagent needed to keep a constant pH over time. There is a nice vantage point for both of these mechanisms, and that is the fact that ions can be detected in a wide range of concentrations, usually 10^{-6} to 10^{-1} mol/L.[6] Environmental applications may be possible with these devices because of their ability to take measurements continuously. They are also portable, inexpensive, and can make in situ measurements. One major flaw is that the selectivity can be lower than desired and the detection limit in certain environmental samples can be somewhat high (10^{-5} mol/L or 1 ppm). In general, potentiometric biosensors used for environmental pollutant detection have utilized enzymes that catalyze the production or consumption of protons. Carbamic and phosphoric pesticides can be monitored by a pH electrode that measures the activity of acetylcholinesterase.[6] Pesticides in a substance can affect the enzyme's activity. These compounds can be measured at concentrations as low as 10^{-9} M because of this enzymatic amplification. Potentiometric biosensors can also measure heavy metals by using the enzyme urease coupled to an ammonium ion sensor. Urease is sensitive to heavy metal ions. Thus, the total concentration of these ions can be estimated by the inhibition of enzyme activity.

2.3.2 Amperiometric Transducers

The second category of transducers used in biosensors is amperometric transducers. Amperiometric biosensors use an enzyme mechanism that catalytically changes an electrochemically non-active analyte into a product that can be reduced or oxidized at a working electrode.[6] The working electrode is kept at a certain potential with respect to a reference electrode. The generated current is linearly proportional to the

electroactive product's concentration. The product's concentration is then proportional to the non-electroactive enzyme substrate. The enzyme-catalyzed reaction allows the concentration of the substrate to be obtained by amperometric detection of H_2O_2 or O_2. Amperiometric biosensors are the most frequently used class of biosensors. However, they have a tiny dynamic range because of the enzyme saturation kinetics. Also, for analyte oxidation to occur, a large over-potential is necessary. Consequently, this can cause interfering compounds to oxidize. These types of transducers do have their advantages: they are inexpensive and use disposable electrodes. This technique has such high reproducibility that repeated calibration is not necessary. The device used for these readings is readily available and compact, allowing for on-site measurements. These transducers also have limitations. One limitation being multiple electroactive compounds can yield false current values. This problem is addressed in clinical applications by implementing selective membranes that control the charge or molecular weight of compounds that have access to the electrode.

2.3.3 Conductometric Transducers

Another category of transducers is conductometric. Enzyme reactions that consume or create ionic species will alter the capacitance/conductance of the solution to a higher or lower degree depending upon the total ionic strength of the material.[6] Many planar interdigitated electrode configurations have been used as conductometric transducers for biosensors. Conductance is temperature sensitive. Thus, double layer charging, Faradaic processes, concentration polarization, and differential methods with internal controls are essential.[6] These transducers have several advantages, such as being

reproducible, inexpensive, and disposable. One drawback is that in order to achieve a reliable reading, the ionic species generated needs to notably alter the total ionic strength. Consequently, this may raise the limit of detection to undesirable levels and yields interference from the sample's variation in ionic strength.

2.3.4 Optical Transducers

Optical transducers are another category. There is a vast array of optical transduction techniques that can be used in biosensors, such as linear optical occurrences including fluorescence, absorption, polarization, phosphorescence, interference, etc. There are also non-linear phenomena like second harmonic generation. The technique applied depends on the application's nature and sensitivities. Fiber optics can generally be utilized with any optical methods in turn increasing their flexibility. Optical biosensor methods include direct detection of the analyte being studied or indirect detection via optical probes. Total Internal Reflection Fluorescence (TIRF) has been used with fiber optic and planar waveguides as signal transducers in many biosensors. In this type of transducer, light travels down a waveguide that creates an evanescent/electromagnetic wave at the surface of the waveguide material that has a higher refractive index than the material adjacent to it. The standing wave's amplitude decreases exponentially the further it penetrates into the medium with the lower refractive index. The fluorescence of a fluorophore, or probe, that is excited inside the evanescent field can be obtained outside the waveguide or by coupling the emission frequencies back into the waveguide.[6] For methods that implement TIRF, the biological sensing element is immobilized on the side of the waveguide. This technique is great for monitoring binding events at a solid-liquid

interface because washing away of unbound analyte is not necessary. Surface Plasmon Resonance (SPR) has also been used for signal transduction in biosensors. This method will be discussed in more detail later. Optical transducer methods have several advantages, such as reproducibility and speed of the measurement. They have been used for microbial and affinity-based biosensors and for enzyme-based biosensors for environmental applications. One main disadvantage of optical monitoring is that the device is often very expensive. Also, the devices are usually much larger than desired for on-site readings.

2.3.5 Acoustic Transducers

Another type of biosensor transducer is the acoustic transducer. These use the principle of the piezoelectric crystal as a mass sensor because there is a linear relationship between the change in the crystal's oscillating frequency and the change in the mass at the surface of the crystal.[6] When these crystals vibrate they create an oscillating electric field where the crystal's resonant frequency relies on its own size, mass, chemical structure, and shape. The frequency can be obtained as a function of mass when the crystal is put in an oscillating circuit. When the difference in mass (Δm) is insignificant in comparison to the crystal's total mass, Δm relates to the change in frequency (f) as:

$$\Delta f = Cf^{2}\frac{\Delta m}{A} \tag{2.2}$$

where A is the area of the electrode, f is the crystal's resonant frequency and C is a constant obtained from the crystal's thickness and material. Acoustical transducers can detect analytes by being coupled with antibodies or enzymes. One great advantage of acoustic transducers is that they are able to detect, in real time, the binding reactions of

chemical compounds in gas or solution with the crystal's solid surface. This technique enables the kinetic assessment of affinity interactions, generally between antigens and antibodies. Also, the cost of the device itself is very little. Of course, as with all devices, the acoustic transducers do have their limitations, which include calibration and format requirements. Every crystal needs to be calibrated because its frequency relies on the geometry of the crystal and the method used to cover the surface with antibody or antigen. The variability lies in the immobilized protein's uniformity on the surface. Acoustic transducers have been utilized in numerous biosensors, one being a detector for atmospheric pollutants that uses immobilized proteins, such as antibodies and enzymes.

2.3.6 Calorimetric Transducers

Another category of transducers is calorimetric. Numerous enzymatic reactions are exothermic and produce heat that can be used as the platform for measuring the reaction rate and concentration of analyte.[8] The changes in temperature are generally obtained by thermistors at the entrance and exit of small immobilized enzyme-containing columns. The surrounding environment is held at constant temperature. Because the conditions are very well controlled, as much as 80% of the heat produced by the reaction can be recorded as a change in temperature in the sample.[8] This can be obtained from the change in enthalpy and the amount that reacted.

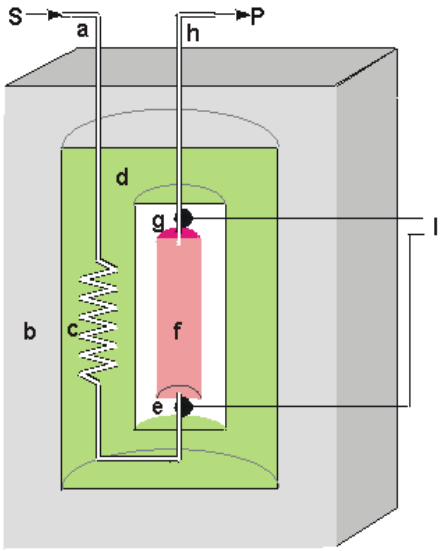

Figure 2-1: Schematic of calorimetric biosensor.

In Figure 2-1 above, the sample stream, (a), travels through the outer insulated box, (b), to the heat exchanger, (c), inside an aluminum block, (d). Then, the stream travels past the reference thermistor, (e), and into the packed bed bioreactor, (f), which holds the biocatalyst. This is where the reaction takes place. The temperature change is obtained by the thermistor, (g), and the solution sent to waste, (h). The external electronics, (l), calculate the variance in resistance and temperature between the thermistors. Thermistors implemented to detect the change in temperature operate by varying their electrical resitance with the temperature. They follow the relationship:

$$\ln \frac{R_1}{R_2} = B\left(\frac{1}{T_1} - \frac{1}{T_2}\right) \tag{2.3}$$

thus:

$$\frac{R_1}{R_2} = e^{B\left(\frac{1}{T_1} - \frac{1}{T_2}\right)} \tag{2.4}$$

where R_1 and R_2 are the resistances of the thermistors at absolute temperatures T_1 and

T_2.[8] B is the thermistor's characteristic temperature constant. When the change in temperature is very tiny, then $B(\frac{1}{T_1}-\frac{1}{T_2})$ is much smaller than one and Equation 2.4 can be simplified by using the approximation that when x << 1, $e^x \sim 1+x$, where x is $B(\frac{1}{T_1}-\frac{1}{T_2})$. Thus:

$$R_1 = R_2(1+B\frac{T_2-T_1}{T_1T_2}) \tag{2.5}$$

When $T_1 \sim T_2$:

$$\frac{\Delta R}{R} = -\frac{B}{T_1^2}\Delta T \tag{2.6}$$

The decrease in electrical resistance $\frac{\Delta R}{R}$ of the thermistor is proportional to the increase in temperature (ΔT).

One main issue with this biosensor is that it is hard to match the characteristic temperature constants of the reference and measurement thermistors.[8] If both thermistors experience an equal movement of only 1 ^{0}C from the background temperature this generates a change in the relative resistances of the thermistors that is equal to 0.01 ^{0}C. This is the same as the whole temperature change caused by the reaction. This is why changes in the temperature of the surrounding environment must be eliminated, which is why the aluminum block in biosensor in Figure 2-1 is very well insulated. The range and sensitivity of thermistor biosensors are fairly low for most of the applications. However, sensitivity can be increased by increasing the heat given off by the reaction.

2.4 Optical Biosensors

Optical biosensors use optical-based transducers for monitoring biological molecules.[5] In general, the bio recognition processes occur at surfaces or interfaces. Optical biosensors are most widely used for biological sensing and they are the largest collection of transducers.[5] Two important research techniques for optical biosensors, include utilizing luminescence or ascertaining changes in the absorption of light between the reactants and products of a reaction.[9] These techniques generally make use of colorimetric test strips, which are one-time use cellulose pads infused with reagents and enzymes. This process is usually utilized for monitoring diabetics' glucose levels, for example. For this sensor, the test strips are composed of horseradish peroxidase, glucose oxidase, and a chromogen. The hydrogen peroxide created by the aerobic oxidation of glucose oxidizes the weakly colored chromogen to a highly colored dye. The process is shown below:

$$\text{chromogen}(2H) + H_2O_2 \xrightarrow{\text{peroxidase}} \text{dye} + 2H_2O \qquad (2.7)$$

Once the test strip is dyed, the results can be assessed by making use of portable reflectance meters, or simply by visual comparison with a colored chart. There are numerous other test strips that use other enzymes, one of which is a biosensor that employs firefly luciferase to sense bacteria in clinical samples or food. Bacteria are lysed (cells destroyed) and the ATP (Adenosine Tri-Phosphate) is released and reacts with oxygen and D-luciferin in a reaction that generates yellow light in high quantum yield.[9]

$$\text{ATP} + \text{D-luciferin} + O_2 \xrightarrow{\text{luciferase}} \text{oxyluciferin} + \text{AMP} + \text{pyrophosphate} + CO_2 + \text{light (562 nm)}$$

(2.8)

There are two methods in which the generated light may be monitored. One is by low voltage inexpensive photodiode devices. The other is by photomultiplier tubes that are costly and use high-voltage. The sensitivity of the latter system is higher than that of the photodiodes. The firefly luciferase enzyme is highly expensive and only comes from the tails of wild fireflies.

As alluded to previously, optical biosensors can be divided into two categories, direct and indirect.[5] For the direct case, the analyte's inherent optical properties are monitored, such as emission, absorption, or refractive index. Examples of the direct case are Scanning Angle Reflectometery (SAR), ellipsometery, and Optical Waveguide Lightmode Spectroscopy (OWLS). For the indirect case, the fluorescence or color of an optically detectable bioprobe is measured. Examples here include Surface Plasmon Resonance (SPR), Total Internal Reflection Fluorescence (TIRF), and Total Internal Reflection Spectroscopy (TIRS). The methods mentioned are non-destructive because they utilize weak radiations to detect signals.

Optical biosensors have their advantages. The first being, they can function in nondestructive operation mode. Their accuracy and sensitivity are very high because their signal-to-noise ratios are better. In general, for optical biosensors, the biological molecules being monitored do not need to be labeled. Also, they can measure events in real time in situ.

2.4.1 (Enzyme-linked Immunosorbent Assays) ELISA

Optical immunosensors are very popular for biological analysis. The ELISA (enzyme-linked immunosorbent assays) technique is a common biosensor approach. This method is used to identify and intensify an antibody-antigen reaction. It monitors the amount of enzyme-linked antigen that is bound to the immobilized antibody. The sensitivity can be improved by making use of enzyme-catalyzed reactions, to give much larger responses. For example, there are enzyme-catalyzed reactions that generate highly fluorescent, colored, or bioluminescent products.

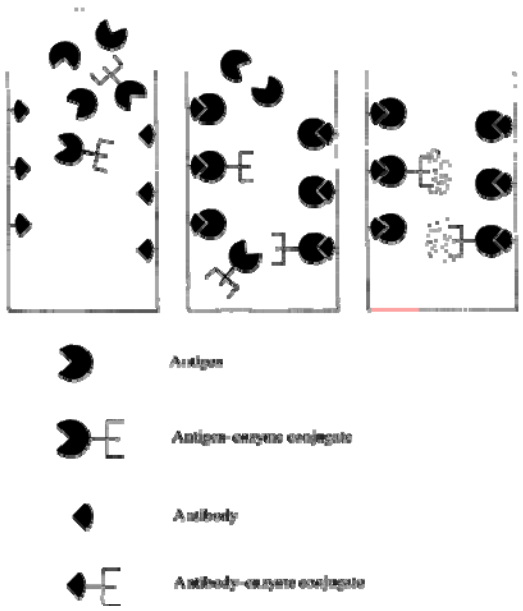

Figure 2-2: Underlying principles of ELISA.

Figure 2-2 displays the underlying principles of ELISA. (a) The antibody with an affinity for the antigen being studied is immobilized on the surface of a tube. A solution of antigen-enzyme conjugate with an unknown concentration of antigen is put in the tube and left to equilibrate. (b) After some time, the antigen-enzyme conjugate along with the

unlabeled antigen will equilibrate to free and bound states based on their concentrations. (c) The material that does not bind is rinsed away. The quantity of bound antigen-enzyme conjugate can be obtained by the rate of enzymatic reaction.

2.4.2 Surface Plasmon Resonance

Surface plasmon resonance (SPR) is another very popular approach for optical biosensors. In the early 1900s, R.M. Wood at Johns Hopkins University discovered that polarized light incident on a diffraction grating with a metal back produced light and dark bands in the reflected light.[10] He postulated theories for what was taking place, but it was not until 1907 that this phenomena was better understood by Lord Rayleigh. He developed a grating theory based only upon the expansion of the scattered electromagnetic field in terms of outgoing waves. He discovered that at wavelengths where one of the spectral orders comes out of the grating at the grazing angle, the scattered field is singular. These particular wavelengths are now known as the Rayleigh wavelengths (λ_R) and they are consistent with Wood's anomalies. Also, the singularities are only observed when the electric field is perpendicularly polarized to the rulings. Thus, they explain the S anomalies.

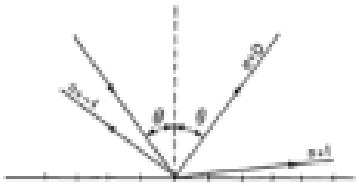

(a)

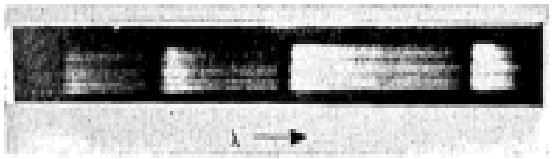

(b)

Figure 2-3: Wood's anomalies: (a) reflected and diffracted spectral orders created by plane waves incident on a reflection grating; (b) spectrogram showing Wood's anomalies.

Further experimentation and research on electron energy losses on thin foils and in gasses was done in the 1950s. One major contribution came from D. Pines at the University of Pennsylvania and D. Bohm at Princeton University when they discovered that the energy losses resulted from the excitation of conducting electrons that produced plasma oscillation or plasmon.[11] As more studies were completed, it came to be known that the energy loss is a consequence of the excitation of a surface plasma oscillation where a portion of the restoring electric field reaches passed the boundary of the specimen being studied. This leads to the conclusion that the surface plasmon oscillation can be altered by any contaminant or film on the surface of the specimen. After a time, this phenomenon was understood as the excitation of electromagnetic evanescent waves at the metal's surface. Later on, in the 1970s, evanescent waves were used to examine ultra-thin metal coatings and films.

Kretchman and Otto verified optical excitation of surface plasmons by using the technique of attenuated total reflection.[10] There are two main methods to optical excitation of surface plasma waves. The first is diffraction at diffraction gratings. The second is attenuated total reflection in prism coupler-based structures. Nylander and Liedberg have extensively studied the sensing applications of surface plasma waves excited by the attenuated total reflection. This particular technique is fairly

uncomplicated, and hence often utilized for biochemical sensing and characterizing thin films. Cullen *et al*. has studied SPR sensing techniques that utilize the diffraction gratings.[12] Thus, grating-based SPR sensors have been examined as a substitute for prism-based mechanisms.

SPR and similar methods in the 1980s that implemented evanescent waves were used for the study of thin films and chemical and biological interactions. Use of these methods enables one to have a closer look at how analytes and immobilized receptors interact in solution in real time, without labeling the analyte. The binding levels and rates can be explained in a multitude of ways to yield pertinent information on the analyte's concentration, or the affinity, specificity, and kinetics of the interaction.

2.4.3 Surface Plasmon Resonance Theory

The phenomenon of SPR takes place when plane-polarized light is incident on a metal film when there is total internal reflection. Total internal reflection can occur when a beam of light is incident on a half circular prism at the planar interface when it travels from a higher refractive index medium to a lower refractive index one. By increasing the angle of incident light, the refracted angle is increased until the critical angle is achieved. At the critical angle all of the incident light is reflected inside the circular prism, hence leading to total internal reflection (TIR). Even though no light transmits through the planar interface when there is TIR, the photons' electric field penetrates roughly a quarter of a wavelength into the reflecting surface.

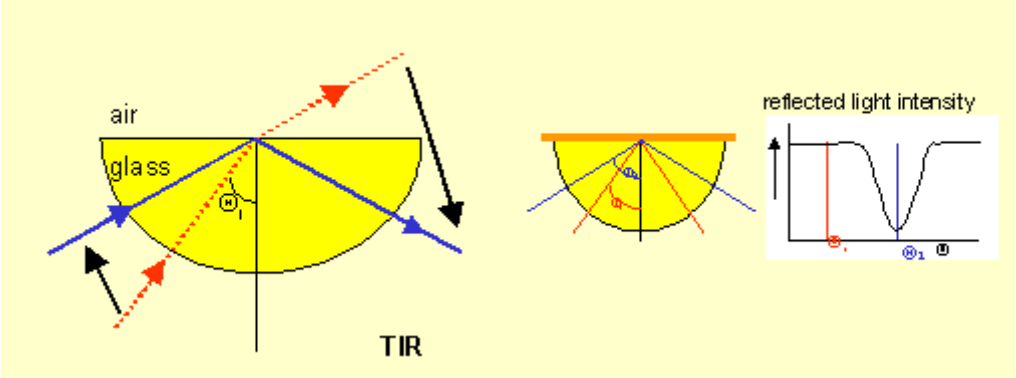

Figure 2-4: Schematic of total internal reflection.

For SPR, the prism is covered with a thin metal film on the planar interface. Generally, gold is used because it yields an SPR signal at suitable combinations of wavelength and reflectance angle.[10] Another advantage is that gold is chemically inert to solutes and solutions that are commonly used for biochemical purposes. Under appropriate coupling conditions, the optical electrical field can interact with the free electrons in the gold surface. The incident photons are then absorbed and that energy is transferred into the surface plasmons.

Electron and photon behavior can only be described correctly with both particle and wave properties. A plasmon is the particle name of the electron density wave.[10] Thus, under specific conditions, the photons are converted to plasmons, consequently leaving a 'gap' in the reflected light intensity.

Because of conservation laws, the conversion from photon to plasmon must conserve energy and momentum. Plasmons have a unique momentum determined by the material on either side of the film and the conducting film's nature.

Resonance takes place when the incident photon's momentum matches the plasmon's momentum. Changing the incident light's angle or wavelength leads to a

change in the relative magnitude of the vector components of the momentum. For SPR, the component parallel to the gold surface is important since plasmons are restricted to the gold film's plane. Consequently, for SPR to occur, there needs to be a particular angle and energy of incident light.

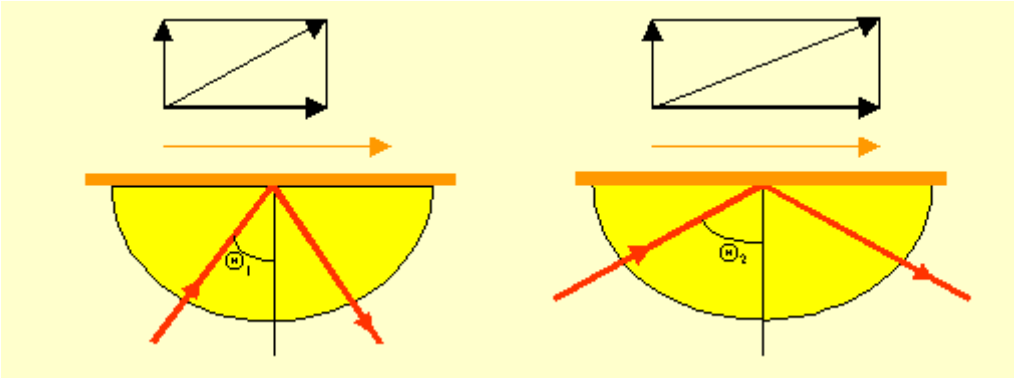

Figure 2-5: Schematic of momentum resonance.

The reflected photons generate an electric field on the opposing side of the interface when there is TIR. In turn, the plasmons produce a field that exists in the material on either side of the film. This particular field is referred to as the evanescent wave because the wave's amplitude exponentially decreases as the distance from the interface surface increases, thus decaying over the length of around one optical wavelength. The evanescent wave travels within about 300nm of the sensor surface.

The photons velocity varies inversely with the refractive index. Similarly, the plasmon's velocity and momentum depends on what the material is comprised of. Due to the momentum change, the angle of incident light at which SPR takes place changes as well. This change can be measured very accurately. This frequently used SPR method is called angular SPR or resonant angle SPR. However, when the angle of incident light is fixed, the wavelength can be adjusted until resonance is obtained. This less common

technique is called spectral SPR or resonant wavelength SPR.

The SPR angle is dependent upon the wavelength of the incident light, the characteristics of the metal film, and the refractive index of the material on both sides of the metal film.[10] The refractive index of the film is temperature sensitive. Thus, it is necessary for the experiments to be completed at a controlled temperature. It is important that the metal have conduction band electrons that can resonate with the incident light at a certain wavelength. Metals where this is possible are gold, silver, copper, sodium, aluminum, and indium. The metal on the surface of the sensor cannot have any sulphides or oxides, and it must not react with other molecules when exposed to aqueous solutions or the atmosphere. Gold is the most suitable metal for SPR. Sodium is too reactive, indium is too expensive, silver is too susceptible to oxidation, aluminum and copper have too broad of an SPR response.[10] Gold is mainly impervious to atmospheric pollutants and oxidation. However, it works well with many chemical modification systems. The total thickness of the gold layer should be around 50nm thick and this thickness is highly significant.

As seen in Figure 2-6 below, the dip in reflective light gets shallow when it is above the optimum reflectance. The dip gets broader when the reflective light is below the optimum reflectance. To achieve a sharp dip, it is necessary for the light source to be p-polarized and monochromatic. Non p-polarized light increases the background intensity of the reflected light and does not play a part in the SPR.

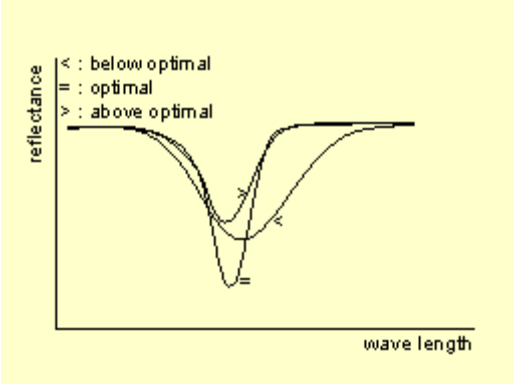

Figure 2-6: Optimum reflectance.

The SPR signal depends solely on the refractive index change of the material that is on the sensing side of the SPR surface. This is due to the fact that during experimentation, the temperature, metal film, and incident light are held constant.

When biomolecules bind to the surface of the sensor, the refractive index at the sensor surface changes. This is seen as a change in resonance wavelength or resonance angle. The change in refractive index is linearly proportional to the amount of bound macromolecules. This is generally the case for protein-protein interactions with refractive index increment (RII) of around 0.18-0.19 ml/g. Several SPR devices change the measured values of wavelength or angle into an arbitrary value that is simple to understand in display. One example is the BIACORE machine, which uses the Resonance Unit (RU). The RU gets converted from the actual angle shift in reflected light.

2.4.4 Fiber Grating Sensors

In 1978, Hill *et al*. at the Canadian Communications Research Center (CRC),

were the first to observe fiber photosensitivity.[13] However, these "Hill gratings" only operate in the visible wavelength range of the writing light, so they are not commonly used. In 1989, Meltz *et al*. solved this problem.[14] They implemented ultraviolet light at 244 nm as their source to create the first Bragg grating in germanium doped fibers with a resonant wavelength that is within the communications window by side writing interferometry. This is the method of "transverse holographics" and it became very popular. It was a stepping stone for researchers to be able to study the construction technologies, optical properties, and applications of fiber gratings.

Fiber sensors have many advantages, such as EMI immunity, electrically passive operation, high sensitivity, and multiplexing capabilities.[15] Fiber sensors that have the ability for distributed sensing have a step up on the competition. Devices with this capability include Fiber Bragg Gratings (FBGs) and other grating-based systems. Gratings are straight-forward, intrinsic sensing instruments that can be photo-inscribed into a silica fiber. They encompass all the same advantages as fiber sensors, plus some extra benefits. They also possess inherent self-referencing capabilities and they can be easily multiplexed along a single fiber. Grating-based sensors have many applications, one of which is the development of "smart structures" using distributed embedded sensing media. In this process, fibers containing sensor arrays are embedded into the materials to enable the monitoring and measuring of strain, load, temperature, and vibration.[15] This allows determination of the structure's health, which can be monitored in real time. Gratings also play an important role as the optical sensing elements in a multitude of fiber sensor constructions, pressure sensors, grating-based chemical sensors, and accelerometers to name a few.

UV-written fiber gratings have lead to major improvements in many areas such as fiber sensors, optical fiber communications, optical computing, and optical information processing.[5] Fiber gratings influence nearly every facet of optical communications such as optical amplification, optical transmitters, and the dispersion compensation to the optical receiver. The technology of fiber gratings has made an impact on the development of semiconductors and fiber lasers by allowing for the creation of extremely spectrally selective feedback elements straight into the fiber core. This allows for the single longitudinal mode output with 100 kHz line width. Another application for fiber gratings is in the area of optical amplifiers where they aid in obtaining gain flattening through the whole bandwidth of optical amplifiers. They also efficiently reduce the Amplified Spontaneous Emission (ASE). This increases the pump efficiency and enables low noise amplification. Fiber gratings are also useful for making Add/Drop Multiplexers and WDM Demultiplexers. In addition, they make excellent sensors because of their noteworthy linear relationship between temperature/stress and the resonant wavelength of the grating. The grating's resonant wavelength is intrinsically independent of the input optical power. This allows for the grating-based sensor's self-referenced capabilities. Thus, eliminating the random variation of the input optical power caused by the physical distortion of the fiber (i.e. macrobending), or the thermal fluctuation of the optical source.

Optical fiber-based sensors have numerous advantages over other environmental sensors. Some of these advantages are: 1.) intrinsically safe in explosive environments; 2.) potentially resistant to ionizing or nuclear radiation; 3.) sensed signal is immune to radio frequency interference (RFI) and electromagnetic interference (EMI); 4.) as a point

sensor, can be used to sense normally inaccessible areas without perturbation of the transmitted signals; 5.) chemically inert, can be readily implemented in biomedical instrumentation and chemical processes due to mechanical flexibility and small size; 6.) easily interfaced with low-loss optical fiber telemetry, and thus allow remote sensing by locating the control electronics for detectors and LEDs/lasers far from the sensor head; 7.) extremely secure and reliable with no risk of sparks or fire; 8.) low weight and volume (1 km of 200 μm silica fiber only weighs 70 gm and takes up a 30 cm^3 volume); 9.) high voltage insulation and absence of ground loops eliminates need for isolation mechanisms such as optocouplers; 10.) large bandwidth enables multiplexing multiple individually addressed point sensors in a fiber network or distributed sensing (continuous sensing along the fiber length); 11.) high accuracy, high sensitivity, and cost-effective.[5]

---

[1] http://chem.ch.huji.ac.il/history/clark_leland.htm

[2] http://www.cranfield.ac.uk/health/researchareas/biosensorsdiagnostics/page18795.jsp

[3] D. W. Lübbers, "How to measure pO_2 of tissue sealed in a transparent chamber: Development and construction of the first optrodes/optodes," *Sensors and Actuators B: Chemical*, **51**, Iss. 1-3, 5-11, (1998).

[4] B. Liedberg, C. Nylander, I. Lundstrom, "Surface plasmon resonance for gas detection and biosensing," Sens. Actuators B, **4**, 299 (1983).

[5] Zhiyong Wang, Ph D Dissertation, (Virginia Tech, 2005).

[6] K. R. Rogers, M. Mascini, "Biosensors for Analytical Monitoring," *Human Exposure and Atmospheric Sciences, EPA*, (2007).

[7] http://www.scientistlive.com/lab/?/Lab_Equipment/2004/12/01/9966/How_to_keep_pH-stat_titrant_addition_under_proper_control/

[8] http://www.lsbu.ac.uk/biology/enztech/calorimetric.html

[9] http://www.lsbu.ac.uk/biology/enztech/optical.html

[10] http://www.sprpages.nl/SPRtheory/SprHistory01.htm

[11] D. Pines, D. Bohm, "A Collective Description of Electron Interactions: II. Collective vs Individual Particle Aspects of the Interactions," *Phys. Rev.* **85**, 338 – 353, (1952)

[12] D. C. Cullen, "Detection of Immuno-complex Formation via Surface Plasmon Resonance on Gold-Coated Diffraction Gratings," *Biosensors*, **3**, 211-225, (1987/88).

[13] J. W. Goodman, "Introduction to Fourier Optics," 3rd ed., Ch. 10 Fourier Optics in

Optical Communications, 400.
[14] G. Meltz; *et al.*, "Formation of Bragg gratings in optical fibers by a transverse holographic method," *Opt. Lett.* **14**: 823, (1989).
[15] A. D. Kersey; *et.al*., "Fiber Grating Sensors," *J. Lightwave Tech.*, **15**(8), (1997).

Chapter 3. Background on Ionic Self-Assembled Multilayers and Long Period Gratings

3.1 Ionic Self-Assembled Multilayers (ISAMs)

The ISAM technique is a layer-by-layer deposition technique that is used to form nm-thick films on a substrate (such as a microscope slide or an optical fiber) that are held together by the ionic bonds created between two oppositely charged polyelectrolytes.[1] These layers display excellent reliability, stability, and homogeneity.[2] The ISAM technique allows for precise control of the thickness and refractive index of the films deposited onto the substrate. These films can be deposited on any surface with a minimum charge density, such as metal, glass, or silica.[3] The films can also be adjusted to incorporate a variety of materials, including proteins, clay platelets, virus particles, etc.[3] ISAMs are inexpensive, and quick and easy to assemble. The ISAM technique illustrates its diversity in being able to utilize many different substrates and materials. In addition, ISAMs deposited on optical fiber gratings have some further advantages, which include: the ability to easily fine tune grating resonances, development of efficient index sensors or index-modulating fiber mechanisms, and applications to biosensors.[4]

The thin polyelectrolyte multilayer (PEM) films created by the ISAM deposition technique have been thoroughly investigated and they have been demonstrated to have potential applications as membranes, sensors, drug delivery agents, and in some polyelectrolyte mechanisms biocompatibility was noted.[5] Other applications for these films include: permselectivity membranes, enzyme active films, light-emitting diodes, electrochromism, nonlinear optics, etc.[6] Most of these applications benefit from procedures for creating organic thin films on the nanoscale level. Due to this fact, over

the years polymer self-assembly is becoming a more widely studied area for the creation of well-defined thin films. The ISAM technique enables control in the vertical direction of the film growth process. These organic self-assembled films encompass two aspects that enable the formation of stable structures in thermodynamic equilibrium. The first is versatile organic synthesis, and the second, spontaneous molecular self-assembly. Making these films requires knowledge from many different disciplines, including material science, organic synthesis, physics, physical chemistry, and electrical engineering.

Decher *et al.*, in the early 1990s developed this layer-by-layer assembly technique.[7] This technique, unlike the traditional self-assembled monolayers (SAMs), can be adjusted to enable multimaterial construction of several compounds without chemical modifications. In the ISAM deposition technique, a negatively charged substrate is placed into a polycation solution, where it adsorbs a layer of polycation molecules because of the strong Coulombic attraction between the substrate and the polycations. Now the surface is positively charged. This limits any further polycation adsorption. Then, the substrate is taken out and rinsed in deionized water to remove any polycation molecules that did not ionically bond. Next, the substrate is placed into a polyanion solution, where it adsorbs a layer of polyanion molecules because of the Coulomb attraction. Again, the substrate is taken out and rinsed in deionized water. These steps are repeated to create a multilayered thin film. Each layer is about 1 nm thick, but the thickness can be varied by altering the pH and ionic strength of the immersion solutions. This process is depicted in Figure 3-1. One monolayer of polycation plus one monolayer of polyanion makes up a bilayer. Films with different

compositions can be created, which are determined by the dipping sequence of the various ionic solutions. For example, ABAB, ABCBAB, etc.

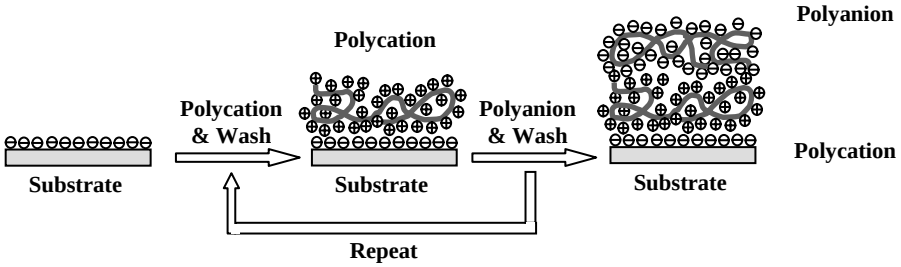

Figure 3-1: Schematic illustration of the ISAM procedure.

These thin films are, to some degree, independent of the initial substrate that they are being deposited on. Following the first couple layers, the characteristics of the layers are controlled by the deposition conditions and the polyanion/polycation pair. Generally, the influence of the substrate disappears after the deposition of a few bilayers.[8] To summarize, the advantages of the ISAM technique are:

1. ISAM film materials are very diverse (i.e. polyelectrolytes infused with proteins, clay platelets, virus particles, etc.);
2. ISAM film thickness can be controlled very precisely at the nm level;
3. ISAM procedure is rapid, easy, inexpensive, and environmentally friendly;
4. Film structure is very flexible and depends on dipping sequence;
5. Substrate materials are very diverse with different sizes, structures, and topology (i.e. glass, mica, metal, silica, etc.);
6. ISAM film refractive index can be controlled by altering the pH of polyelectrolyte solutions and using different materials;

7. ISAM films are thermally stable, reliable, and of good quality.[4]

3.1.1 ISAM Film Characterization

Techniques and procedures for understanding ISAM films fall into two categories: *ex situ* and *in situ* methods. Some *in situ* methods are the following: surface force measurements[9], atomic force microscopy (AFM)[10], second harmonic generation (SHG)[2], attenuated total reflection Fourier transform infrared spectroscopy (ATR-FTIR)[11], quartz crystal microbalance[12], zeta potential[13], optical waveguide lightmode spectroscopy (OWLS)[14], surface plasmon spectroscopy[15], scanning angle reflectometry (SAR)[16], optical reflectometry in stagnation point flow cells[13], and ellipsometry[17]. *Ex situ* methods are: X-ray/neutron-ray reflectometry[1], UV/Vis spectroscopy[1], and nuclear magnetic resonance (NMR).[18]

3.1.2 Ellipsometry Studies on ISAM Films on Glass Slides

Ellipsometry can be used for characterization of film thickness and optical constants (such as extinction coefficients and film refractive index). The device implemented for such experiments is a Variable Angle Spectroscopic Ellipsometer (VASE) designed by J. A. Woollam Co. The experiments were performed with ISAM film coated glass slides from Fisher Scientific Inc. The materials were Poly(allylamine hydrochloride) (PAH) and Poly[1-[4-(3-carboxy-4-hydroxyphenylazo) benzenesulfonamido]-1, 2-ethanediyl, sodium salt (PCBS). Both were prepared at 10 mM concentrations. PAH was the polycation and PCBS was the polyanion. Figure 3-2 a and b depict the molecular structures of PAH and PCBS, respectively. PAH is a low

refractive index material and PCBS is a high refractive index material.

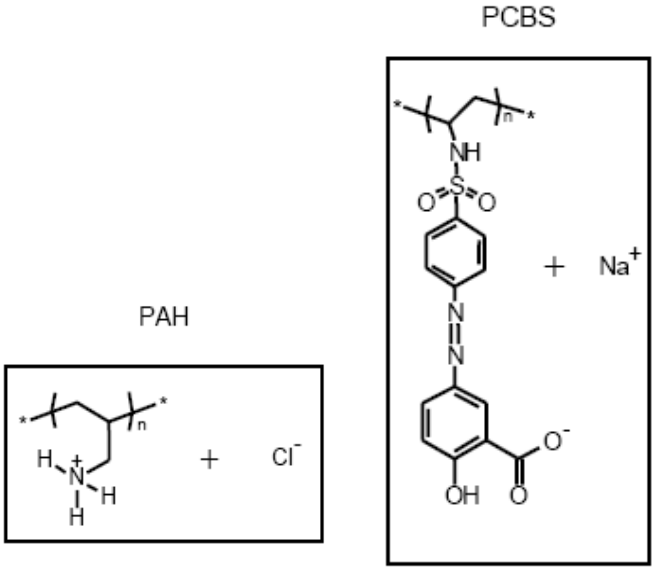

(a) (b)

Figure 3-2: Molecular structure of (a) Poly(allylamine hydrochloride), (PAH) and (b) Poly[1-[4-(3-carboxy-4-hydroxyphenylazo) benzenesulfonamido]-1, 2-ethanediyl, sodium salt (PCBS).

The glass slides were prepared by the RCA cleaning process.[19] Ellipsometry is an extremely sensitive measurement technique that uses polarized light to characterize thin films, surfaces, and material microstructures. It achieves its sensitivity from the determination of the relative phase change in a beam of reflected polarized light.

3.1.3 Ellipsometry Results

My predecessor, Zhiyong Wang, performed studies of many PAH/PCBS ISAM films using ellipsometry on glass slides. The first study was on the dependence of ISAM film thickness and refractive index on the variation of the pH's of the polyelectrolyte solutions. PAH and PCBS were used at 10 mM concentrations. Multiple sample slides

were constructed with different pH values for the PAH and PCBS. The pH of the PCBS solutions went from 6.0 to 8.0 and the pH of the PAH solutions went from .06 to 9.0. Each of the films consisted of 20 bilayers of PAH/PCBS.

Figure 3-3 a, b, c, and d show how the thickness and refractive index of the ISAM films vary with respect to the pH of the polyelectrolyte solutions used. As can be seen in the figures, as the pH of the PAH is increased, while the pH of the PCBS is kept constant, the film thickness increases and refractive index of the film decreases.

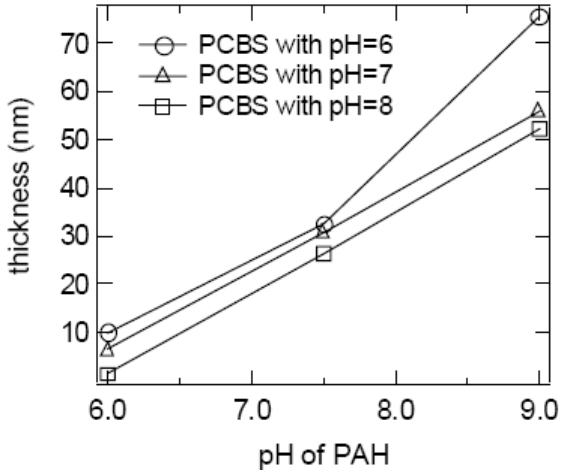

(a)

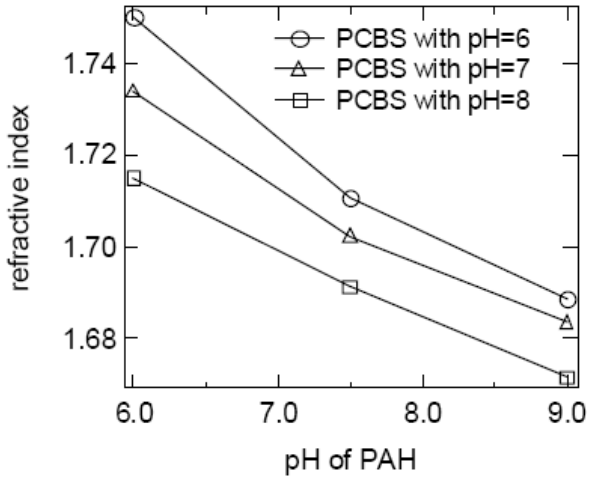

(b)

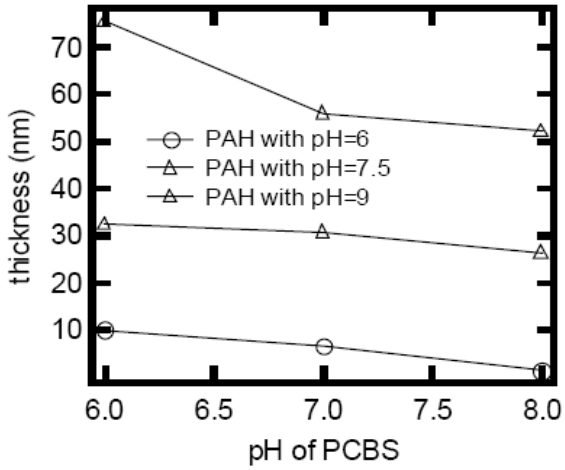

(c)

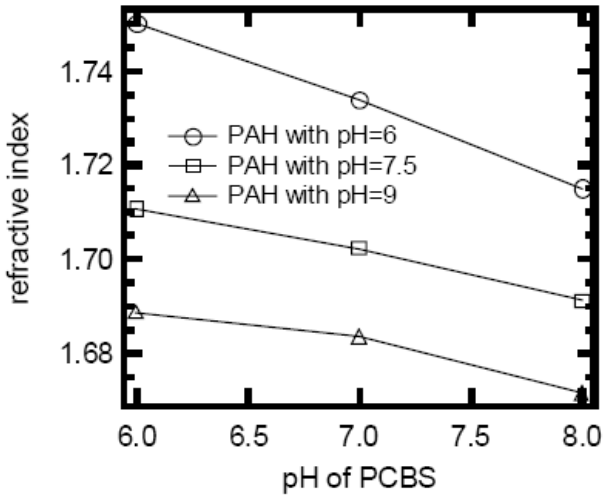

(d)

Figure 3-3: Refractive index and thickness of 20 bilayer PAH/PCBS ISAM film measured using ellipsometery. (a) Thickness vs. pH of PAH. (b) Refractive index vs. pH value of PAH. (c) Thickness vs. pH of PCBS. (d) Refractive index vs. pH value of PCBS.

This process occurs because PAH and PCBS are both weak electrolytes. Thus, changes in the pH will alter the charge density of the adsorbing polymer. As the pH drops below the pK_a value of PCBS (~ 5 or 6), the charge density of the PCBS decreases because its acid groups become protonated. However, as the pH of the PAH is increased above its

pK_a value (~ 9), its amine groups become deprotonated. Hence, the charge density of the PAH will decrease. As the charge density decreases, there is less repulsion between neighboring charges. This allows more polymer chains to adsorb on the substrate with loops and tails to induce thicker layers. PCBS has a higher refractive index than PAH. Thus, a higher percentage of PCBS yields a higher composite index of the film. However, a higher percentage of PAH yields a lower composite index. Thus, the thickness and refractive index of the ISAM films can be controlled precisely by altering the pH values of the polyelectrolyte solutions being used.

3.2 Long Period Gratings (LPGs)

Long Period Gratings (LPGs) are photo induced variations in the refractive index of an optical fiber that couple light from the core of a single mode optical fiber into the cladding of the fiber at certain wavelengths, creating one or several attenuation bands in the fiber transmission.[20] The figure below depicts the mechanism of the LPG.

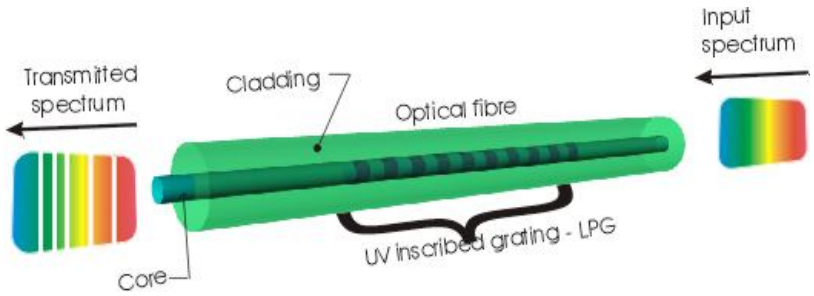

Figure 3-4: Schematic of transmission spectrum of an LPG in an optical fiber.

The LPG couples light from the core mode to the cladding mode, and the cladding modes are attenuated rapidly. As a result, the transmission spectrum of the LPG is made

up of a series of attenuation bands, as displayed in Figure 3-4 above. Every attenuation band corresponds to the coupling from the core mode to a cladding mode. There is total internal reflection in the core mode, since the index of refraction is slightly higher in the core than it is in the cladding. Thus, most of the light's intensity is in the core. The cladding has a higher index of refraction than the air surrounding it. As schematically illustrated in Figure 3-5, while light is highly transmitted at most wavelengths, there are specific wavelengths where very strong attenuation is observed. These are the wavelengths where light is coupled out of the core and into the cladding mode.

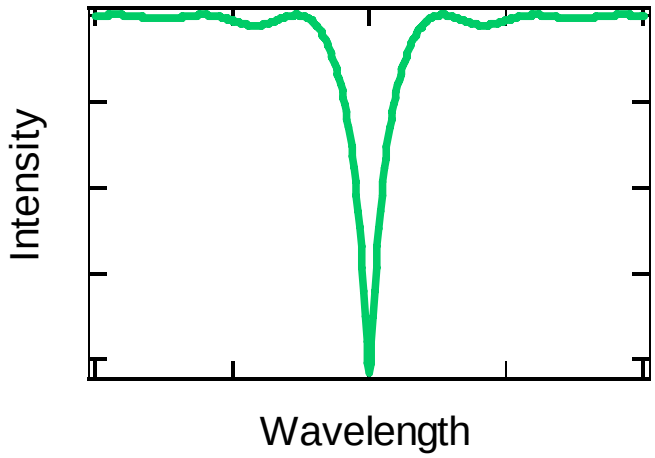

Figure 3-5: Sketch of transmission spectrum of an LPG in an optical fiber.

LPGs have been used in filtering procedures such as band-rejection and gain-flattening. They have also been used for temperature and strain sensing. In this thesis, we will describe how LPGs can be implemented for biosensing. One very useful characteristic of LPGs is their sensitivity to the refractive index of the material surrounding the fiber cladding in the grating region, which, for this work, is the ISAM film. This is a result of the dependence of the attenuation band wavelengths on the cladding mode's effective refractive index. The effective refractive index of the cladding

modes depends on the refractive index of the surrounding environment. This sensitivity allows LPGs to be used as index sensors because of the change in attenuation and/or wavelength of the LPG bands.

3.2.1 Differences Between Fiber Bragg Gratings (FBGs) and Long Period Gratings (LPGs)

An optical fiber that has a refractive index in its core that varies periodically along the length of the fiber is called a fiber grating. Fiber gratings can be separated into two categories depending upon the period of the grating. The first category is short period fiber gratings, which are called Fiber Bragg Gratings, or FBGs. The second category, which will be the one focused on in this dissertation is Long Period Gratings, or LPGs. They have a period in the range of 100 μm to 1 mm. An LPG can be created by ultraviolet (UV)-induced modulation of the fiber core's refractive index.[20]

Figure 3-6 (a) depicts a schematic of a typical FBG. FBGs are spectral filters. They generally reflect over a narrow range of wavelengths and transmit all other wavelengths. FBGs are based upon the principle of Bragg reflection. When light travels through the fiber core, the reflected wave, (which consists of light reflected off interfaces of high and low refractive indices) can have constructive interference for one wavelength. That wavelength is highly reflected. If the wavelength is twice the spacing of the high index regions in the fiber, the reflected waves with the same wavelengths will constructively interfere and create a strong reflection or strong transmission. On the other hand, the reflected waves with different wavelengths will cancel each other out by destructive interference and lead to low transmission or low reflection. In a typical FBG,

the grating period is about 535 nm for a Bragg wavelength of 1550 nm. FBGs are generally between 1 mm and 25 mm long.

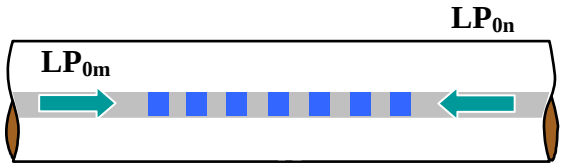

(a)

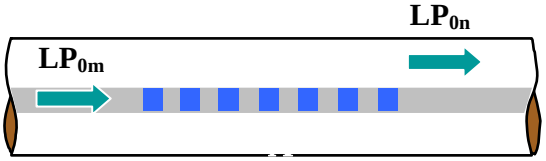

(b)

Figure 3-6: (a) Fiber Bragg Grating (Reflection Grating), (b) Long Period Grating (Transmission Grating).

Figure 3-6 (b) depicts a schematic of a typical LPG. An LPG has a core with periodic alternating segments of higher and lower refractive index. In contrast to FBGs, LPGs couple co-propagating modes with close propagation constants. Thus, the period of the LPG can greatly exceed the wavelength of radiation propagating in the fiber. Because LPGs couple co-propagating modes, their resonances can only be seen in transmission spectra. The transmission spectrum has dips at the wavelengths corresponding to resonances with different cladding modes in a single mode fiber. In contrast to FBGs, LPGs do not produce reflected light and can serve as spectrally selective absorbers. LPGs are generally between 3 and 5 cm long. Thus, the FBG acts as a reflection grating and the LPG acts as a transmission grating.

3.2.2 LPG Simulations

Zhiyong Wang also performed simulations to examine the optical properties of LPGs. Erdogan's theory was utilized to evaluate the LPGs.[21] To simplify things, it was assumed that the UV-induced variation in the refractive index of the core is described by:

$$\delta n_{core}(z) = \overline{\delta n_{core}}(z)\{1 + \nu \cdot \cos[\frac{2\pi}{\Lambda} z + \phi(z)]\} \tag{3.1}$$

where $\overline{\delta n_{core}}$ is the "dc" index change spatially averaged over a grating period, ν is the fringe visibility of the index change, Λ is the grating period, and ϕ(z) describes grating chirp.[4] The LPGs used in this research are uniform gratings with no chirp, so ϕ(z) = 0 and $\overline{\delta n_{core}}$ is a constant in Equation (3.1). Also, for simplicity, the fringe visibility ν = 1.

3.2.3 Phase Matching Curves (PMCs)

The phase matching conditions used for calculating LPG mode coupling come from the following equations:

$$\delta = \frac{1}{2}(\beta_1 - \beta_2 - \frac{2\pi}{\Lambda}) = \pi(n_{eff\,1} - n_{eff\,2})(\frac{1}{\lambda} - \frac{1}{\lambda_D}) \tag{3.2a}$$

where $$\lambda_D = (n_{eff\,1} - n_{eff\,2})\Lambda \tag{3.2b}$$

where δ is the detuning parameter, assumed to be constant along z. When δ = 0, the strongest mode coupling between mode '1' and mode '2' occurs. β_1 and β_2 are the propagation constants of material 1 (fiber core) and 2 (fiber cladding), respectively. β is determined by the optical fiber structure and its dispersion. Even inside a single mode fiber, different wavelengths will propagate at slightly different velocities. n_{eff1} and n_{eff2} are the effective refractive indices of the core and cladding, respectively; and λ is the wavelength.

Equation 3.2 above is used to compute the Phase Matching Curves (PMCs) of the LPG. The PMCs represent the grating period, Λ, as a function of the resonant wavelength, λ_{res}, for which $\delta = 0$. In this particular case, only mode coupling between the other fiber modes and the fundamental mode were investigated. The fiber parameters selected where: the radius of the fiber core a = 3.2 μm, the fiber cladding radius b = 59.2 μm, the surrounding material was air with index $n_{air} = 1$, the core index, n_1, and the cladding index, n_2, were calculated based upon Sellmeier's equation. The calculated results for the PMCs of the single mode fiber (SMF) are displayed in Figure 3-7.

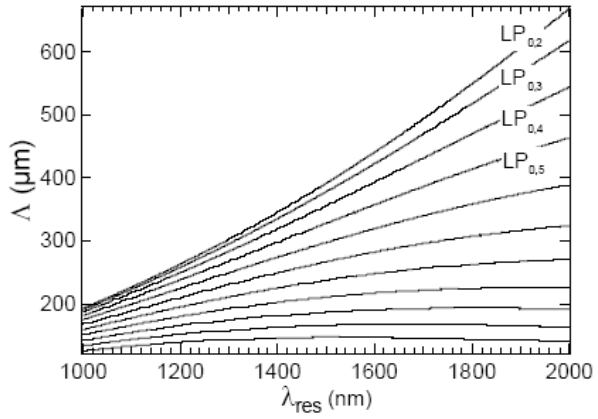

Figure 3-7: LPG phase matching curves. The grating period (Λ) as a function of resonant wavelength (λ_{res}) when $\delta = 0$. Going from the top of the figure to the bottom, the lines are fiber modes $LP_{0,2}$ through $LP_{0,12}$.

From Figure 3-7 several important observations can be made: (1) For a specific grating period, the LPG can couple the energy of the fundamental mode into multiple other modes simultaneously at different resonant wavelengths; (2) For a certain resonant wavelength, a particular grating period can be chosen to allow the LPG to couple the fundamental mode into a certain fiber mode; (3) The higher the coupled fiber mode order, the shorter the grating period required to achieve mode coupling; (4) The slope, $d\Lambda/d\lambda_{res}$

progressively decreases from the lower order modes to the higher order modes.[4] Consequently, $d\lambda_{res}/d\Lambda$ progressively increases from lower order mode to higher order mode. This shows that the change in λ_{res} as a result of the change in Λ gets larger as the order of the coupled fiber mode increases for the same LPG. The change in Λ can result from the change in strain on the grating or the change in ambient temperature. Consequently, the sensitivity of the LPG to strain or temperature increases with increased coupled fiber mode order for the same LPG.

3.2.4 Simulated LPG Transmission Spectra

Dr. Wang also created a model to simulate the LPG transmission spectra. The radius of the fiber core, a, was chosen to be 5 μm, the radius of the fiber cladding, b, was chosen to be 62.5 μm, the surrounding material was air with $n_{air} = 1$, the index of the core, n_1, was 1.455, and the index of the cladding, n_2 was 1.45. The grating length, L, was 10 mm, and the grating period, Λ, was 240 μm. The resonant wavelength, λ_{res} was around 1410 nm and the coupled fiber mode was $LP_{0,12}$.

Figure 3-8 displays the LPG transmission spectrum variations as a function of length L and δn_{core} of the LPG. As L increases, the LPG bandwidth becomes narrower, while the δn_{core} which is needed to maintain the grating strength becomes smaller. For example, δn_{core} must be 0.0014 for a grating of L = 5 mm to cause the maximum attenuation as illustrated in Figure 3-8 a. However, δn_{core} only needs to be 0.0007 for a grating of L = 10 mm as depicted in Figure 3-8 b.

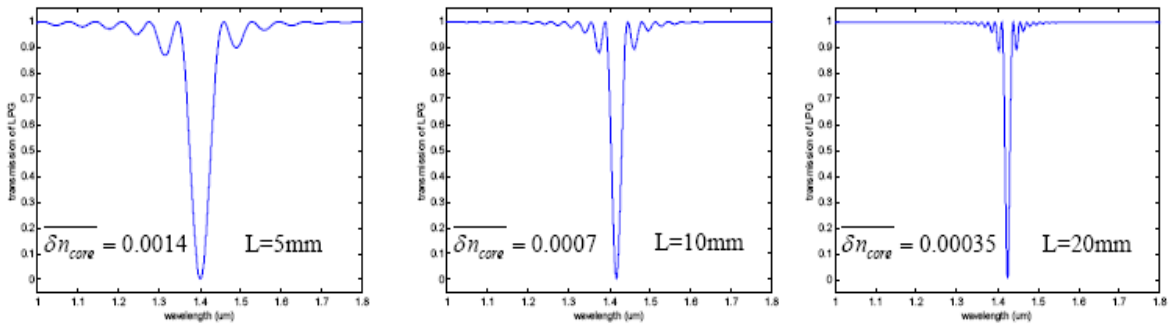

(a) (b) (c)

Figure 3-8: Progression of LPG spectra with grating length, L, and δn_{core}. (a) L = 5 mm and δn_{core} = 0.0014; (b) L = 10 mm and δn_{core} = 0.0007; (c) L = 20 mm and δn_{core} = 0.00035.

3.3 Effects of ISAMs on LPGs

ISAMs deposited on LPGs lead to remarkable shifts in resonant wavelength, even for films less than 1 nm thick. This enables them, in turn, to be used as sensors. Record shifts in resonant wavelength (40 nm) were observed for film thickness of only 25 nm.[3]

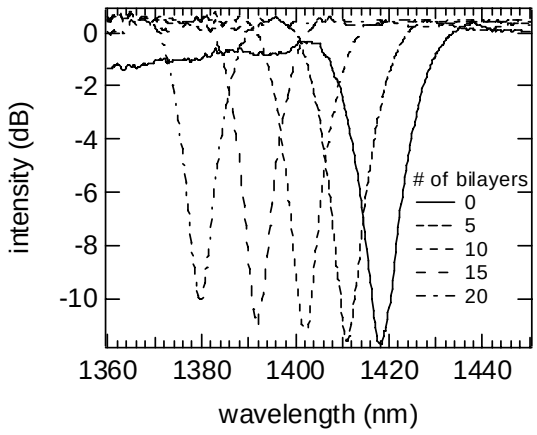

(a)

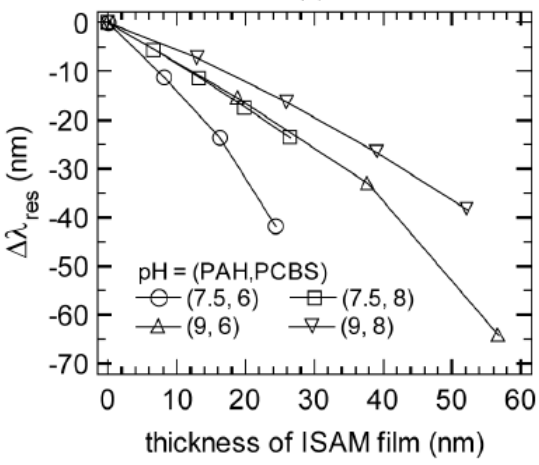

(b)

Figure 3-9: Experimental results of ISAMs coated on LPG. (a) LPG transmission spectra with 0, 5, 10, 15, and 20 bilayers of PAH/PCBS ISAM films with the pH of the PAH set at 9.0 and the pH of the PCBS set at 8.0. (b) $\Delta\lambda_{res}$ of the LPG as a function of the ISAM film thickness with various pH combinations of PAH/PCBS [(7.5/6.0), (7.5/8.0), (9.0/6.0), (9.0/8.0)] which yield the corresponding refractive indices (n) [1.7101, 1.6912, 1.6887, 1.6715], respectively.
* 1 bilayer is approximately 2.6 nm thick when the pH of PAH is 9.0 and pH of PCBS is 8.0.

Figure 3-9 a displays the shift in LPG resonant wavelength as the number of bilayers of ISAM film (and, hence, its thickness) are increased. The ISAM film was made from PAH at pH 9.0 and PCBS at pH 8.0. Figure 3-9 b further depicts this point by indicating the change in resonant wavelength as a function of the film thickness for numerous pH combinations of PAH and PCBS ionic solutions. A record large shift in resonant wavelength of 1.6 nm/nm was observed for the case when the pH of the PAH was 7.5 and the pH of the PCBS was 6.0.[3] The equation for LPG resonance is:

$$\lambda_{res} = (n_{core} - n_{clad})\Lambda \tag{3.3}$$

where λ_{res} is the resonant wavelength, n_{core} is the effective refractive index of the core mode, n_{clad} is the effective refractive index of the cladding mode, and Λ is the grating

period. Since the effective refractive index of the coupled cladding mode is important, it is possible to see resonant wavelength shifts when thin films with a higher index than the cladding are deposited onto the exterior of the cladding. Looking again at Figure 3-9, it is observed that λ_{res} shifts as a result of changes in the thickness of the ISAM film, as well as changes in the film's refractive index. Changes in ISAM deposition conditions result in changes in the films' refractive indices. It has been shown, now, that this creates remarkable shifts in the resonant wavelength when the refractive index of the film is larger than the cladding.[3] This can be explained by looking at the coupling mechanism of ISAM films adsorbed on LPGs.

In general, the evanescent tail of the cladding mode field travels 100-200 nm into the ambient material. All of the ISAM films studied here are thinner than this. Hence, the cladding mode enters the ISAM and the air surrounding it. The effective refractive index, n_{eff}, of a guided mode can be approximated by[3]:

$$n_{eff}{}^2 \approx \iint n^2(r) \cdot \left|E(r)\right|^2 \cdot dA \tag{3.4}$$

where n(r) is the fiber's refractive index profile, $\iint dA$ represents an integration over the cross-sectional area of the fiber, and E(r) is the mode field distribution. Equation (3.4) above explains that a mode's effective index is related to the average refractive index of the area where light is present, weighted by the local intensity profile. In general, a cladding mode tests both the surrounding low index air and the high index ISAM. The average ambient index constructed from air and 10-50 nm-thick ISAM films is the same as that of a bulk medium with an index lower than silica. The average of the ambient index is also dependent upon the refractive index and thickness of the film. Thicker films result in a greater contribution from the ISAM to the average index.

3.3.1 Theoretical Results of ISAMs Coated on LPGs

Dr. Wang performed several more LPG simulations to understand the previous results. First, PMC variations of the grating were simulated to study how the refractive index, n_3, and the thickness, d, of the ISAM films on the LPGs effect them. This was done by separately changing n_3 and d, and then, changing n_3 and d together. For n_3, the values chosen were 1.5, 1.6, 1.7, and 1.8. For d, the values used were 0, 20, 40, 60, 80, and 100 nm, respectively. One higher order cladding mode, $LP_{0,12}$, and one lower order cladding mode, $LP_{0,4}$, were chosen to examine PMC behavior of higher and lower order modes. Dr. Wang performed the simulations using Matlab.

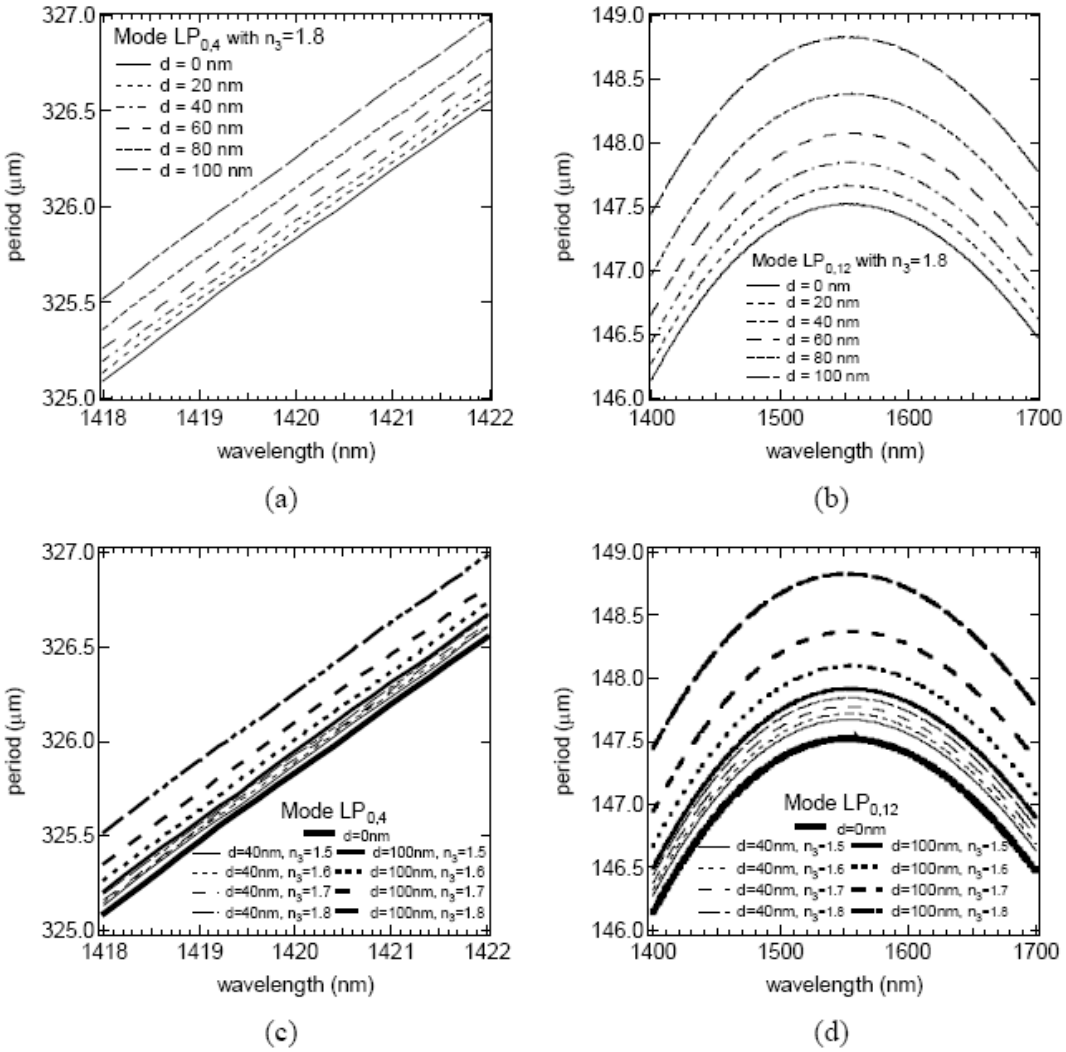

Figure 3-10: Phase Matching Curves (PMC) shift as a function of film thickness, d, and film refractive index, n_3. (a) PMC of $LP_{0,4}$ mode shifts with d (d = 0, 20, 40, 60, 80, 100 nm) at n_3 = 1.8; (b) PMC of $LP_{0,12}$ mode shifts with d (d = 0, 20,40, 60, 80, 100 nm) at n_3 = 1.8; (c) PMC of $LP_{0,4}$ mode shifts with n_3 (n_3 = 1.5, 1.6, 1.7, 1.8) at d = 40 nm and d = 100 nm, (d) PMC of $LP_{0,12}$ mode shifts with n_3 (n_3 = 1.5, 1.6, 1.7, 1.8) at d = 40 nm and d = 100 nm.

Figure 3-10 illustrates the PMC shifts as functions of n_3 and d of the ISAM film. The $LP_{0,12}$ mode has a wider wavelength range than the $LP_{0,4}$ mode to clearly display the variations. The wide wavelength range around 1550 nm was purposely chosen to show

the turnaround point in the PMC. The turnaround point will be discussed in much more detail later. In Figure 3-10 a the PMC of the $LP_{0,4}$ mode shifts with d at $n_3 = 1.8$. Figure 3-10 b also shows that the PMC of the $LP_{0,12}$ mode shifts with d at $n_3 = 1.8$. It is also observed that when n_3 is fixed, the PMCs of $LP_{0,4}$ and $LP_{0,12}$ move upwards as d increases. The magnitude of the PMC shift is not uniform even though there is a uniform 20 nm increment increase in d. The PMC curve shift increases as d is increased from 0 to 100 nm. This implies that sensitivity to d increases with increased d. The PMC of the $LP_{0,12}$ mode shifts much more quickly than the $LP_{0,4}$ mode. This implies that the sensitivity of $LP_{0,12}$ to d is much greater than $LP_{0,4}$.

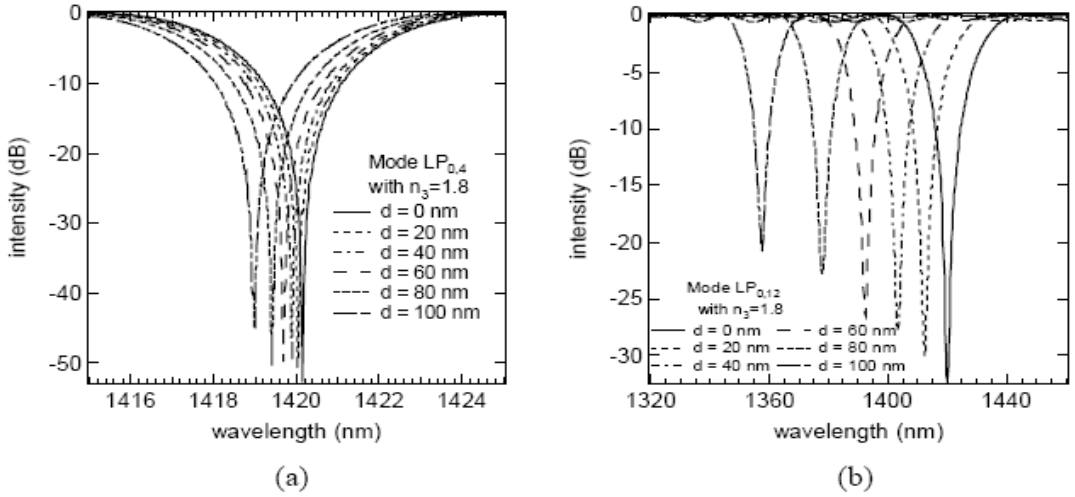

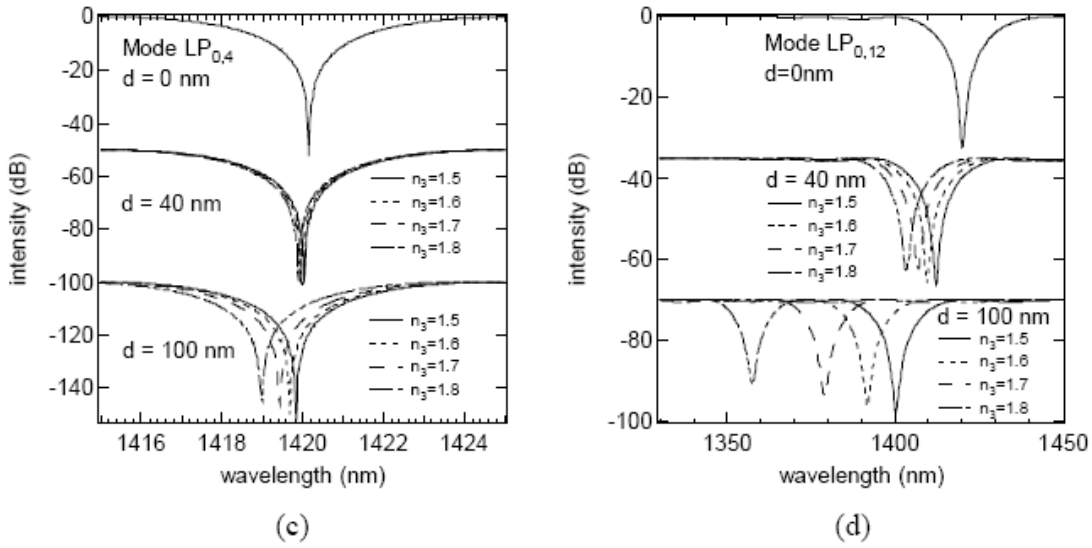

Figure 3-11: Transmission spectra of LPG shifts as a function of film thickness, d, and film refractive index, n_3. (a) Spectra of $LP_{0,4}$ mode shifts with d (d = 0, 20, 40, 60, 80, 100 nm) at n_3 = 1.8; (b) spectra of $LP_{0,12}$ mode shifts with d (d = 0, 20, 40, 60, 80, 100 nm) at n_3 = 1.8; (c) spectra of $LP_{0,4}$ mode shifts with n_3 (n_3 = 1.5, 1.6, 1.7, 1.8) at d = 40 nm and d = 100 nm; (d) spectra of $LP_{0,12}$ mode shifts with n_3 (n_3 = 1.5, 1.6, 1.7, 1.8) at d = 40 nm and d = 100 nm.

Figure 3-11 shows how the LPG transmission spectra shift as functions of n_3 and d of the ISAM film, respectively. For comparison sake, the conditions for selecting periods for $LP_{0,4}$ and $LP_{0,12}$ was to have their resonant wavelengths equal to 1420 nm. To fulfill the criteria, the period for $LP_{0,4}$ needed to be 324.82 μm and the period for $LP_{0,12}$ needed to be 146.28 μm. Figure 3-11 a – d depict the changes in the LPG transmission spectra corresponding to the same circumstances of Figure 3-10 a – d. For comparison sake with the experimental LPG spectra, Figure 3-11 uses different wavelength ranges than those of Figure 3-10. In addition, the $LP_{0,12}$ spectra use a smaller wavelength range to clearly display the variations.

Figure 3-11 yields a great deal of important information and insight that guided

some of the work in this present thesis. (1) When n_3 is kept fixed and d increases, the spectra for both $LP_{0,4}$ and $LP_{0,12}$ shift towards shorter wavelengths. The spectral shift increases as d is increased for 0 to 100 nm. This fact implies that the sensitivity to d increases with increased d; (2) When d is kept fixed and n_3 increases, the $LP_{0,4}$ and $LP_{0,12}$ resonances shift to shorter wavelengths, and the rate of change increases with the magnitude of n_3. This implies that the sensitivity to n_3 increases as n_3 is increased; (3) When d is kept fixed and n_3 increases, the spectra shift to the left. The magnitude of the shift for each 0.1 increment of n_3 is larger at larger d. This implies that the sensitivity to n_3 increases as d increases; (4) When either n_3 or d is kept fixed, the $LP_{0,12}$ spectrum shifts a good deal more than the $LP_{0,4}$ spectrum. This implies that the sensitivity of $LP_{0,12}$ to n_3 and d is much greater than $LP_{0,4}$. This last observation results from two features. First, higher order modes interrogate material that is further from the fiber's core. Consequently, changes in refractive indices and film thicknesses far from the core have a greater effect. Second, the PMC of the higher order mode operates closer to the turnaround point because it has a smaller gradient. This means that tiny adjustments for any parameter cause large shifts in the resonant wavelength. What is remarkable here is that even though these thin films are only at the nanometer level, the LPG's resonant wavelength has the ability to shift more than 60 nm for $LP_{0,12}$ with film thickness of 100 nm. This is illustrated clearly in Figure 3-11 b. Also, by examining Figure 3-10, it is observed that the PMCs display the same behaviors as the corresponding grating's spectra.

3.3.2 Experimental and Theoretical Results Compared

Dr. Wang performed his simulations based upon the experimental data of n_3 and d that he obtained through ellipsometry and theoretical analysis. Figure 3-12 below depicts the comparison between the simulated and experimental LPG transmission spectra with no ISAM coating.

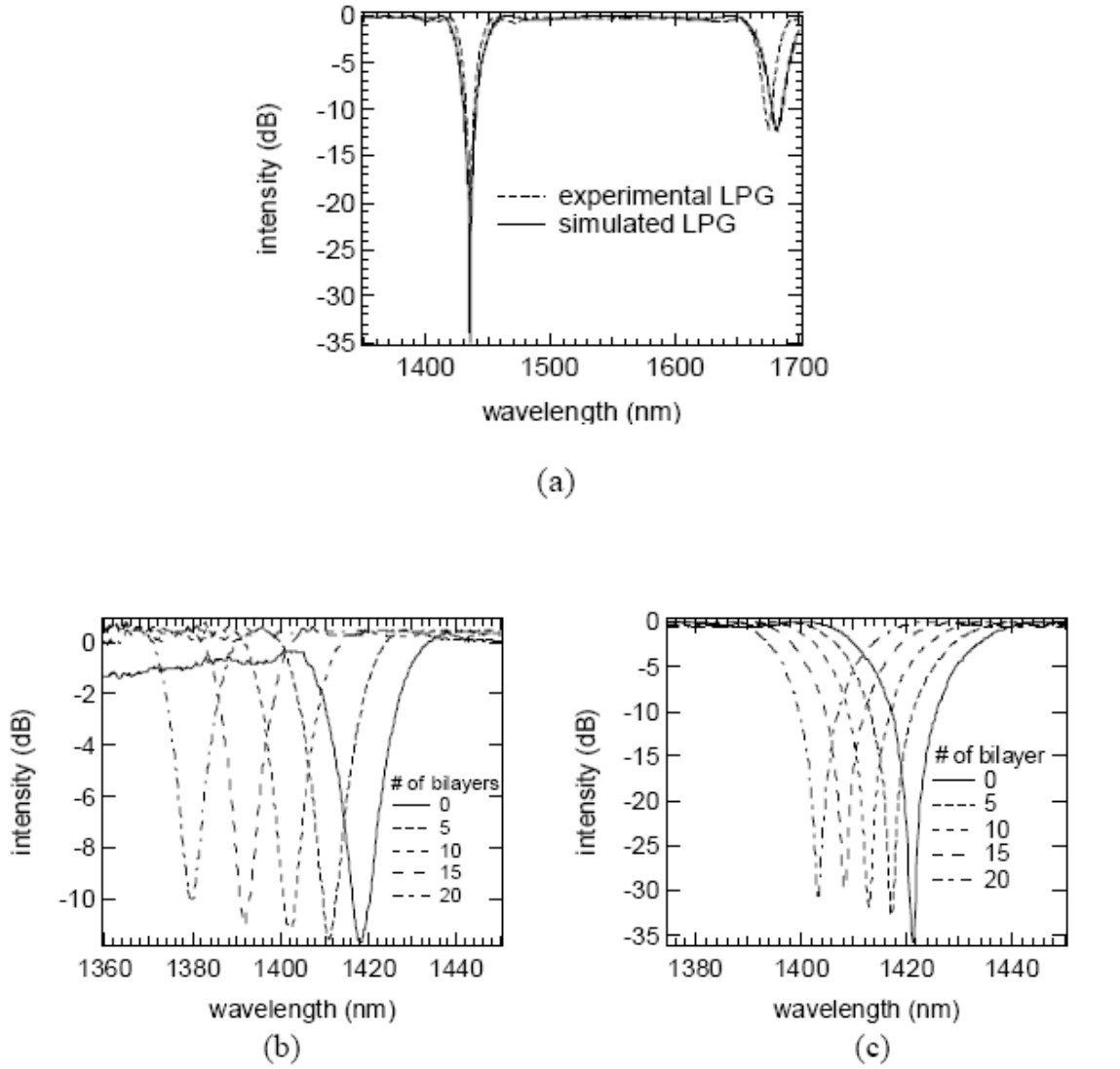

Figure 3-12: Comparison between experimental and simulated LPG transmission spectra. (a) Spectra of LPG without ISAM films; (b) experimental LPG transmission spectra with 0, 5, 10, 15, and 20 bilayers of PAH/PCBS with pH of PAH set at 9.0 and pH of PCBS set at 8.0; (c) simulated LPG spectra with same conditions.
* 1 bilayer is approximately 2.6 nm thick with pH of PAH at 9.0 and pH of PCBS at 8.0.

These results coincide remarkably. The experimental LPG is an $LP_{0,12}$ mode. Figure 3-12 b illustrates the experimental LPG transmission spectra with different bilayers/thicknesses of PAH/PCBS where the pH of the PAH was 9.0 and the pH of the PCBS was 8.0. Here, one bilayer is around 2.6 nm thick. The simulated LPG transmission spectra shown in Figure 3-12 c has different bilayers of PAH/PCBS also for pH of PAH at 9.0 and pH of PCBS at 8.0. The simulated results are close in appearance to the experimental results except that there is a larger shift in resonant wavelength for the experimental results.

3.4 Turnaround Point (TAP) LPGs

Upon examination of Figure 3-7 it is observed that the PMCs of several of the higher order modes, such as $LP_{0,9} - LP_{0,12}$, do not monotonically increase as the resonant wavelength increases. In other words, the grating period, Λ, does not monotonically increase for increased resonant wavelengths for which $\delta = 0$. To see this more easily, Figure 3-7 was magnified as shown in Figure 3-13. Here it is observed that initially Λ increases with increased λ_{res} (slope = $d\Lambda/d\lambda_{res} > 0$), but the slope slowly decreases. Then, at a particular λ_{res}, the slope is zero. After the zero point, Λ decreases as λ_{res} increases ($d\Lambda/d\lambda_{res} < 0$) and the slope decreases. The spot in the PMC where the slope is zero is known as the Turnaround Point (TAP) of the grating. It is denoted by the solid black dots are in Figure 3-13. An LPG with a period written near the TAP is called a TAP LPG.

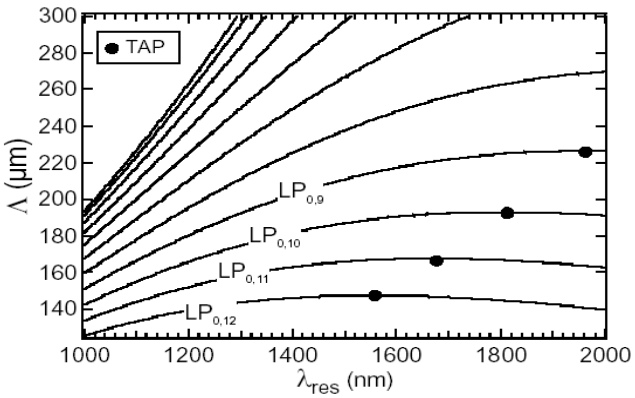

Figure 3-13: Magnified view of Figure 3-7. LPG phase matching curves. The grating period (Λ) as a function of resonant wavelength (λ_{res}) when $\delta = 0$. Going from the top of the figure to the bottom, the lines are fiber modes $LP_{0,2}$ through $LP_{0,12}$.

Thus in special cases, the cladding modes may have a TAP of the grating where the slope switches from positive to negative. As the order of the cladding mode increases, the TAP of that cladding mode shifts to shorter wavelengths. Gratings operating around the TAP are much more sensitive to changes in the surrounding environment, such as the thickness and refractive index of a film on the cladding. TAP LPGs are, therefore, much more useful as biosensors than LPGs operating away from the TAP. Also, at the TAP, the sensitivity is manifested as a change in strength of the broadband attenuation, rather than a shift in wavelength of the narrowband attenuation, which will be illustrated later.

3.4.1 TAP LPG Optical Characteristics

Dr. Wang simulated the PMC and evolution of the transmission spectra of TAP LPGs using computer modeling. The fiber parameters used are the same as described previously, fiber core radius a = 3.2 μm, fiber cladding radius b = 59.2 μm, surrounding

material is air with n_{air} = 1, core and cladding indices, n_1 and n_2 were again calculated using Sellmeier's equation. The high-order mode $LP_{0,12}$ was used to show the properties of the TAP LPG. The TAP was at Λ = 147.3 μm with λ_{res} ~ 1550 nm. The length of the LPG was chosen to be 50 mm and $\overline{\delta n_{core}}$ = 0.000148.

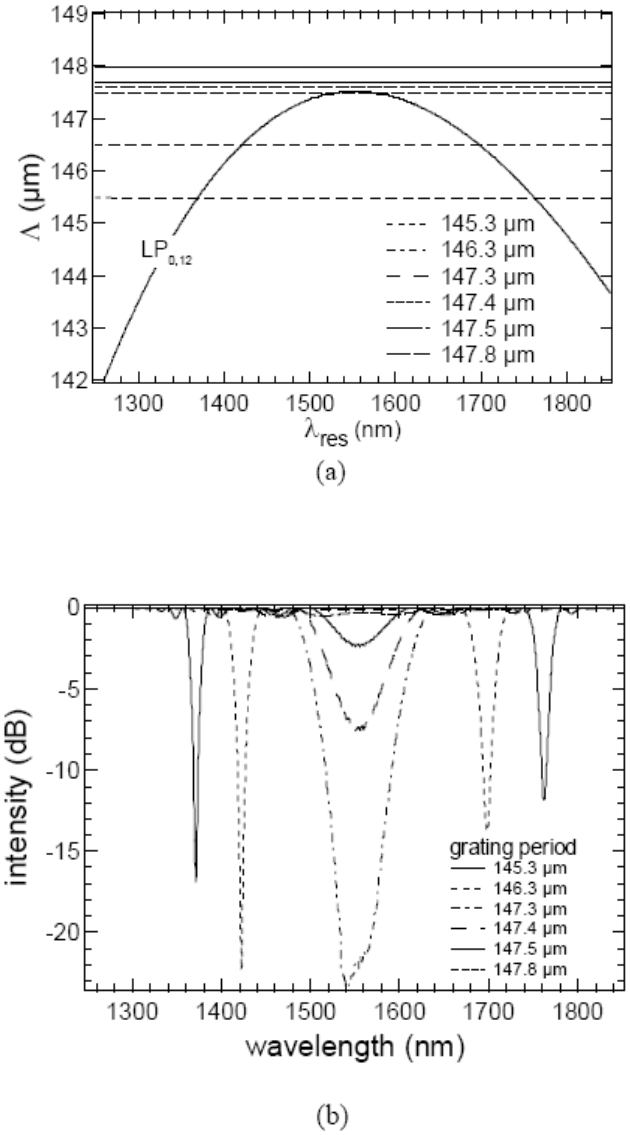

Figure 3-14: TAP LPG optical properties. (a) The solid curve symbolizes the PMC of the $LP_{0,12}$ mode. The dashed horizontal lines symbolize the various grating periods, which are (from bottom to top) 145.3, 146.3, 147.3, 147.4, 147.5, and 147.8 μm, respectively; (b) the corresponding LPG transmission spectra at the same grating periods.

In Figure 3-14 a the solid black curve is the PMC of the $LP_{0,12}$ mode. The horizontal lines are the different grating periods. Figure 3-14 b shows the corresponding LPG transmission spectra at the different grating periods. In Figure 3-14 a, the grating period of either 145.3 μm or 146.3 μm intersect the PMC at two separate resonant wavelengths. Consequently, the grating spectrum resulting from that grating period has two attenuation peaks at those two resonant wavelengths, as can be seen in Figure 3-14 b. Each peak has the narrowband characteristic of conventional LPGs. When the period gets close to 147.3 μm at the TAP, the two attenuation peaks move closer together. When the period equals 147.3 μm at the TAP, the two narrowband attenuation peaks merge into one, single, broadband, strong attenuation peak. When the period moves away from the TAP, the grating period does not intersect the PMC at any wavelengths, and the single, broadband attenuation peak becomes smaller. The grating strength, or amplitude of the peak, decreases in proportion to the separation between the grating period and the PMC. Eventually, the period shifts far enough so that no resonance occurs, which can be seen for the grating period at 147.8 μm. In the vicinity of the TAP, small changes in the thickness or refractive index of the film on the fiber cladding result in very large changes in the transmitted light intensity at the resonant wavelength. This is very evident in Figure 3-14. While Figure 3-14 shows the case of a changing grating period, in the experiments to follow, the grating period is fixed and the PMC shifts upward, which has exactly the same effect.

3.4.2 Theoretical Results of ISAM Coated TAP LPGs

TAP LPGs have very high sensitivity. Thus, it makes sense that ISAM coated

TAP LPGs make excellent ultra-sensitive optical sensors. Dr. Wang studied the TAP LPG index sensitivity by simulating the ISAM coated TAP LPG variations in transmission spectra due to changing the film parameters n_3 (film refractive index) and d (film thickness). Dr. Wang showed that LPG index sensitivity would significantly increase by implementing TAP LPGs instead of using conventional LPGs.

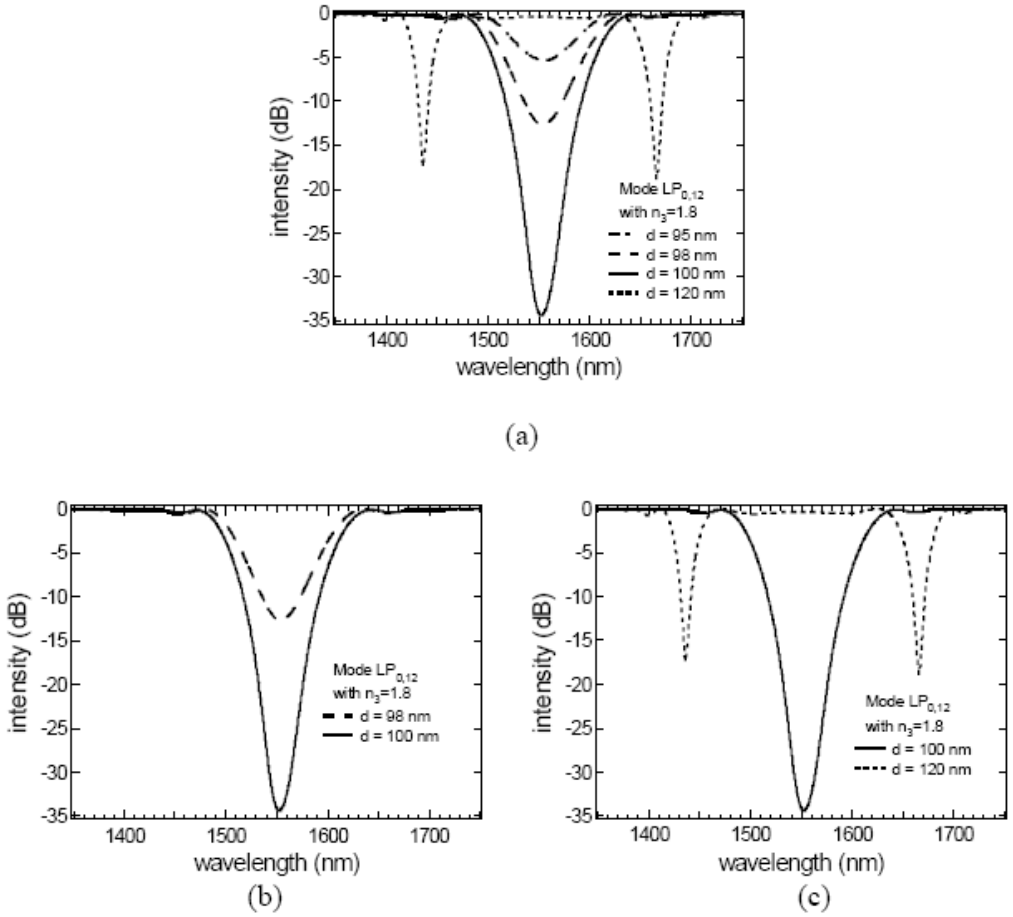

Figure 3-15: Simulated film-coated TAP LPG transmission spectra for $LP_{0,12}$ mode at n_3 = 1.8. (a) d = 95, 98, 100 and 120 nm; (b) optical intensity-based sensor at d = 98, and 100 nm; (c) dual peak-based sensor at d = 100 and 120 nm.

For these simulations, all the parameters are the same as the previous ones, except this time the grating period is 148.61 μm, which means the TAP is at d = 100 nm. Figure 3-

15 depicts the transmission spectrum of the $LP_{0,12}$ mode of the ISAM coated TAP LPG with $n_3 = 1.8$. It should be noted that when the grating is operating closer to the TAP its sensitivity is much greater. Figure 3-15 b illustrates a single peak optical intensity based sensor, while Figure 3-15 c shows a dual peak sensor. Either of these sensors can significantly improve LPG sensitivity. This is very valuable for LPG sensor applications in addition to biosensors.

3.4.3 Procedure of Etching LPGs

A schematic of the setup for all the experiments performed in this thesis is illustrated in Figure 3-16. An Ando AQ6317 Optical Spectrum Analyzer (OSA) was used along with a LS-1 Tungsten Halogen White-Light Source from Ocean Optics, Inc. The white light source was optimized for the VIS-NIR (360-2500 nm). FC buffered fiber adapters from Fiber Instrument Sales, Inc were also used, as well as a Fujikura CT-07 fiber optic cleaver.

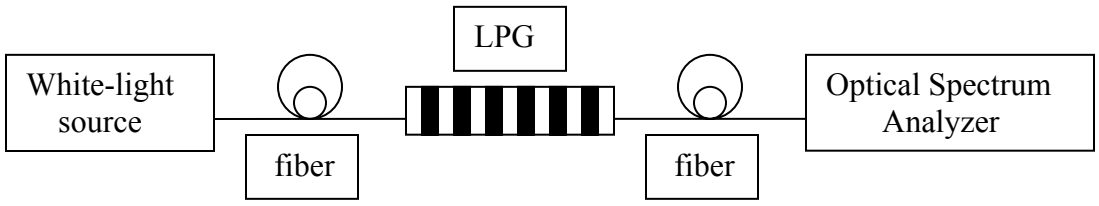

Figure 3-16: Schematic of experimental setup for LPGs.

One way to tune an LPG to the TAP is by etching it with hydrofluoric acid (HF).

In the experiments to follow, I used a solution of 90% deionized water and 10% HF for this process. Etching is the process of dipping the fiber grating into the HF acid solution to gradually reduce the thickness of the cladding. This alters the cladding mode properties in the fiber, which causes the resonant wavelength to shift, as can be seen in Figure 3-17. The two attenuation peaks begin far apart from each other and move closer together with successive amounts of etching. The two peaks eventually combine into one peak at the TAP.

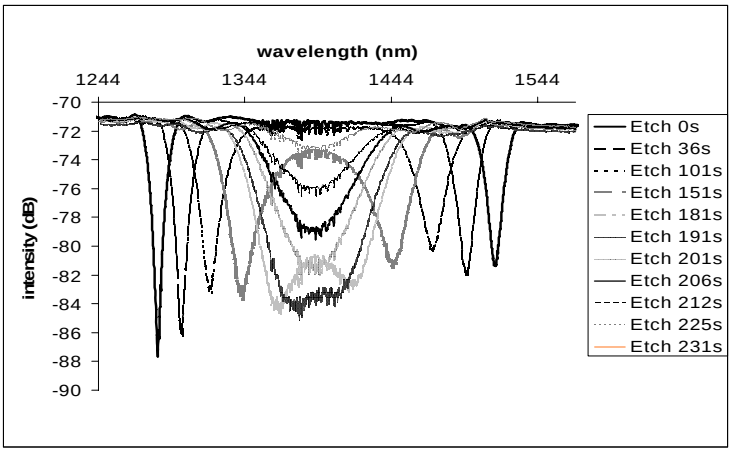

Figure 3-17: HF etching LPG to the Turn-Around-Point (TAP) of the LPG in PBS (Phosphate Buffered Saline) solution.

In the above experiment, the operating point of the LPG was set at the TAP when immersed in phosphate buffered saline solution (PBS). There are two benefits to this optical intensity based TAP LPG sensor: (1) it is possible to make biosensor systems with inexpensive photo detectors rather than expensive optical spectrum analyzers by monitoring the transmitted intensity at the wavelength of the TAP; (2) the sensitivity of the LPG is significantly increased when the operating range is set at the TAP of the LPG. This also illustrates the versatility of the sensor since experiments can be performed in solution as well as in air.

3.4.4 ISAM Removal

It can be very useful and beneficial be able to reuse the same LPG for many experiments without altering any of its properties. To illustrate this removable aspect of the ISAM films, an LPG spectrum with no ISAM film coating is compared to an LPG spectrum where the ISAM coating has been removed using a sulfuric/nitric acid solution.

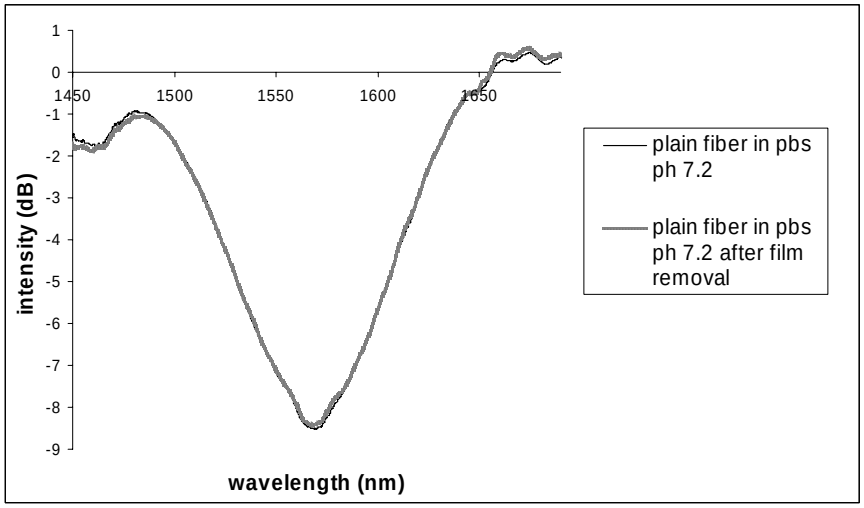

Figure 3-18: Comparison of LPG transmission spectra without ISAM film coating and LPG transmission spectra after removal of ISAM films.

PAH and PCBS were used as the ISAM films. The pH of PAH was 7.0 and the pH of the PCBS was 7.0. The acid solution was 95% sulfuric acid and 5% nitric acid. In the ISAM removal procedure, the acid mixture is placed in a glass beaker and heated to around 80 ^{0}C. Then, the ISAM coated LPG part of the fiber is immersed into the solution for 25 minutes. Figure 3-18 displays two LPG spectra, one taken before films were deposited, and one taken after films were removed. This experiment shows that the ISAM films are able to be removed with negligible variation in the spectra by immersion in the acid mixture. In this thesis, the same LPG is reused dozens of times. This removable feature

of the ISAM films on the LPGs assures the comparability and repeatability of experimental results. Furthermore, it improves the cost-efficiency, flexibility, and time-efficiency of experiments.

---

[1] G. Decher, "Fuzzy Nanoassemblies: Toward Layered Polymeric Multicomposites," *Science*, **277**, 1232-1237, (1997).

[2] J.R. Helfin, C. Figura, D. Marciu, Y. Liu, R. Claus, "Thickness dependence of second-harmonic generation in thin films fabricated from ionically self-assembled monolayers," Appl. Phys. Lett., **74**, 495-497, (1999).

[3] Z. Wang, J.R. Heflin, R. H. Stolen, S. Ramachandran, "Highly sensitive optical response of optical fiber long period gratings to nanometer-thick ionic self-assembled multilayers," Appl. Phys. Lett., **86**, 223104 (2005).

[4] Zhiyong Wang, Ph D Dissertation, (Virginia Tech, 2005).

[5] O.M. Tanchak, C.J. Barrett, "Swelling Dynamics of Multilayer films of Weak Polyelectrolytes," *Chem. Mater*. **16**, 2734-2739, (2004).

[6] E.S. Forzani, M.A. Perez, M.L. Teijelo, E.J. Calvo, "Redox Driven Swelling of Layer-by-layer Enzyme-Polyelectrolyte Multilayers," Langmuir, **18**, 9867-9873, (2002).

[7] Gero Decher, et al., *Multilayer Thin Films*, (Wiley press, ISBN: 3527600574, 2002).

[8] Charles Brands, Ph.D Dissertation, (Virginia Tech, 2003).

[9] Lowack, K., Helm, C.A., "Polyelectrolyte Monolayers at the Mica/Air Interface: Mechanically Induced Rearrangements and Monolayer Annealing," *Macromolecules* **28**, 2912-2921, (1995).

[10] P. Lavalle, C. Gergely, F.J.G. Cuisinier, G. Decher, P. Schaaf, J.C. Voegel, C. Picart, "Comparison of the Structure of Polyelectrolyte Multilayer Films Exhibition a Linear and an Exponential Growth Regime: An in Situ Atomic Force Microscopy Study," Macromolecules **35**, 4458-4465, (2002).

[11] M. Muller, T. Rieser, P.L. Dubin, K. Lunkwitz, "Selective Interaction Between Proteins and the Outermost Surface of Polyelectrolyte Multilayers – Influence of the Polyanion Type, pH and Salt," *Macromol. Rapid, Commun*. **22**, 390-395, (2001).

[12] E.J. Calvo, R. Etchenique, L. Pietrasanta, A. Wolosiuk, C. Danilowicz, "Layer-by-Layer Self-Assembly of Glucose-Oxidase and Os(bpy)(2)Cipych2Nh- Poly(Allylamine) Bioelectrode," *Anal. Chem*. **73**, 1161-1168 (2001).

[13] N.G. Hoogeveen, M.A.C. Stuart, G. Fleer, M.R. Bohmer, "Formation and Stability of Multilayers of Polyelectrolytes," *Langmuir* **12**, 3675-3681, (1996).

[14] C. Picart, P. Lavalle, P. Hubert, F.J.G. Cuisinier, G. Decher, P. Schaaf, J.C. Voegel, "Buildup Mechanism for Poly(L-lysine)/Hyaluronic Acid Films onto a Solid Surface," *Langmuir* **17**, 7414-7424, (2001).

[15] R. Advincula, E. Aust, W. Meyer, W. Knoll, "In-situ Investigations of Polymer Self-Assembly Solution Adsorption by Surface Plasmon Spectroscopy," Langmuir 12, 3536-3540, (1996).

[16] P.A. Ngankam, P. Lavalle, J.C. Voegel, L. Szyk, G. Decher, P. Schaaf, F.J.G. Cuisinier, "Influence of Polyelectrolyte Multilayer Films on Calcium-Phosphate Nucleation," *J. Am. Chem. Soc*. **122**, 8998-9004, (2000).

[17] J.J. Harris, M.L. Bruening, "Electrochemical and in-Situ Ellipsometric Investigation of

the Permeability and Stability of Layered Polyelectrolyte Films," *Langmuir* **16**, 2006-2013, (2000).
[18] L.N.J. Rodriguez, S.M. Depaul, C.J. Barrett, L. Reven, H.W. Spiess, "Fast Magic-Angle-Spinning and Double-Quantum H-1 Solid-State NMR-Spectroscopy of Polyeletrolyte Multilayers," *Adv. Mater*. **12**, 1934, (2000).
[19] W. Kern, D.A. Poutinen, *RCA Rev.* **31**, 187, (1970).
[20] Z. Wang, J.R. Heflin, R.H. Stolen, S. Ramachandran, "Analysis of optical response of long period fiber gratings to nm-thick thin-film coatings," *Opt. Exp*. **13**, 8, 2808, (2005).
[21] Turan Erdogan, "Fiber Grating Spectra," *Journal of Lightwave Technology* **15**, 1277-1294, (1997).

Chapter 4. Studies of the Sensitivity of ISAM LPGs

4.1 Materials

In this research, the effects of different materials for incorporation into ISAM films on LPGs were carefully studied. Many different sensitivity tests were performed, and the results of these experiments will be analyzed and discussed in this chapter. The materials used include Poly(allylamine hydrochloride) (PAH) purchased from Sigma Aldrich, Poly[1-[4-(3-carboxy-4-hydroxyphenylazo) benzenesulfonamido]-1, 2-ethanediyl, sodium salt (PCBS) purchased from Sigma Aldrich, Polyacrylic acid (PAA) – sodium salt purchased from Aldrich, silica nanoparticles from Nissan Chemical Industries, and Sodium Poly[2-(3-thienyl)ethyloxy-4-butylsulfonate] (PTEBS).

4.1.1 Poly(allylamine hydrochloride) (PAH)

The molecular structure for the polycation PAH is shown in Figure 4-1.

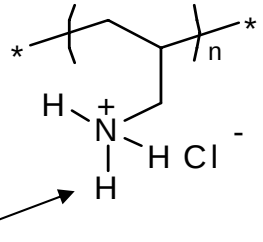

Positively charged

Figure 4-1: Molecular structure of PAH.

PAH is a low refractive index material that is transparent in appearance. PAH does not contain any delocalized π electrons and has a refractive index in the vicinity of 1.5. In

the experiments to follow, PAH was dissolved in deionized water to a concentration of 10 mM.

4.1.2 Poly[1-[4-(3-carboxy-4-hydroxyphenylazo) benzenesulfonamido]-1, 2-ethanediyl, sodium salt (PCBS)

The molecular structure for the polyanion, PCBS, can be seen in Figure 4-2.

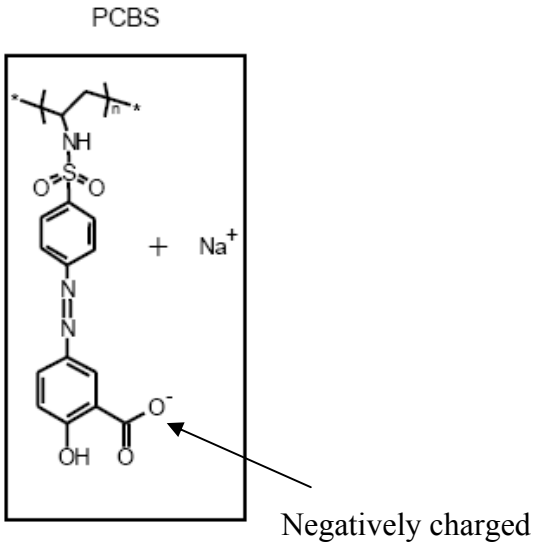

Figure 4-2: Molecular structure of PCBS.

PCBS is a high refractive index material that is brown in appearance. PCBS has a highly conjugated side chain and has a refractive index in the vicinity of 1.8. In the following experiments, PCBS was dissolved in deionized water to a concentration of 10 mM.

4.1.3 Polyacrylic acid (PAA), Sodium Salt

The molecular structure for the polyanion, PAA, is shown in Figure 4-3. PAA has no conjugated electrons and has a refractive index around 1.5. PAA is transparent in appearance. In the experiments to follow, the PAA was also dissolved in deionized water to the concentration of 10 mM.

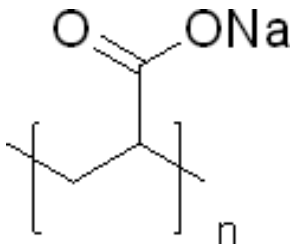

Figure 4-3: Molecular structure of PAA.

4.1.4 Silica Nanoparticles

The silica nanoparticles used in this research are called Nissan SNOWTEX-C. They have a milky white appearance. The particles are colloidal silica and have numerous applications for fibers, paper, catalysts, and steel. They have also been used by the semiconductor industry to aid in the polishing of silicon wafers. SNOWTEX-C is a colloidal silica mixture created by dispersing amorphous spherical, silica particles with negative charges into water.[1] At the surface of the particles are OH ions with an electric double layer created by alkali ions. The repulsion amongst the same negatively charged particles allows for stabilization. When the charge balance is disturbed, the colloidal silica will aggregate, leading to gelation or high viscosity of the solution.[1] Figure 4-4 is a

Scanning Electron Microscope (SEM) of these 40 nm diameter silica nanoparticles as an antireflection coating.[2]

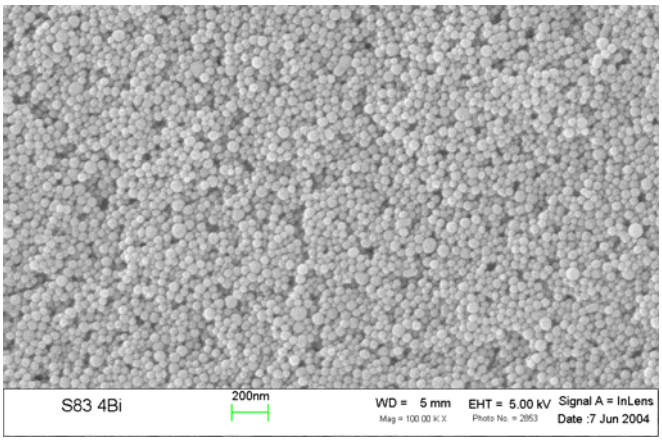

Figure 4-4: Scanning Electron Microscope (SEM) image of 40 nm diameter silica nanoparticles.

The negatively-charged silica nanoparticles are used with the PAH polycation to make ISAM films. The PAH creates a thin shell, approximately 1 nm thick, around each nanoparticle to switch the exterior charge from negative to positive. This then enables the deposition of the next layer of silica nanoparticles. Spheres are unable to fill space (i.e. about 40% of the volume is comprised of air void space). This is important for anti-reflection coatings due to the fact that it decreases the refractive index of the film to 1.30, which is close to the ideal refractive index value of 1.22 for an anti-reflection coating on a glass substrate.[2] There are two main benefits to utilizing nanoparticle ISAM films on LPGs. (1) The affinity ligands have the ability to bind to the surface of every nanoparticle in the porous film. This is in contrast to solely polyelectrolyte films where the affinity ligand only binds to the surface of the film. The increased surface area of nanoparticle ISAM films enables the target molecules to bind to a greater volume of the

film, which, in turn, increases sensitivity. (2) The 40 nm diameter particles create bilayers that are ~25 nm thick (less than 40 nm because a portion of the spheres rests in the previous layer). This enables the ISAM films to build up more quickly, which yields greater sensitivity.

4.1.5 Sodium Poly[2-(3-thienyl)ethyloxy-4-butylsulfonate] (PTEBS)

The molecular structure of the polyanion PTEBS is shown in Figure 4-5. PTEBS is a water soluble thiophene polymer. It is a brown powder that has an orange color in basic solutions and a dark green color in acidic solutions. It is a semiconducting polymer with a conjugated backbone.

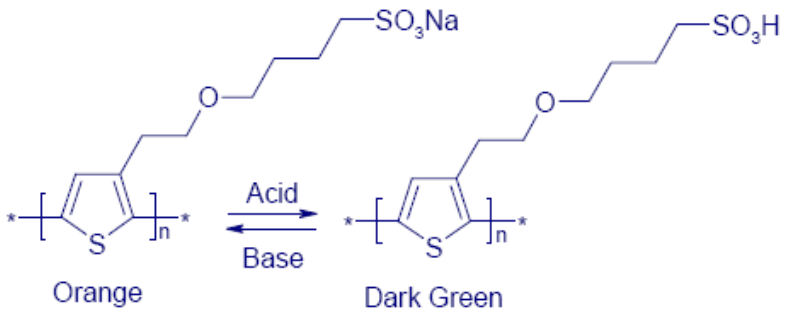

Figure 4-5: Molecular structure of PTEBS.[3]

4.2 Experimental Results of ISAM Sensitivity Studies on TAP LPGs

4.2.1 PAH/PCBS

Figure 4-6 a and b are a comparision of an ISAM sensitivity experiment in air and in phosphate buffered saline solution (PBS) using PAH and PCBS. The pH of the PAH was adjusted to 7.0 using HCl and NaOH. The pH of the PCBS was also adjusted to 7.0. Figure 4-6 a is an experiment using an LPG that was etched to be at the TAP in air. Four bilayers of PAH/PCBS were deposited onto the fiber grating using the ISAM technique. Figure 4-6 b is a similar experiment, but a different LPG is used here. This LPG was etched to be at the TAP when immersed in PBS. The resulting transmission spectra can be seen below.

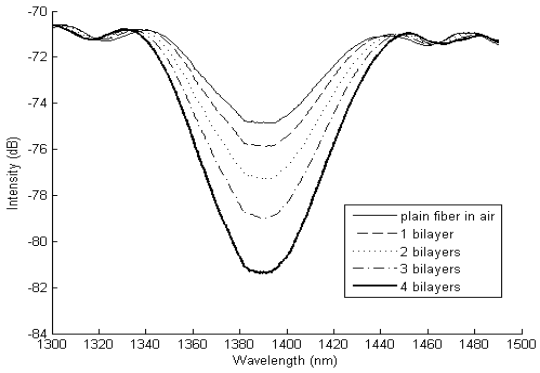

(a)

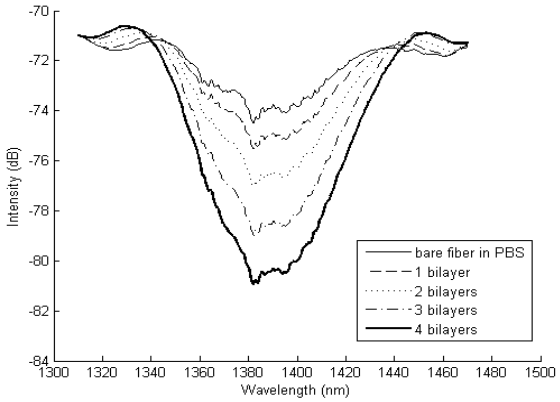

(b)

Figure 4-6: (a) LPG response to addition of bilayers of PAH/PCBS in air. (b) LPG response to addition of bilayers of PAH/PCBS in PBS.

In both cases, as the number of bilayers was increased, the sensitivity of the LPG (as measured by the additional attenuation produced by an additional bilayer) increased as well. This is because as the ISAM film thickness increases the LPG begins to operate closer to the TAP, which is the highest point of sensitivity in the fiber. It is very important to note here that the results are nearly identical for the two experiments. Each bilayer yields almost the same downward shifts in the attenuation peak for both experiments. This is great news because it shows that the results are not compromised by performing an experiment in solution, and many of the real-world applications of biosensors will be in solution. Furthermore, it shows that the sensitivity level is essentially independent of the substance in which the readings are being taken. As a result, this is an extremely versatile sensor platform. In Figure 4-6 b there is some repeatable "noise", which may be due to the HF etching process of the fiber, but further testing will have to be done to verify this. However, this "noise"

does not significantly effect the results or the capability to detect tiny spectral shifts from adsorbed analytes.

4.2.2 PAH/PAA

Figure 4-7 is a comparison of the LPG sensitivity to ISAM films measured in air using PAH/PCBS and PAH/PAA. In the latter case, PAH is the polycation and PAA is the polyanion. Both were adjusted to pH 7.0 using NaOH and HCl. PAH and PAA have low refractive indices and the resultant film has a refractive index of about 1.5. As a result, there are very tiny decreases in the transmitted light intensity at the resonant wavelength, as seen in Figure 4-7 a. In contrast, for a high refractive index material, such as PCBS, in correspondence with a low refractive index material, such a PAH, there are much larger shifts in the transmitted light intensity, as shown in Figure 4-7 b. This confirms that the sensitivity of the LPG increases when high refractive index materials are used. As can be seen by comparing Figure 4-7 a and b, the decreases in the transmission spectra are 4-5 times smaller for the PAH/PAA trial than for the PAH/PCBS trial. This is due to the lower refractive index of PAA. Thus, one way to obtain a more sensitive sensor would be to build a platform using polyelectrolytes that have high refractive indices.

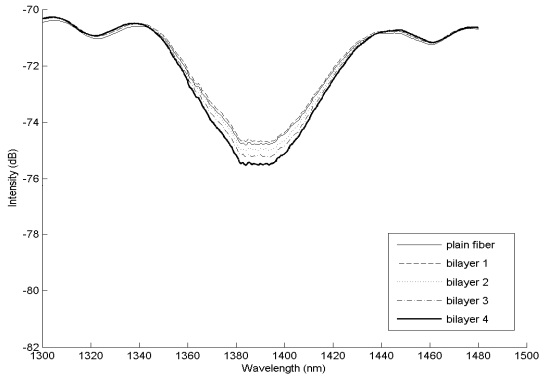

(a)

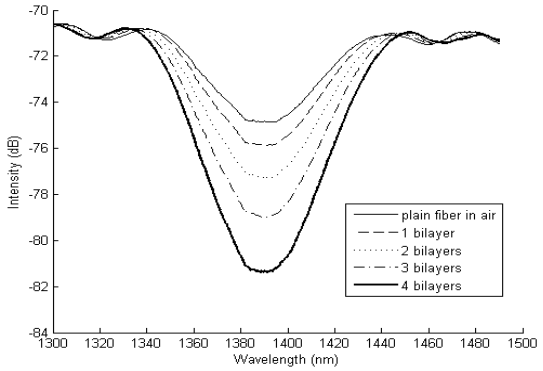

(b)

Figure 4-7: (a) LPG response to the deposition of bilayers of two low refractive index materials (PAH and PAA); (b) LPG response to addition of bilayers of PAH/PCBS. Both sets of spectra are measured in air.

It is also important to note that the simulations discussed in the previous chapter indicate that depositing a high refractive index film on the fiber increases the sensitivity to additional adsorbed materials even if those materials do not have a high refractive index themselves. Hence, experiments are not restricted to high refractive index analytes. This is because the high refractive index film forces the mode profile of the cladding mode outwards toward the surface, consequently, increasing the sensitivity to any surface material.

4.2.3 PAH/PTEBS

In this experiment, the polycation was PAH and the polyanion was PTEBS. The pH of the PAH was adjusted to 4.0 and the pH of the PTEBS was adjusted to 3.5 using NaOH and HCl. Again, this experiment was performed in air and compared to the PAH/PCBS experiment in air.

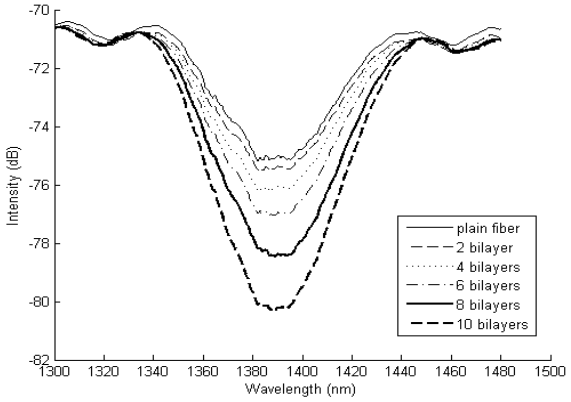

(a)

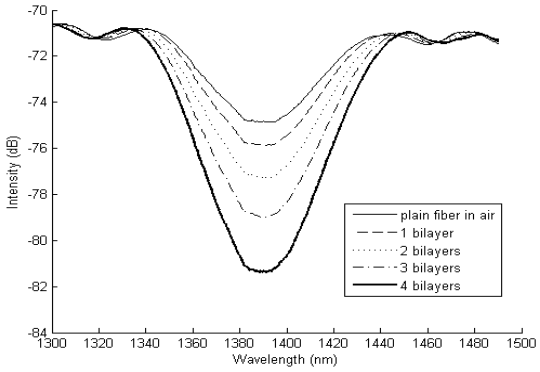

(b)

Figure 4-8: (a) LPG response to deposition of bilayers of PAH and PTEBS; (b) LPG response to addition of bilayers of PAH/PCBS in air.

It was hoped that this combination of materials would be more sensitive than that of the PAH/PCBS, but, unfortunately, that was not the case. It was thought that the refractive index of PTEBS would be higher than that of PCBS since PTEBS is a semiconducting polymer, but it was not. As can be seen in Figure 4-8 a for PAH/PTEBS ten bilayers were needed to reach the TAP. Whereas, for PAH/PCBS, only four bilayers were deposited to reach the TAP as can be seen in Figure 4-8 b.

4.2.4 PAH/Silica Nanoparticles

To further increase the sensitivity of the ISAM LPG sensor, incorporating silica nanoparticles into the ISAM film was explored. Nanoparticles provide increased film thickness and surface area for binding of probe and target molecules. With just one layer of 40 nm diameter silica nanoparticles, there is a very significant shift in the transmitted light intensity at the resonant wavelength, as shown in Figure 4-9. This extremely large shift is due to the thickness of the nanoparticles bilayer, which is about 20 nm. In contrast, a bilayer of PAH/PCBS is 1-2 nm. Therefore, the shift in intensity is much larger for the nanoparticles bilayer. Depositing two bilayers of PAH/PCBS (at pH 7.0/7.0) after just one bilayer of PAH and silica nanoparticles pushes the LPG past the TAP causing the spectrum to split into two peaks. If larger silica nanoparticles were to be used, there would be an even larger shift in the light intensity. Thus, another way to make a more sensitive sensor might be to incorporate larger silica nanoparticles into the film, if the increased Rayleigh scattering does not adversely affect the spectrum.

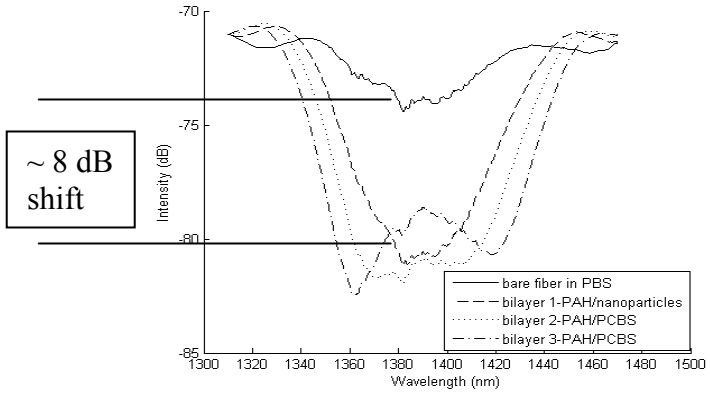

Figure 4-9: LPG response to one bilayer of 40 nm diameter silica nanoparticles and PAH, along with the additional response to two bilayers of PAH/PCBS.

It is important to note that the experiment shown in Figure 4-9 was performed in PBS solution, which again illustrates the versatility of the sensor.

The experiment illustrated in Figure 4-10 b is similar to the previous ones, except here the grating has been etched such that the attenuation band completely disappears because the nanoparticle layer creates such a large shift. One bilayer of PAH and 40 nm diameter silica nanoparticles was then deposited, and yielded about a 2.0 dB decrease in transmission. This was close to the LPG's starting point when just the bilayers of PAH/PCBS were deposited onto the LPG in the experiment shown in Figure 4-10 a. These experiments were also performed in PBS solution. The pHs of the PAH and of the nanoparticles were adjusted to 7.0 using NaOH and HCl.

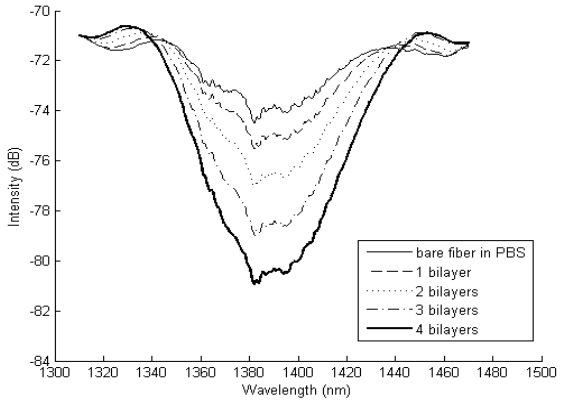

(a)

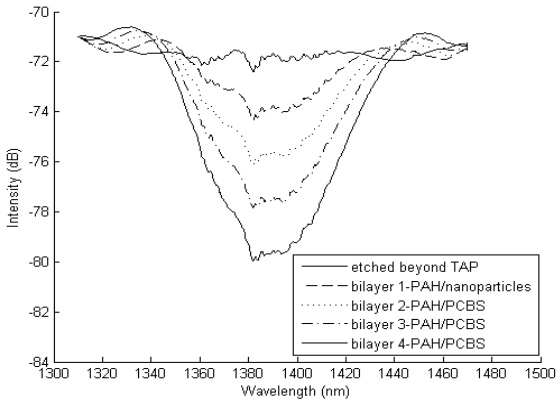

(b)

Figure 4-10: (a) LPG response to addition of bilayers of PAH/PCBS in PBS; (b) LPG etched beyond the TAP with deposition of one bilayer of PAH/silica nanoparticles and three bilayers of PAH/PCBS.

It can be seen that the first nanoparticle bilayer in Figure 4-10 b caused a 1.8 dB shift in attenuation, while the first bilayer for the PAH/PCBS (without nanoparticles) experiment in Figure 4-10 a yielded only a 1.0 dB shift in attenuation. Furthermore, the shifts in attenuation with the underlying nanoparticle layer are also greater as more bilayers of PAH/PCBS are deposited. The silica nanoparticle ISAM films have a fairly low

refractive index which may counteract the potential sensitivity increases as a result of increased surface area and thickness. Consequently, titania nanoparticles would be more likely to yield an even greater increase in LPG sensitivity. This is because the bulk refractive index of titania is about 2.5, which would create a film refractive index of about 1.9 for 40% void space.

4.3 Real-time Binding of ISAM Films

As a result of working in collaboration with a company (Prime Photonics) on another project, we got the opportunity to monitor the binding events that take place when ISAM layers are absorbed on the LPG in real-time. This was accomplished by monitoring the change in intensity at the wavelength of the TAP (~ 1570 nm) by placing a spike filter in front of the light source as the ISAMs were deposited onto the TAP LPG. As can be seen in Figure 4-11, the photodiode voltage decreases as each ISAM layer is deposited. The decrease in voltage corresponds to a decrease in transmitted light intensity at the wavelength of the TAP. The whole deposition and binding process was captured for each layer of film, which took around 3 minutes. These results verify the fact that it is possible to make biosensor systems with inexpensive photodectors rather than expensive optical spectrum analyzers. They also show that the sensor platform can be used to monitor real-time binding kinetics *in-situ*. This system could be used to monitor real-time binding of biotin-streptavidin, anthracis protective antigen, and prostate specific antigen testing.

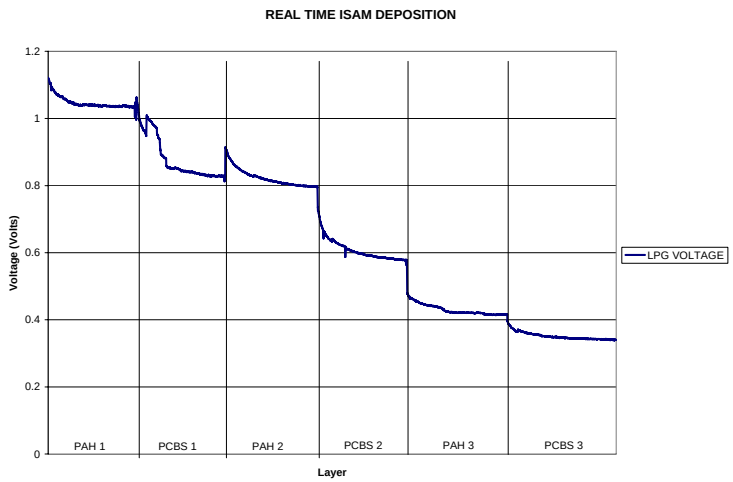

Figure 4-11: Real-time binding events between bilayers of PAH/PCBS ISAM films (at pH 7.0 and 7.0) taken during film deposition on the TAP LPG fiber. Each cycle is around 3 minutes.

4.4 Different TAP LPGs

Much later in this research, a different set of TAP-LPGs was obtained from OFS Laboratories. These LPGs were designed to significantly increase the dynamic range and sensitivity compared to the previous LPGs that had been used. These LPGs have a 35.0 dB overall decrease in transmitted intensity at the TAP, whereas, the older LPGs have only a 12.0 dB overall decrease in intensity at the TAP. This can be seen in Figure 4-12 a and b, which is a comparison of an old LPG to a new LPG. It should be noted here that along with these new LPGs, a new light source was also implemented. The setup is still the same as that in Figure 3-16. Instead of the white-light source, a Agilent 83437A Broadband Light Source from Agilent Technologies was used. This light source was much more powerful than the previous one and transmitted light at wavelengths of 1310, 1430, 1550, and 1650 nm.

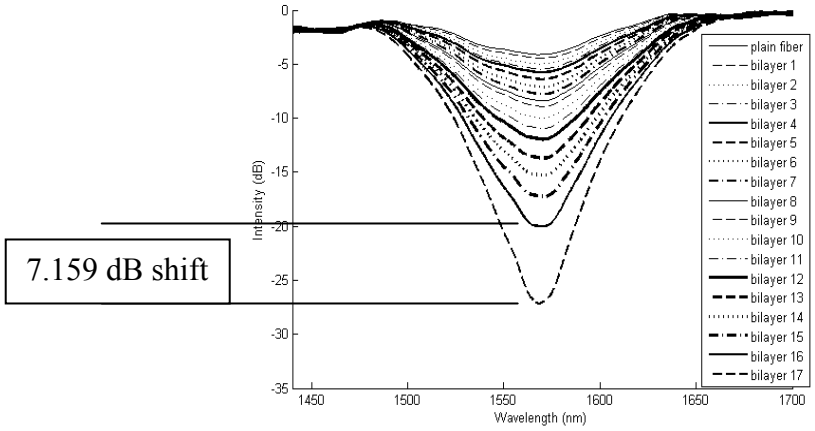

(a)

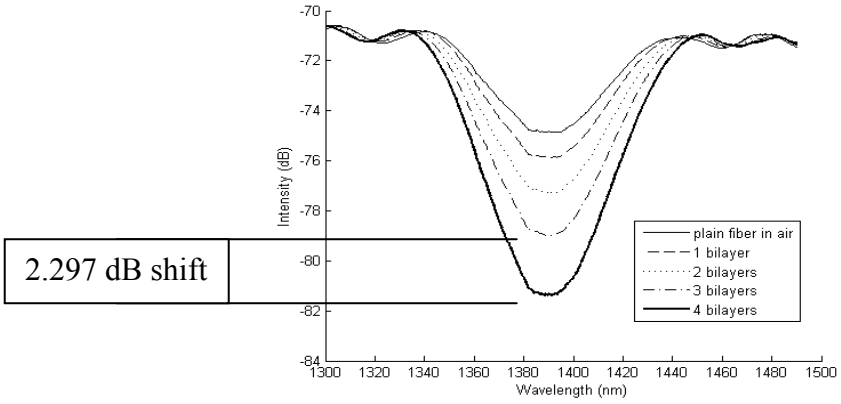

(b)

Figure 4-12: (a) Newer, more sensitive LPG response to bilayers of PAH/PCBS;
(b) Prior LPG response to bilayers of PAH/PCBS.

It can be seen in Figure 4-12 a and b that more than four times as many bilayers of PAH/PCBS can be deposited on the new LPG before it gets to the TAP. Furthermore, near the TAP, the spectrum has a 7.159 dB shift for the last bilayer for the new LPG, whereas, for the old LPG, there is only a 2.297 dB shift near the TAP. These new LPGs will enable construction of a sensor with drastically increased sensitivity and dynamic range, particularly when one considers the fact that dB corresponds to a logarithmic

transmission scale.

---

[1] Nissan Chemical America Corporation, Nissan Chemical Industries, 2001-2004.

[2] Yancey, S. A.; Zhong, W; Heflin, J. R.; Ritter, A. L. The influence of void space on antireflection coatings of silica nanoparticle self-assembled films, *J. Appl. Phys*. 2006, **99**, 034313:1-10.

[3] http://www.adsdyes.com/products/pdf/polythiophene/ADS2000P_DATA.pdf

Chapter 5. Implementation and Optimization of the ISAM LPG Biosensor

5.1 Anthrax Biosensor

Biosensors have important applications for homeland security. They have the ability to detect harmful, or even deadly, chemicals, pollutants, etc. that may be used in biological warfare. The following experiment tests the ability of a TAP-LPG to detect the B. *Anthracis* (Anthrax) Protective Antigen (PA), which is secreted by the bacteria as the gateway of infecting host cells with Anthrax toxin. Anthrax is made up of three proteins: the protective antigen (PA), the edema factor (EF), and the lethal factor (LF).[1] These three proteins function together to travel into a cell and inhibit the signaling pathways. This leads to apoptosis (cell death). Each protein is nontoxic alone. When they are combined, they create the lethal anthrax symptoms.

The 83 kDa PA consists of anti-parallel β-sheets with four functional domains.[2] Domain I is the amino terminal domain, which contains two calcium ions and the cleavage area for proteases to activate the protein. The product of the cleavage leads to the creation of the amino terminal fragment a20. Domain II is involved in the creation of the hexamer and contains a flexible loop that helps with membrane insertion. Currently, Domain II has no known function. Domain IV is needed for receptor binding.

The PA and its antibody were obtained from Biodesign International, Inc. Antibodies are part of a category of proteins known as immunoglobulins, which are a family of proteins produced by plasma cells that bind to invading organisms and destroy them. Antibodies are the body's best defense against disease. These proteins occur

naturally in the immune system in response to antigens. Antigens are foreign materials in the body.

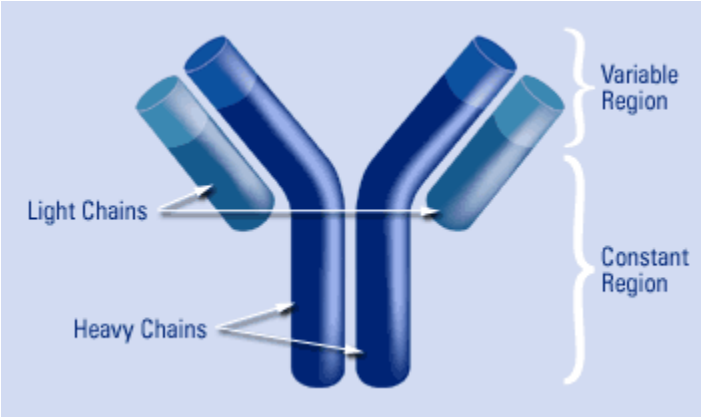

Figure 5-1: General schematic of an antibody.

Immunoglobulins are generally "Y" shaped and comprised of two light chains and two heavy chains.[3] There are two categories or isotypes of light chains known as lambda and kappa. Isotypes are genetic variations or differences in the constant regions of the heavy and light chains. The heavy chains contain five different isotypes (gamma, delta, alpha, epsilon, and mu) that each have different biological functions.

The light and heavy chains are made of two domains: the variable region and the constant region. The variable region is at the top of the arms of the "Y" and acts as the antigen binding site. Antibodies vary in the constant region. This leads to one of five immunoglobulin isotypes – IgG, IgA, IgD, IgM, or IgE.[3] Through the constant and variable domains, antibodies have the ability to bind, neutralize, and aid in eliminating pathogens along with their toxins.

5.1.1 Buffer Solutions

For these biosensor experiments, the most common buffer solution used is Phosphate Buffered Saline (PBS) solution. Another buffer some times used is Sodium Phosphate buffer. The following procedure was followed to make this Sodium Phosphate buffer. The two materials used were Na_2HPO_4 and NaH_2PO_4 purchased from Sigma-Aldrich. 9.71 g of Na_2HPO_4 and 3.791 g of NaH_2PO_4 were dissolved in 1 L of DI water. Then, the pH of the buffer was adjusted to 7.2 using NaOH and HCl. The other, more commonly used buffer, PBS, was made by dissolving 40 g of NaCl, 5.76 g of $Na_2HPO_47H_2$, and 0.95 g of KH_2PO_4 in 500 mL of DI water. This combination yields a 10 M PBS solution. Then, 100 ml of that solution was added to 900 ml of DI to create the 1 M solution used in experimentation. This solution was also adjusted pH 7.2 using NaOH and HCl. The materials for this buffer were obtained from the Winkel lab.

5.1.2 Experimental Procedure

Here, 1.5 bilayers of PAH (pH 7.0)/PCBS (pH 7.0) ISAM film were deposited onto a bare LPG that was etched beyond the TAP in air. Figure 5-2 depicts this optical-intensity based biosensor which uses the anthracis antibody-protein system [bare LPG -> ISAM -> antibody -> antigen], measured in air. As can be seen in Figure 5-2 there is a large increase in the attenuation at the resonant wavelength. Next, the antibody, which was supplied as 100 μg lyophilized from 100 μl of PBS, was dissolved into 100 μl of deionized water to a concentration of 1 mg/ml. Then, 5 mg of 1-ethyl-3-(3-dimethylaminpropyl) carbodiimide hydrochloride (EDC) crosslinker was dissolved in 1 ml of PBS and this solution was added to the antibody solution. EDC enables the PA

antibody to covalently link to the amines on the outer PAH layer of the ISAM film. This antibody solution was deposited onto the LPG as the probe molecule and incubated for two hours on the fiber. Again there was a significant decrease in the transmitted light intensity (~2 dB shift). Lastly, the anthrax protein (i.e. target molecule) PA, which was supplied as 100 μg of protein lyophilized from 1 ml of 10 mM BisTris pH 8.5 containing 1.25% trehalose, was dissolved in 1 ml of PBS to the concentration of 0.1 mg/ml. This solution was deposited onto the LPG and incubated for fifteen minutes. As can be seen in Figure 5-2, the PA was detected by the antibody (i.e. probe molecule) and binding took place. There was again a significant decrease (2.333 dB or 41.6%) in the transmitted light intensity at the resonant wavelength. The concentration of PA used is far above the desired sensitivity (< 1 μg/ml). However, this preliminary proof-of-principle demonstration has the possibility of improvement in sensitivity by several orders of magnitude. The improvements can come from optimizing the procedure for attaching the PA antibody to the film surface on the fiber, using high index underlying layers and nanoparticles, by implementing the new TAP LPGs obtained from OFS (which are engineered for much higher sensitivity and dynamic range), as well as the more powerful Agilent 83437A Broadband Light Source from Agilent Technologies.

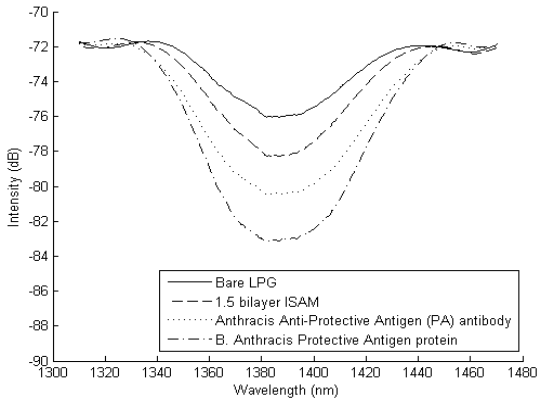

Figure 5-2: Direct EDC cross-linking of carboxylates on the Anthrax protective antigen antibody to amines on ISAM-coated fiber. Antibody dissolved in 100 µl of deoinized water to concentration of 1 mg/ml, then mixed with EDC and PBS. Protective antigen dissolved in 1 ml of PBS to concentration of 0.1 mg/ml.

5.2 Biotin-Streptavidin Biosensor

In order to study approaches for increasing the biosensor sensitivity, we focused on the system of biotin and streptavidin. These materials are far better characterized and more heavily studied, as well as being substantially less expensive.

5.2.1 Materials

5.2.1.1 Biotin

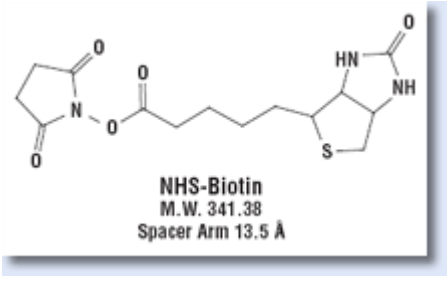

Figure 5-3: Molecular structure of NHS-Biotin.

The structure of NHS-Biotin, which was initially used in this research is shown in Figure 5-3. Biotin is also referred to as vitamin B7 or vitamin H. It is a water-soluble B-complex. Biotin plays an important role as a cofactor in the catalysis of essential metabolic reactions to synthesize fatty acids in gluconeogenesis, and to metabolize leucine. Biotin is also a key factor in the Citric acid cycle (how biochemical energy is created in aerobic respiration). Biotin aids in numerous metabolic chemical conversions, as well as assisting in the transfer of carbon dioxide. Furthermore, biotin is good for holding a constant blood sugar level. Also, it can aid in strengthening nails and hair.

Biotin can attach to numerous chemical sites. This process is called biotinylation. Biotinylation can be used to examine protein interactions and localizations, and DNA replication and transcription. Biotin tightly binds to the trameric protein, avidin (as well as streptavidin and neutravidin). There is a very high affinity binding constant between biotin and avidin (greater than 10^{15} M^{-1}).[4] This is the highest known affinity between any protein and its ligand. Frequently, this is implemented in various biotechnical applications. Due to the very high affinity between biotin and avidin, biotin is of great use in molecular biology as a chemical tag on nucleic acid probes or antibodies. Avidin and streptavidin can be coupled to enzymes, fluorescent dyes, or colloidal gold. This enables detection by chromogenic reactions, which, in turn, enables detection of biotin-labeled probes or antibodies.

5.2.1.2 Avidin

Avidin is a glycoprotein. It is present in the tissues and egg whites of reptiles, birds, and amphibians. It is comprised of four subunits that are identical and have a

combined mass of 67,000 - 68,000 daltons. Every subunit contains 128 amino acids and binds one molecule of biotin. Carbohydrates make up around 10% of avidin's total mass. Avidin is unaffected over a large range of temperature and pH. It is extremely helpful in protein purification and has fairly high nonspecific binding.

5.2.1.3 Streptavidin

Streptavidin is a 60,000 dalton tetrameric protein that is purified from the bacterium Streptomyces avidinii. Streptavidin has an extremely high affinity for biotin (on the order of $\sim 10^{15}\ M^{-1}$). Its affinity is slightly lower than that of biotin and avidin, but it is still one of the strongest known non-covalent interactions. This very strong affinity between biotin and streptavidin is a result of the shape-specificity of the biotin-binding pocket on streptavidin. This enables the generation of van der Waals interactions and numerous hydrogen bonds.[5] One of the most common uses of streptavidin is the detection or purification of certain biomolecules. The extremely strong bond between biotin and streptavidin can enable the attachment of numerous biomolecules onto a solid substrate or to one another.

5.2.1.4 Differences and Similarities Between Avidin and Streptavidin

Avidin and streptavidin are fairly different in composition. Also, as mentioned earlier, the affinity constant for biotin and streptavidin is slightly lower than that of biotin and avidin. However, avidin and streptavidin are extremely similar in other ways. They both create tetrameric complexes where each subunit binds to only one molecule of

biotin. Avidin and streptavidin tetramers can both be dissociated by guanidine hydrochloride into their component subunits, although streptavidin is more resistant to the dissociation. Avidin is much more water-soluble than streptavidin. Streptavidin also does not have avidin's extensive glycosylation. One main difference between streptavidin and avidin is that at neutral pH, streptavidin is almost neutral. Whereas, avidin holds a positive charge at neutral pH.

One major advantage of using biotin is that many biotin molecules can couple to a protein, and the biotinylated protein has the ability to bind multiple molecules of streptavidin. The biotinylated protein's biological activity can be preserved as long as the biotinylation process is done under careful circumstances. This can be used to increase the sensitivity of various biosensor approaches. The biotin-streptavidin mechanism can be utilized by linking the streptavidin covalently with various ligands such as fluorochromes, enzymes, or EM markers. This mechanism has the capability to be used in examining a large range of biological structures and processes. The biotin-streptavidin mechanism has been shown to be able to detect antigens, glycoconjugates, or nucleic acids by implementing biotinylated antibodies, lectins, or nucleic acid probes, respectively.

5.2.1.5 Biotin-(Strept)avidin System Advantages

There are numerous benefits that the biotin-(strept)avidin mechanism has over direct coupling of the marker to a lectin, antibody, or nucleic acid probe. These include: (1) (Strept)avidin can be made with high fluorochrome to protein ratios.[6] Furthermore, avidin conjugates are extremely stable. (2) Because (strept)avidin and biotin have such a

large affinity for each other, stable complexes are quickly generated between the biotin-labeled protein and the (strept)avidin conjugate. (3) The biotin-(strept)avidin mechanism has amplification capability because of the multiple binding sites. This can increase sensitivity. (4) Biotin-(strept)avidin system reagents can defeat the issue of background fluorescence that occurs occasionally when rhodamine or fluorescein-labeled antibodies are implemented. At times, these conjugates adsorb nonspecifically to tissues, but fluorochrome-conjugated avidin D does not. (5) Even when two or three primary antibodies are present from the same species, simultaneous localization of more than one antigen in the same tissue section can be achieved. (6) Just one single labeled conjugate (i.e. streptavidin or avidin) is necessary because it can be implemented with numerous antibodies, biotinylated lectins, or probes.

5.2.2.6 Biotin-Streptavidin Chemistry

Figure 5-4 describes the chemistry behind the biotin-streptavidin experiments. It should be noted that the figure is not drawn to scale. By examining Figure 5-4, it can be seen that 1.5 bilayers of ISAM is deposited onto the LPG using the ISAM deposition technique. The outermost layer is PAH. Then, the biotin is deposited and binds with the PAH. Next, the streptavidin is deposited and binds with the biotin. Chemically, when the biotin is dissolved in PBS at pH 7.2, it reacts with the amine groups of the PAH to form a stable amide bond. The streptavidin has four identical amino acid containing subunits that can each bind to one molecule of biotin. An amino acid contains both a primary amine group and a carboxyl group. When the streptavidin is dissolved in PBS at

pH 7.2, the amino acid-containing subunits can react with the biotin to form hydrogen bonds.

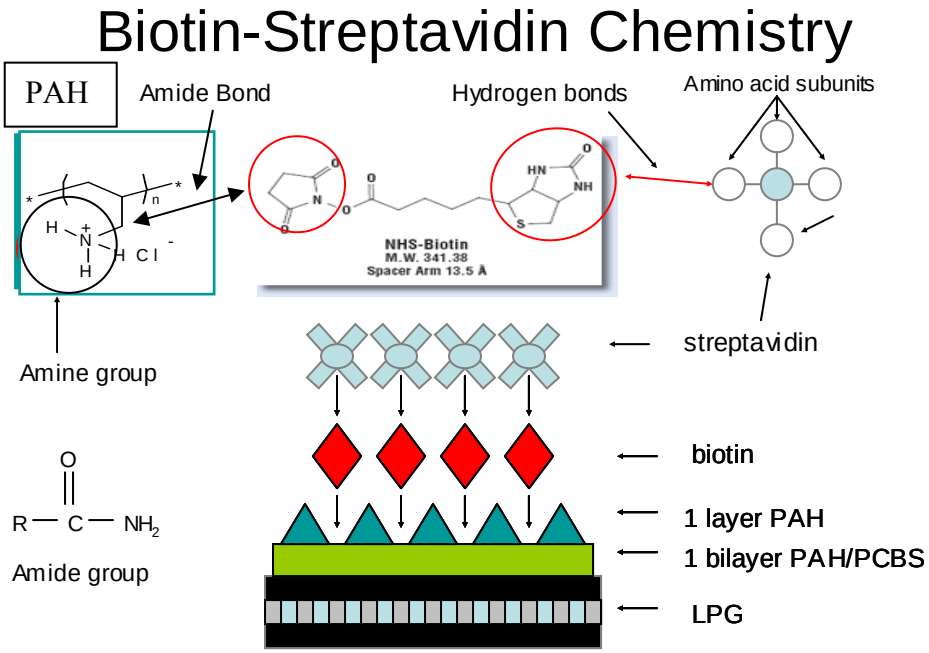

Figure 5-4: Chemistry involved in the binding kinetics of the biotin-streptavidin system onto an ISAM coated LPG.

5.2.2 Prior Biosensor Results

For the biotin-streptavidin biosensor experiments, the biotin-N-hydroxysuccinimide ester (NHS-biotin) and streptavidin (SA) were purchased from Sigma-Aldrich Corp. Upon arrival, these chemicals were immediately placed in the freezer. For comparison, the first set of results that will be discussed are from an experiment that Zhiyong Wang performed. His procedure was as follows:

1. The LPG spectrum was taken at room temperature prior to any film deposition.

2. PAH and PCBS ISAM films were deposited onto the LPG with the outermost layer being PAH. In this particular experiment 1.5 bilayers of PAH/PCBS at pH 7.0/7.0 were deposited onto the LPG. The spectrum was taken at room temperature in air.
3. Biotin was taken out of the freezer and immediately dissolved in the Sodium Phosphate buffer to the concentration of 1 mg/ml. This solution was stirred for 15 minutes.
4. The LPG was immediately immersed into the biotin solution and incubated for 45 minutes (suggested time 30-60 minutes).
5. The LPG was immersed in the Sodium Phosphate buffer/PBS buffer for 3 minutes. Then, the LPG was rinsed with Sodium Phosphate buffer/PBS buffer and the LPG spectrum was taken at room temperature in air.
6. The streptavidin was taken out of the freezer and immediately dissolved in the Sodium Phosphate buffer to the concentration of 0.1 mg/ml. This solution was also stirred for 15 minutes.
7. The LPG was immediately immersed into the streptavidin solution and incubated for 45 minutes.
8. Step 5 was repeated.

For LPG-based biosensors, the ligand/target binding event generates a change in film thickness or refractive index or both in the ambient material surrounding the LPG cladding. This, in turn, causes the measurable change in LPG transmission spectrum. At present, the biotin-streptavidin mechanism is the most commonly used system for examining numerous biological processes and structures and for clinical purposes.[7] The

biotin and streptavidin act as the antibody and antigen, respectively for this biosensor demonstration. The streptavidin is immobilized on the fiber grating through the biotinylated PAH, which was deposited on the LPG using the ISAM technique.[8] The LPG used for the following experiment was UV-induced on TrueWave RS^{TM} fibers with a grating period of 112 μm and length of 5 cm.[8] This produced gratings that couple the fundamental mode to the $LP_{0,14}$ cladding mode. These Turnaround Point (TAP) LPGs were obtained from OFS Laboratories.

Zhiyong used a TAP-LPG to examine the sensitivity to streptavidin concentration used. By diluting 0.1 mg/ml streptavidin, the following concentrations were obtained: 0.0125 mg/ml, 0.025 mg/ml, 0.05 mg/ml, and 0.075 mg/ml. To obtain a larger dynamic range before performing the experiment, Zhiyong etched the fiber slightly with the HF solution. It is important to note that for this experiment all measurements were taken in air.

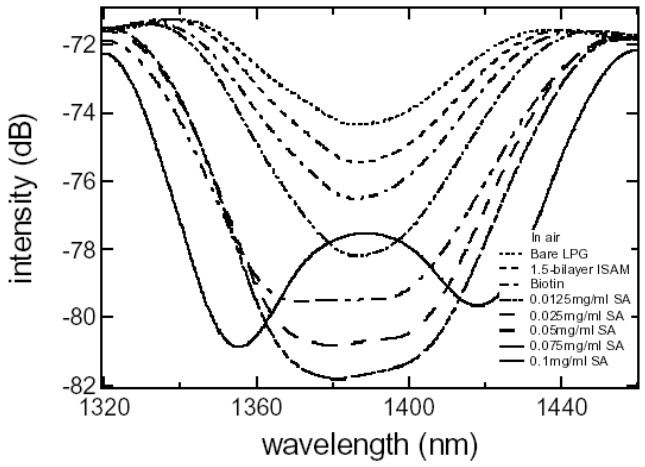

(a)

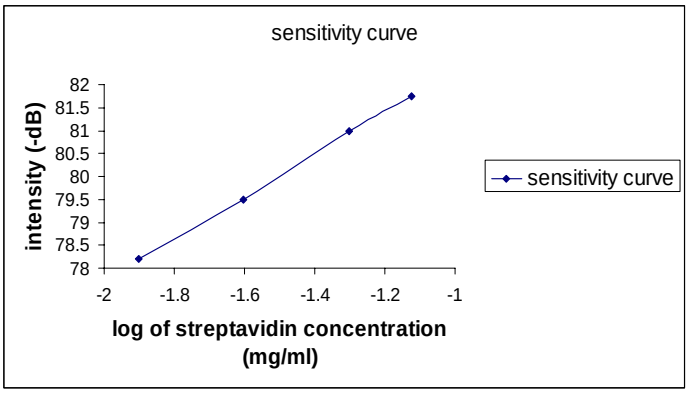

(b)

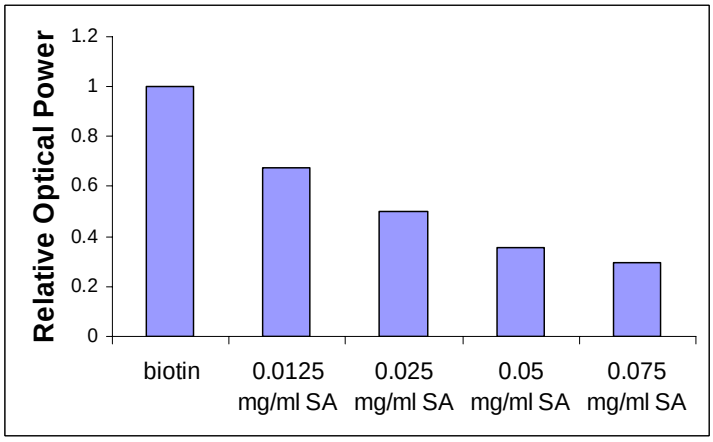

(c)

Figure 5-5: (a) Study of sensitivity to concentration of SA utilizing optical-intensity based biosensor and biotin-SA system [bare LPG->ISAM->biotin->SA], measured in air; (b) sensitivity curve of log of streptavidin concentration in mg/ml; (c) decrease in relative optical power after each deposition of increasingly higher streptavidin concentrations.

Figure 5-5 displays the results from the sensitivity study. It can be seen that for the streptavidin concentration of 0.0125 mg/ml, there was about a 1.7 dB shift in intensity (i.e. ~ 32.4% decrease in transmitted light intensity). This large shift implies that it may be possible to detect even lower concentrations of streptavidin. Figure 5-5 a also shows that the dynamic range for the optical intensity-based biosensor is from 0 mg/ml to 0.075

mg/ml for this approach. Because of the characteristic of TAP LPGs, the single broadband attenuation peak splits into two peaks after the streptavidin concentration surpasses 0.075 mg/ml. One could etch the TAP LPG further back to obtain a larger dynamic range and then perform the experiment again. Figure 5-5 b shows the sensitivity curve of the log of the streptavidin concentrations in mg/ml. As can be seen, the sensitivity of the LPG increased as higher concentrations of streptavidin where deposited. Furthermore, Figure 5-5 c shows the decrease in relative optical power after each deposition of increasingly higher streptavidin concentrations.

5.2.3 Biotin-Streptavidin Sensitivity Study

I performed a similar experiment to Zhiyong's biotin-streptavidin experiment. In my experiment, however, I used one of the newer, more sensitive LPGs along with the more powerful Agilent 83437A Broadband Light Source. I also performed this experiment in PBS as opposed to in air. I made some slight changes in the experimental procedure to obtain improved results. My procedure is as follows:

1. The LPG spectrum was taken at room temperature in PBS solution prior to any film deposition.
2. PAH and PCBS ISAM films were deposited onto the LPG with the outermost layer being PAH. In this experiment, 1.5 bilayers of PAH/PCBS at pH 7.0/7.0 were deposited onto the LPG. The spectrum was taken at room temperature in PBS.
3. 10 mg of biotin was taken out of the freezer and placed into 9 ml of Sodium Phosphate buffer plus 1 ml of ethanol. This solution was pipetted for about 20

s.

4. The LPG was immediately immersed into the biotin solution and incubated for 45 minutes.
5. The LPG was immersed in the Sodium Phosphate buffer/PBS buffer for 3 minutes. Then, the LPG was rinsed with Sodium Phosphate buffer/PBS buffer and the LPG spectrum was taken at room temperature in PBS.
6. The streptavidin was taken out of the freezer and 9 ml of Sodium Phosphate buffer plus 1 ml of 1 mg/ml BSA was added to it. The solution was pipetted for about 20 s.
8. The LPG was immediately immersed into the lowest streptavidin concentration and incubated for 45 minutes.
9. Step 5 was repeated.
10. The same procedures were performed for each concentration of streptavidin.

The results of the experiment can be seen in Figure 5-6. The first change made to Zhiyong's procedure was that the experiment was performed in PBS solution. This illustrates the versatility of the sensor since experiments can be performed in solution as well as in air and many of the real-world applications will be in solution. The second change was to add ethanol to the biotin solution. This was done to improve the ability of biotin to dissolve into solution, which was a problem previously. Zhiyong stirred the biotin solution for 15 minutes, but I only stirred mine a couple of seconds. This was done because the biotin reacts very quickly and it is important to get the solution onto the fiber before any reactions occur. BSA was added to the streptavidin because this prevents the streptavidin molecules from "sticking" to the sides of the glass beaker (thus making the

concentration of streptavidin that goes onto the fiber lower). All of the aforementioned changes were made upon the suggestions of Dr. Rik Obiso, a biochemist familiar with these materials.

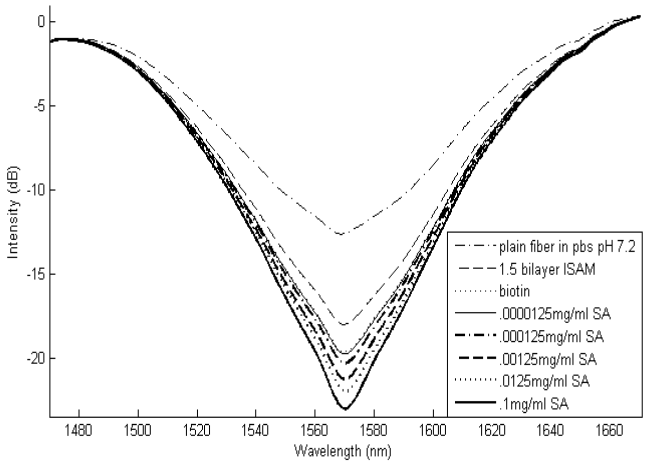

(a)

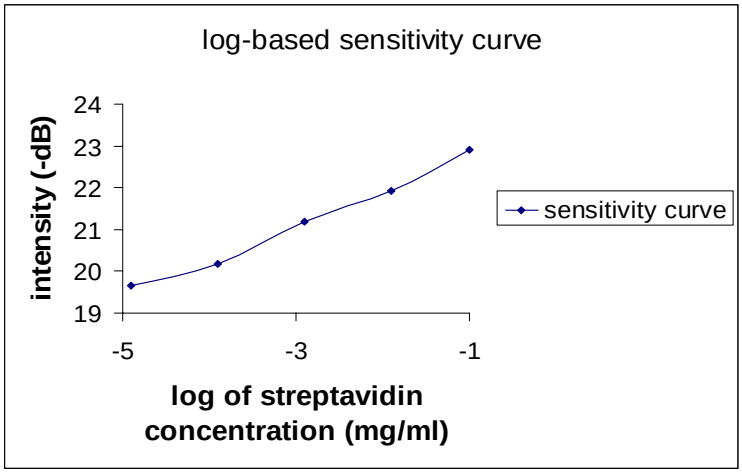

(b)

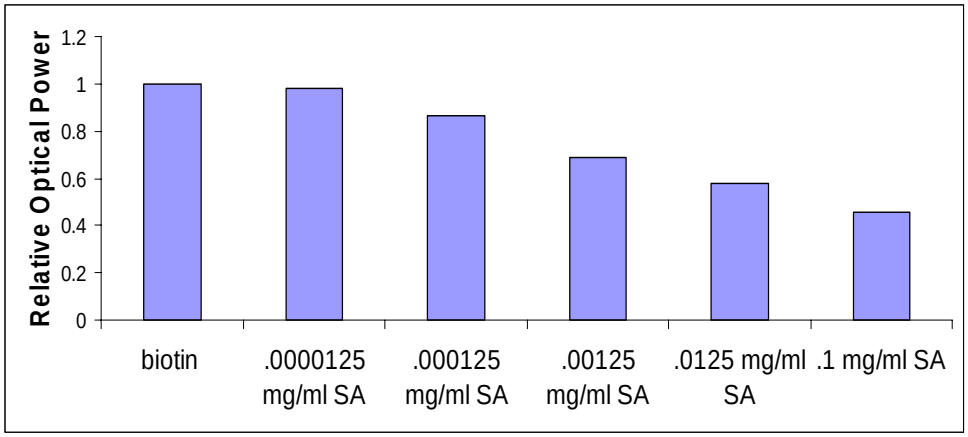

(c)

Figure 5-6: (a) Study of sensitivity to concentration of SA by optical-intensity based biosensor and biotin-SA system [bare LPG->ISAM->biotin->SA], measured in PBS; (b) sensitivity curve of log of streptavidin concentration in mg/ml; (c) decrease in relative optical power after each deposition of increasingly higher streptavidin concentrations.

The results obtained represent a substantial increase in sensitivity compared to those obtained previously. Figure 5-6 a shows the LPG transmission spectra for each concentration of streptavidin. Figure 5-6 b displays the log-based streptavidin sensitivity curve, and Figure 5-6 c depicts the decrease in relative optical power after each deposition. In Zhiyong's experiment, the lowest streptavidin concentration that he detected was 0.0125 mg/ml. In the present study, the lowest detectable signal is at 0.000125 mg/ml (0.125 μg/ml or 125 ng/ml) streptavidin. A concentration 100 times smaller is detected here. Also, in Zhiyong's study, for the steptavidin concentration of 0.0125 mg/ml (12.5 μg/ml or 12500 ng/ml), there was about a 1.7 dB shift or about a 32.4% decrease in the transmitted light intensity. However, in my study, for the same streptavidin concentration, there was a 2.359 dB shift, or a 42% decrease in the transmitted light intensity at the resonant wavelength. Furthermore, for the streptavidin

concentration of 0.000125 mg/ml, there was a 0.645 dB shift, or a 14% decrease in the transmitted light intensity.

5.2.3.1 Further Improved Biotin-Streptavidin Study

Up until this point, one problem still remained in the biotin-streptavidin studies, which was that incomplete surface coverage of biotin binding was taking place, which is suggested by the fairly small spectral shifts after the biotin was deposited. For Zhiyong's study, the biotin shift was about 1 dB. For my study, it was about 1.5 dB. To ensure the maximum amount of binding between biotin and streptavidin, it is important to have the largest possible amount of biotin absorbed onto the fiber. This allows for the maximum number of binding sites for streptavidin. After many, many trials and errors with different methods, different types of biotin, and consultations with a biochemist, Dr. Rik Obiso, it was determined that a form of biotin specifically noted for higher water solubility might lead to the greatest amount of biotin binding to the ISAM films. EZ-Link NHS-LC-LC-Biotin (succinimidyl-6-(biotinamido)-6-hexanamido hexonaoate) was purchased from Pierce.

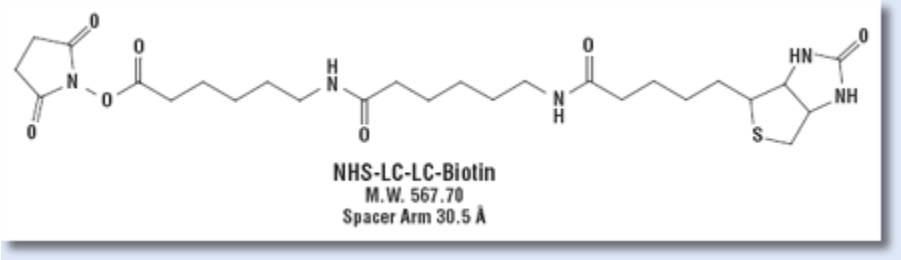

Figure 5-7: Molecular structure of NHS-LC-LC-Biotin.

The molecular weight is 567.70, which is much larger than the previously used biotin's molecular weight of 341.38. The spacer arm length of the new biotin is 30.5 Angstroms, whereas, the spacer arm length of the previous biotin was only 13.5 Angstroms. This longer spacer arm increases the availability of the binding sites for streptavidin. Furthermore, this biotin was much more soluble in solution than the previous biotin, which provides the possibility of greater surface coverage through use of higher concentrations. Thus, the longer spacer arm and increased solubility yielded much more biotin binding. This can be seen in Figure 5-8 a which shows a 3.096 dB biotin shift. The increase in biotin binding sites for the streptavidin generated an overall sensitivity increase for the sensor. This is visible in Figures 5-8 a, b, and c. The experimental procedure was the same as before and a 10 mM biotin solution was used. One other factor that led to increased sensitivity was that the biotin and streptavidin were deposited at points much closer to the TAP of the LPG, which is the most sensitive area of the grating.

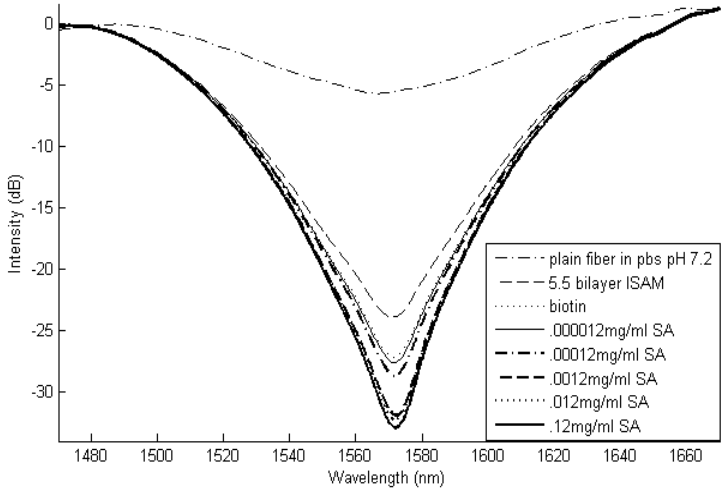

(a)

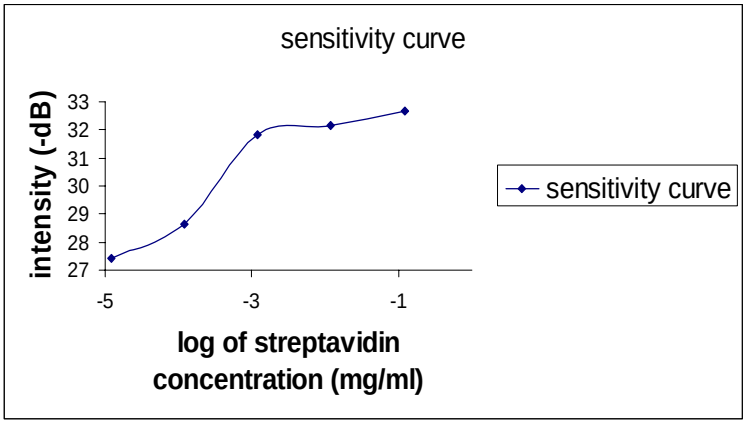

(b)

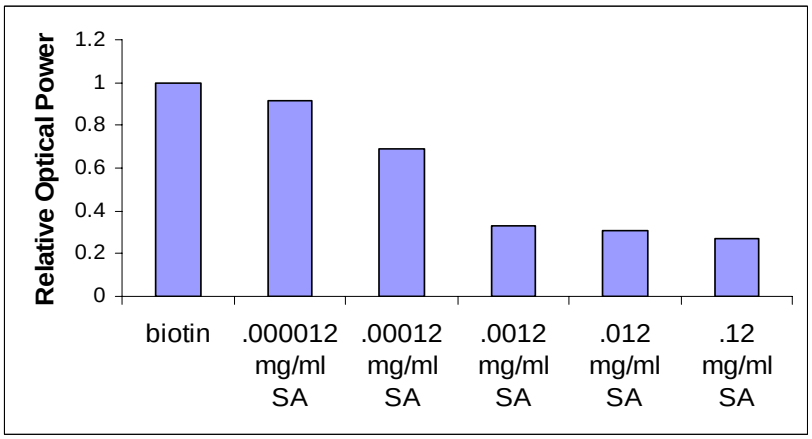

(c)

Figure 5-8: (a) Study of sensitivity to concentration of SA by optical-intensity based biosensor and biotin-SA system [bare LPG->ISAM->biotin ->SA], measured in PBS; (b) sensitivity curve of log of streptavidin concentration in mg/ml; (c) decrease in relative optical power after each deposition of increasingly higher streptavidin concentrations.

Figure 5-8 a depicts the change in LPG transmission spectra after each deposition. Figure 5-8 b shows the sensitivity curve for streptavidin, and Figure 5-8 c illustrates the decrease in relative optical power after each deposition. Due to the aforementioned improvements, the lowest detectable streptavidin concentration was 0.000012 mg/ml (0.012 μg/ml or 12.0 ng/ml). This is a factor of 10 more sensitive than the previous

study, and a factor of 1000 more sensitive than Zhiyong's study. Here, there was a 0.399 dB shift, or an 8.8% decrease, in the transmitted light intensity for 0.000012 mg/ml streptavidin. Also, for 0.012 mg/ml (12.0 μg/ml or 12000 ng/ml) streptavidin, there was a 5.153 dB shift, or a 69.5% decrease, in the transmitted light intensity at the resonant wavelength. In the previous experiment, there was only a 42% decrease for this concentration.

One important fact to note here is that this system reached saturation when 0.0012 mg/ml (1.2 μg/ml or 1200 ng/ml) SA was deposited. This means that after 0.0012 mg/ml of streptavidin was absorbed all (or almost all) of the biotin binding sites were taken. These results are confirmed in Figure 5-9, where the experiment was repeated and saturation again occurred after 0.0012 mg/ml streptavidin was deposited. This is also evident in Figure 5-9 b because the sensitivity curve starts to level off after a certain point.

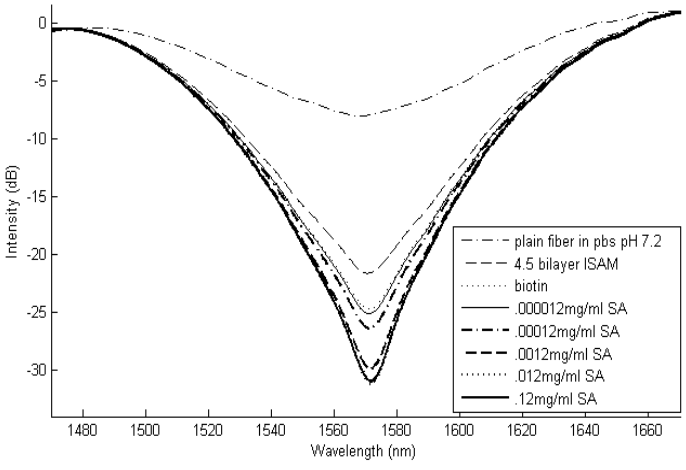

(a)

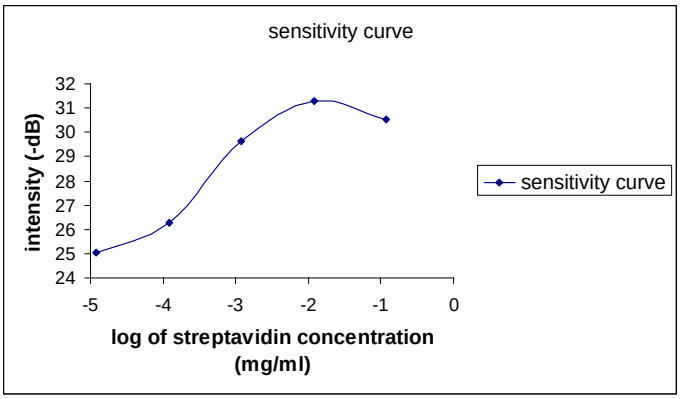

(b)

Figure 5-9: (a) Study of sensitivity to concentration of SA by optical-intensity based biosensor and biotin-SA system [bare LPG->ISAM->biotin->SA], measured in PBS; (b) sensitivity curve of log of streptavidin concentration in mg/ml.

To further illustrate the improvements in sensitivity of the biotin-streptavidin sensor system over time, Figure 5-10 shows the decrease in relative optical power for around 0.012 mg/ml (12 μg/ml or 12000 ng/ml) streptavidin in each of the three systems. 0.012 mg/ml was Zhiyong's lowest detectable concentration of streptavidin. The decrease is visibly larger for each system, implying an increase in sensitivity each time.

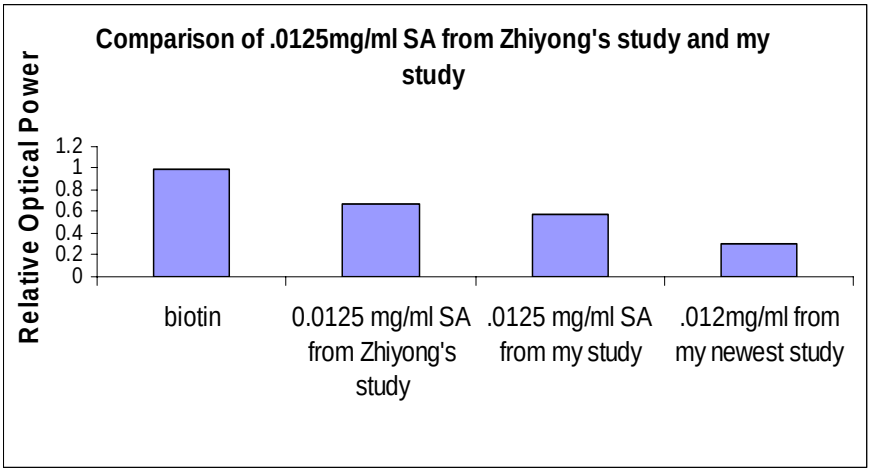

Figure 5-10: Comparison of decrease in relative optical power for Dr. Wang's biotin-streptavidin study and my biotin-streptavidin study for the streptavidin concentration of ~ 0.0125 mg/ml.

5.3 Prostate Specific Antigen Biosensor

I have performed an extensive study on the potential use of fiber optic biosensors for the early detection of prostate cancer. The concept for this system is similar to those just discussed. The prostate specific monoclonal antibody (Mab) is immobilized on an ISAM film. Then, different concentrations of the prostate specific antigen (PSA) are detected. The detailed experimental procedure will be discussed shortly.

5.3.1 Materials and Significance

The two main materials for this sensor, of course, are the PSA and the monoclonal antibody (Mab) to the PSA. A monoclonal antibody is a kind of protein created in the laboratory that can find and bind to substances in the body, such as tumors.[9] They can be used by themselves or to carry toxins, drugs, or radioactive substances directly to a tumor. A monoclonal antibody is used in this study because they have much higher

specificity than polyclonal antibodies, and high specificity is critical for biosensors. The Mab to the PSA used in this experiment is Mouse IgG_1 and the affinity constant is currently undetermined.

PSA is a 34 kDa glycoprotein generated by the cells of the prostate gland.[10] It is a single polypeptide chain of 240 amino acids with calculated molecular weight of 26,496 for the peptide region.[11] PSA exists in tiny amounts in the serum of normal men. Oftentimes, the concentrations of PSA are increased when prostate cancer or other prostate disorders are present.[12] Currently, the most effective way to measure PSA levels for early diagnosis of prostate cancer is a blood test. Generally, the higher the PSA level, the higher the probability that cancer is there. However, other factors besides cancer can cause or contribute to elevated PSA levels. Since PSA is created by the body and can be utilized to detect disease, it is often called a tumor/biological marker.[13] It is normal for men to have small concentrations of PSA in their blood, but prostate cancer or benign conditions can elevate PSA levels. As men get older, both benign prostate conditions and prostate cancer occur more often. PSA levels on their own do not provide doctors with sufficient information to differentiate between benign prostate conditions and cancer. Consequently, the doctor will take the PSA test results into consideration when determining if checking for further signs of prostate cancer is necessary. The doctor may look for a pattern of increasing PSA levels over time instead of just one instance of elevated PSA. There are several risk factors that increase a man's chances of getting prostate cancer such as: age, family history, race, and diet. Age is the most common one. Almost 65% of prostate cancer cases take place in men who are 65 years of age or older.[13]

A cut-off level of 4.0 ng/ml of PSA in the blood test is commonly used as the decision limit, even though it does not relate to any specific reference value.[14] PSA concentrations in serum elevate with age.[15] Hence, the reference values are age dependent. The upper reference limits obtained on the basis of the 95th percentile are 2.5 ng/ml in the age group of 40-49 years, 3.5 ng/ml at age 50-59 years, 4.5 ng/ml at age 60-69, and 6.5 ng/ml at age 70-79 years.[16] However, these values are some times debated. The probability of detecting prostate cancer in a man with serum PSA of 4.0 ng/ml is about 20% and it is similar when PSA is in the range of 2.6-4.0 ng/ml.[16]

5.3.2 PSA Sensor Experiment

For this experiment, the materials used were PAH/PCBS at pH 7.0/7.0, PBS at pH 7.2, biotin purchased from Sigma Aldrich, streptavidin purchased from Sigma Aldrich, unconjugated protein A purchased from Rockland, No-Weigh Sulfo-SMCC (sulfosuccinimidyl 4-[N-maleimidiomethyl]cyclohexane-1-carboxylate) cross-linker tubes purchased from Pierce, PSA and Mab to PSA both purchased from Meridian Life Science Inc.

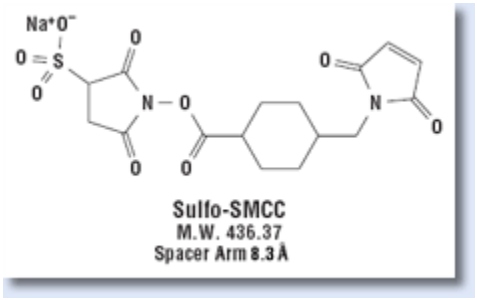

Figure 5-11: Molecular structure of Sulfo-SMCC (sulfosuccinimidyl 4-[N-maleimidiomethyl]cyclohexane-1-carboxylate) cross-linker.

Sulfosuccinimidyl-4-(*N*-maleimidomethyl)cyclohexane-1-carboxylate (Sulfo-SMCC) is a non-cleavable, water-soluble, and membrane impermeable crosslinker.[17] It has an amine-reactive *N*-hydroxysuccinimide (NHS ester) and a sulfhydryl-reactive maleimide group. NHS esters can react with primary amines at pH 7.0-9.0 to create stable amine bonds. Amines are functional groups and organic compounds that have a basic nitrogen atom with a lone pair.[18] A maleimide is a chemical compound with the formula $H_2C_2(CO)_2NH$.[19] Maleimides can react with sulfhydryl groups at pH 6.5-7.5 to create stable thioether bonds. A thioether, which is similar to a sulfide, is a functional group that has the structure R^1-S-R^2.[20] The maleimide groups of Sulfo-SMCC and SMCC are extremely stable up to pH 7.5.

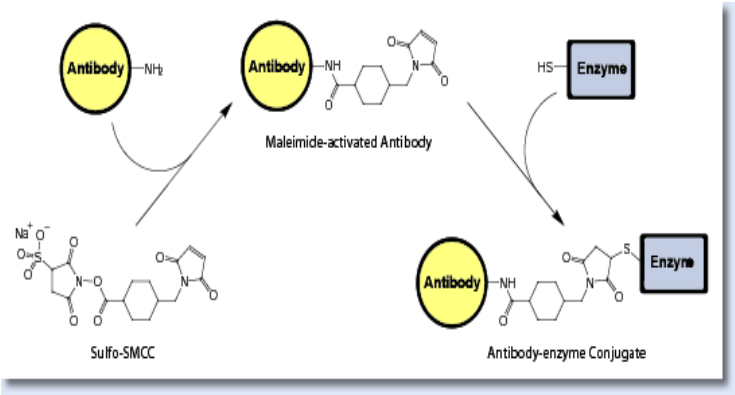

Figure 5-12: Sulfo-SMCC reaction to create maleimide-activated antibody followed by linkage to an enzyme.

Oftentimes, Sulfo-SMCC is implemented in the creation of antibody-enzyme and hapten-carrier conjugates, as shown in Figure 5-12.[17] In this situation, the NHS ester reacts first with the antibody, extra crosslinking reagent is removed, then the sulfhydryl-containing enzyme molecule gets added. This reaction yields the creation of certain antibody-enzyme conjugates. Sulfo-SMCC generates stable maleimide-activated carrier proteins

that can spontaneously react with sulfhydryls.[17] In this situation, the Sulfo-SMCC or NHS ester reacts with the lysine residues on the carrier protein, which makes them reactive maleimides.

In the present work, this crosslinking process is used to attach the protein A to streptavidin, as described in the procedure below. Protein A is a 42 kDa surface protein originally found in the cell wall of the bacteria staphyloccus aureus. It is useful in biochemical research because of its ability to bind to various antibodies, such as the Mab to the PSA in this case. Potein A binds with moderate affinity to the mouse IgG_1 from the Mab to the PSA.[21]

5.3.2.1 PSA Biosensor Chemistry

Figure 5-13 illustrates the chemistry involved in the PSA biosensor. It should again be noted that this figure is not drawn to scale. The binding process between the PAH and the biotin is the same as previously mentioned in Section 5.2.2.1. This time, however, the streptavidin is first cross-linked with protein A. The protein A was supplied chromatographically pure. The crosslinking process involves the use of the Sulfo-SMCC crosslinker, which contains an amine-reactive NHS ester and a sulfhydryl-reactive maleimide group. The crosslinker was supplied as > 90% pure by quantitative NMR (the highest standard for crosslinker purity). First the protein A, which has a sulfhydryl group reacts with the N and O to complete the maleimide group and form a stable thioether bond. Then, the streptavidin reacts with the crosslinker to form stable amine bonds. The streptavidin was supplied affinity purified and has a molecular weight of 60 kDa. Thus, in the end, protein A is crosslinked with streptavidin. This protein A/streptavidin

solution is deposited on the fiber. The streptavidin still has amino acid groups left to bind with the biotin on the fiber (in the same way as mentioned in Section 5.2.2.1) and form hydrogen bonds. After the streptavidin binds to the biotin, the protein A is left exposed to bind to the Mab to the PSA. When the Mab is deposited, it binds to the protein A. Then, the PSA can be deposited and it will bind to the Mab.

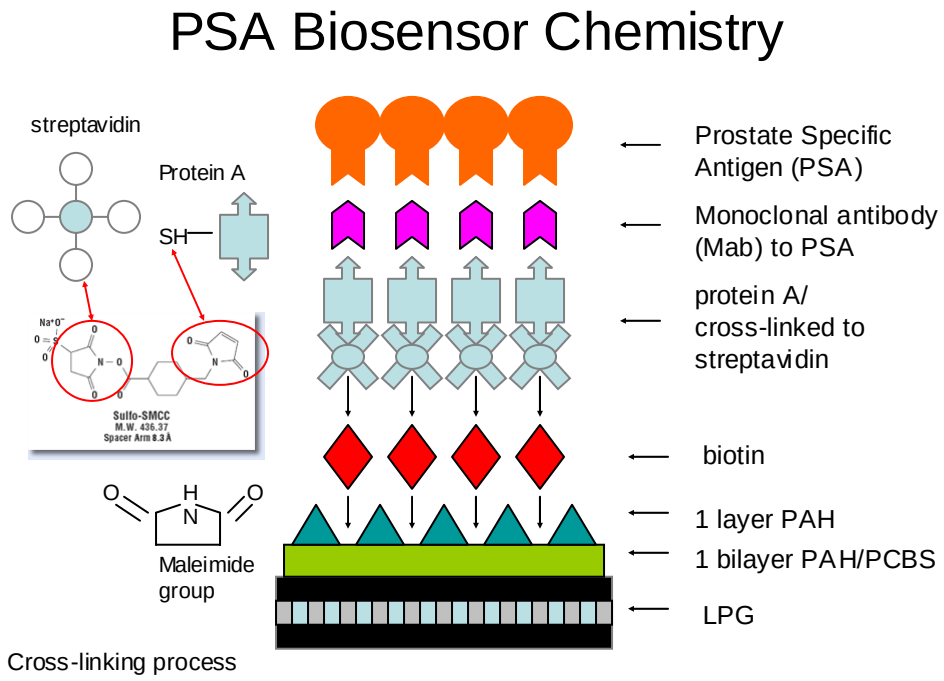

Figure 5-13: Chemistry involved in the binding processes of the PSA biosensor.

The experimental procedure designed by biochemist, Dr. Rik Obiso, was as follows:

1. The LPG spectrum was taken at room temperature in PBS solution prior to any film deposition.

2. PAH and PCBS ISAM films were deposited onto the LPG with the outermost layer being PAH. In this experiment, 1.5 bilayers of PAH/PCBS at pH 7.0/7.0 were deposited onto the LPG. The spectrum was taken at room temperature in PBS.

3. 5 mg of unconjugated protein A was dissolved in 1ml of PBS. Protein A is a "generic" protein that will bind to the Mab to the PSA.

4. 200 μl of the protein A solution was placed into a cross-linker tube and incubated in the refrigerator for two hours.

5. 300 μl of PBS was added to the 200 μl of protein A solution after incubation.

6. The protein A/PBS solution was then placed into a spin column and centrifuged.

7. 1 mg of streptavidin was dissolved in 1 ml of PBS.

8. 200 μl of streptavidin solution was added to the centrifuged protein A/PBS solution.

9. This protein A/PBS/SA solution was incubated in the refrigerator overnight. This allows the protein A to link to the SA.

10. The protein A/PBS/SA solution was also centrifuged.

11. 10 mg of NHS-biotin was taken out of the freezer and placed into 10 ml of PBS. This solution was pipetted for about 20 s.

12. The LPG was immediately immersed into the biotin solution and incubated for 45 minutes.

13. The LPG was immersed in the Sodium Phosphate buffer/PBS buffer for 3 minutes. Then, the LPG was rinsed with Sodium Phosphate buffer/PBS buffer and the LPG spectrum was taken at room temperature in PBS.

14. The centrifuged protein A/PBS/SA solution was then placed onto the fiber and incubated for 45 minutes. This allows the SA to bind to the biotin and the protein A becomes the exterior binding site for the Mab to the PSA.

15. Step 13 was repeated.

16. The Mab to the PSA at a concentration of 1.6 mg/ml (as supplied) was deposited on the fiber and incubated for 45 minutes. This allows the protein A to bind to the Mab.

17. Step 13 was repeated.

18. The LPG was immediately immersed into the lowest PSA concentration for 45 minutes.

19. Step 13 was repeated.

20. The same procedure was performed for each concentration of PSA.

Figure 5-14 shows the results of this PSA experiment. As can be seen, the smallest detectable concentration of PSA was 0.14 mg/ml (120 μg/ml or 120000 ng/ml). For this concentration, there was a 0.213 dB shift or a 5% decrease in the transmitted light intensity at the resonant wavelength. Obviously, this is not nearly sufficient for clinical detection, which requires 4.0 ng/ml at least. There is great room for improvement in this system which will be discussed later.

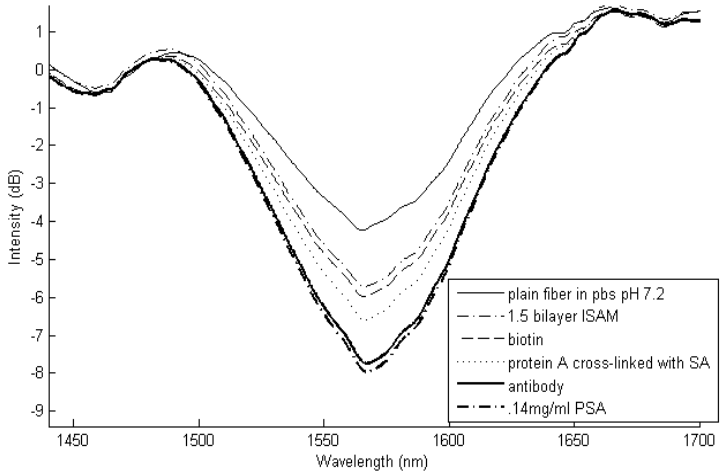

Figure 5-14: (a) Study of sensitivity vs. concentration of PSA by utilizing optical -intensity based biosensor and biotin-protein A/streptavidin system [bare LPG->ISAM-> biotin ->Protein A/SA -> Mab to PSA -> PSA], measured in PBS.

5.3.3 Experimental Procedure for Direct Cross-linking PSA Sensor

It was suggested by biochemist Dr. Rik Obiso to perform an experiment where the Mab to the PSA was directly cross-linked to the outer layer of ISAM film.

5.3.3.1 Direct Crosslinking PSA Biosensor Chemistry

Figure 5-15 illustrates the chemistry involved in the direct crosslinking PSA biosensor. The figure is not drawn to scale. Again, the binding procedure for the ISAM on the LPG is the same as mentioned earlier in Section 5.2.2.1. This time, however, the Mab was mixed with EDC and Sulfo-NHS. The EDC reacts with the carboxyl group on the Mab to form an amine-reactive intermediate group. The intermediate is unstable in aqueous solution. The addition of Sulfo-NHS stablilizes the amine-reactive intermediate

by converting it to an amine-reactive sulfo-NHS ester. The new amine-reactive sulfo-NHS ester has sufficient stability to permit two-step crosslinking procedures, which allows the carboxyl group on the Mab to remain unaltered. Since this is the case, the amine group on the PAH can combine with the new intermediate to form a stable amide bond with the Mab. Once the Mab is linked to the PAH then the PSA can be deposited and bind to the Mab.

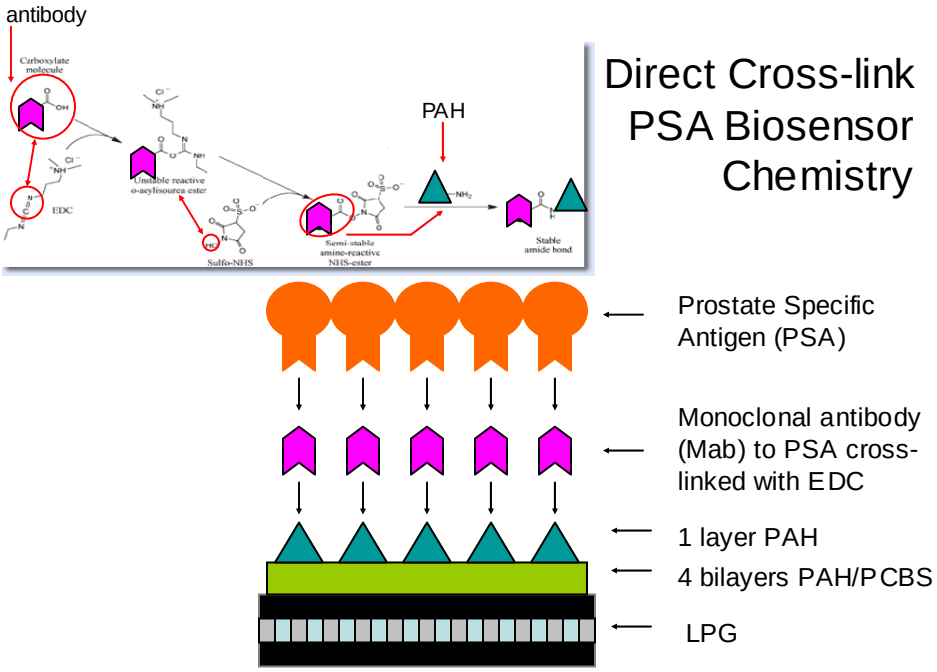

Figure 5-15: Chemistry involved in the binding kinetics of the direct crosslink PSA biosensor.

The experimental procedure was as follows:

1. The LPG spectrum was taken at room temperature in PBS solution prior to any film deposition.

2. PAH and PCBS ISAM films were deposited onto the LPG with the outermost layer being PAH. In this experiment, 4.5 bilayers of PAH/PCBS at pH 7.0/7.0 were deposited onto the LPG. The spectrum was taken at room temperature in PBS.

3. 6 μl of antibody at a concentration of 1.6 mg/ml was added to 34 μl of PBS at pH 6.0.

4. 10 mg of EDC was dissolved into 10 ml of PBS at pH 6.0.

5. 40 μl of the EDC solution was added to the antibody solution. EDC enables the Mab to the PSA to covalently link to the amines on the outer PAH layer of the ISAM film.

6. 10 mg of sulfo-NHS was dissolved into 10 ml of PBS at pH 6.0.

7. 60 μl of NHS solution was added to the antibody/EDC solution.

8. Waited 15 minutes for reaction to take place at room temperature.

9. Put 160 μl of (3-Mercaptopropyl)-trimethoxysilane into 1440 μl of PBS at pH 6.0.

10. 40 μl of 3-merc-tri-silane solution was added to the NHS/antibody/EDC solution to stop the reaction between the antibody, EDC, and NHS.

11. Placed the NHS/antibody/EDC/(3-Mercaptopropyl)-trimethoxysilane solution onto the fiber.

12. Incubated solution for 1.5 hours.

13. The LPG was immersed in the Sodium Phosphate buffer/PBS buffer for 3 minutes. Then, the LPG was rinsed with Sodium Phosphate buffer/PBS buffer and the LPG spectrum was taken at room temperature in PBS.

14. The LPG was immediately immersed into the lowest PSA concentration and incubated for 45 minutes.

15. Step 13 was repeated.

16. The same procedures were performed for each concentration of PSA.

Figure 5-16 a shows the results of the first direct cross-linking PSA experiment. As can be seen, for this experiment, the smallest detectable concentration of PSA was 0.014 mg/ml (14 μg/ml or 14000 ng/ml). For 0.014 mg/ml PSA there was a 0.311 dB shift, or a 7% decrease in the transmitted light intensity. For 0.14 mg/ml PSA concentration, there was a 2.152 dB shift, or a 39% decrease in the transmitted light intensity at the resonant wavelength. This system was able to detect a factor of 10 lower PSA concentration than the previous one. However, this is still not good enough for clinical studies. More improvement on this system is necessary, which will be examined shortly.

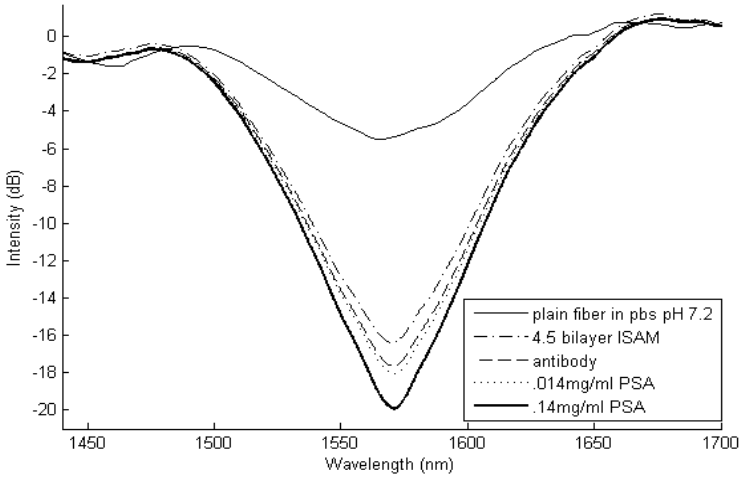

(a)

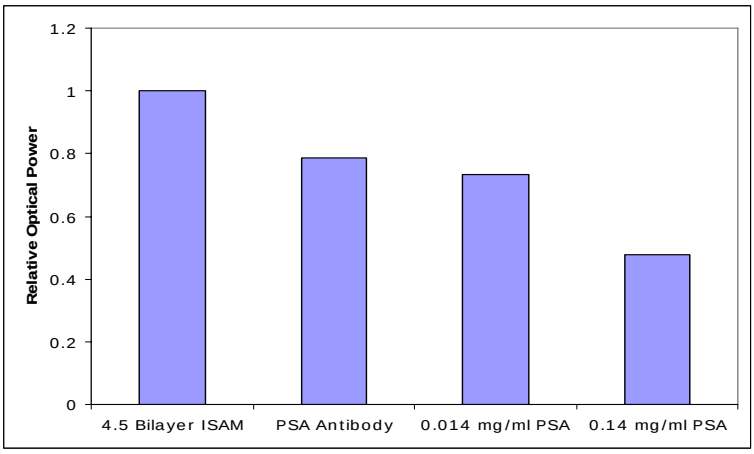

(b)

Figure 5-16: (a) Direct EDC cross-linking of carboxylates on antibody to amines on ISAM-coated fiber. 6 μl of 1.6 mg/ml antibody mixed with 34 μl PBS, then mixed with EDC and NHS. Prostate specific antigen mixed with PBS and detected at concentrations of 0.014 mg/ml and 0.14 mg/ml; (b) decrease in relative optical power after each deposition of increasingly higher PSA concentrations.

Figure 5-16 b shows more clearly the decrease in relative optical power after each deposition.

Figure 5-17 displays the result of another trial of the direct crosslinking PSA biosensor. The procedure was the same as above, but this time 5.5 bilayers of ISAM film were deposited in order to get the spectrum closer to the TAP to increase the sensitivity of the sensor. Also, this time the antibody concentration was 9.9 mg/ml, instead of 1.6 mg/ml. The other small change was that each PSA concentration was incubated 2 hours instead of 1.5 hours to ensure maximum binding. Figure 5-17 a depicts the change in LPG transmission spectrum after each deposition. IN the previous experiment, the smallest detectable PSA concentration was 0.014 mg/ml. In this experiment, the smallest detectable PSA concentration was 0.0001164 mg/ml

(0.1164 μg/ml or 116.4 ng/ml). This means that the improvements made to the procedure enhanced the sensor's sensitivity by a factor of 100. For 0.0001164 mg/ml PSA, there was a 0.334 dB shift, which corresponds to a 7.4% decrease in transmission. For the PSA concentration of 0.001164 mg/ml there was a 1.277 dB overall shift, or a 25.5% overall decrease in transmission. Finally, for 0.01164 mg/ml PSA, there was a 2.575 dB overall shift, or a 44.7% overall decrease in the light transmission at the resonant wavelength. However, in the prior experiment, for 0.014 mg/ml (14 mg/ml or 14000 ng/ml) antigen, there was only a 0.311 dB shift or a 7% decrease in intensity.

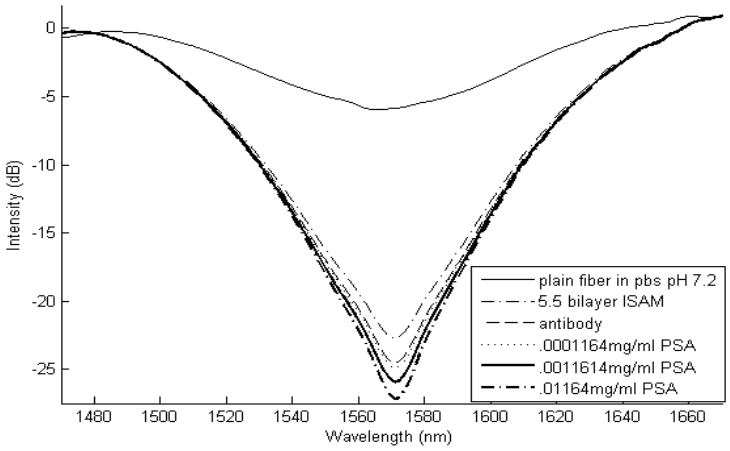

(a)

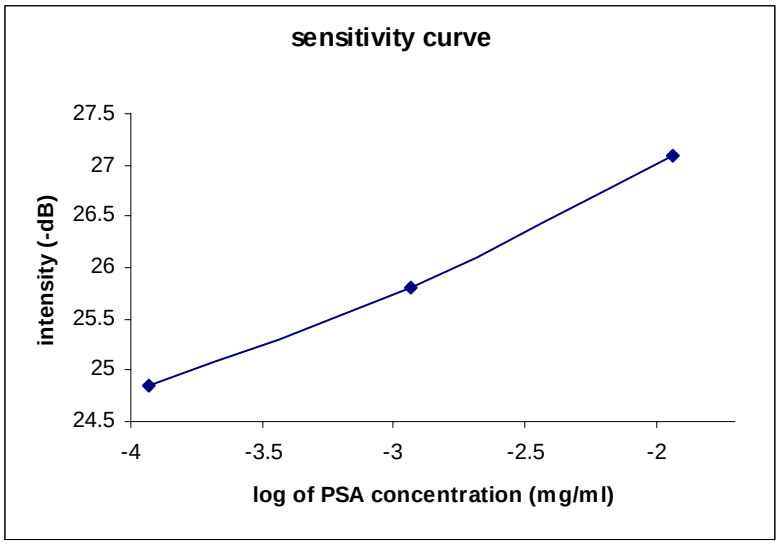

(b)

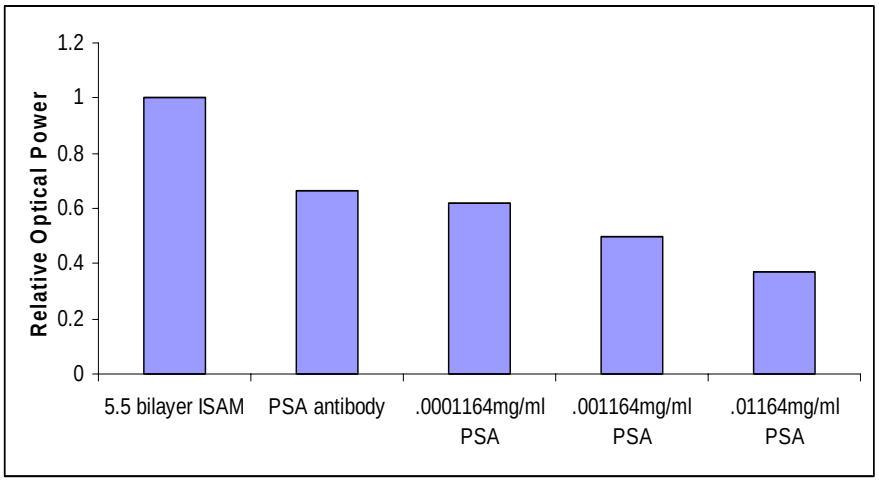

(c)

Figure 5-17: (a) Direct EDC cross-linking of carboxylates on antibody amines on ISAM-coated fiber. 6 µl of 9.9 mg/ml antibody mixed with 34 µl PBS, then mixed with EDC and NHS. Prostate specific antigen mixed with PBS and detected at concentrations of 0.0001164 mg/ml, 0.001164 mg/ml, and 0.01164 mg/ml; (b) sensitivity curve of log of PSA concentration in mg/ml; (c) decrease in relative optical power after each deposition of increasingly higher PSA concentrations.

Figure 5-17 b shows the sensitivity curve for PSA, and Figure 5-17 c illustrates the decrease in relative optical power after each deposition.

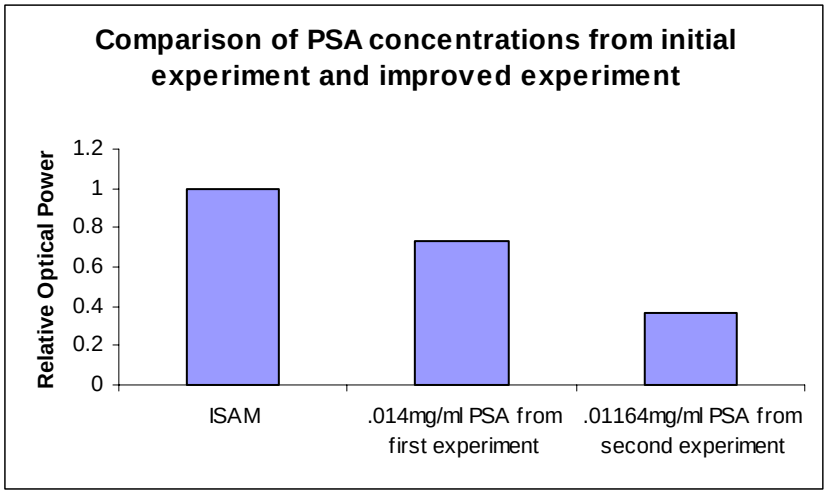

Figure 5-18: Comparison of decrease in relative optical power from the first two experiments for the PSA concentration of ~ 0.014 mg/ml.

A comparison of the decrease in relative optical power for these two experiments can be seen in Figure 5-18. The vast improvements between the two trials can be visibly observed.

I made one further improvement to the direct-crosslink procedure in an attempt to obtain better antibody coverage. In step 3 of the procedure, instead of adding 6 μl of antibody, I added 18 μl. The concentration of the antibody was again 9.9 mg/ml, instead of 1.6 mg/ml. Making this important change did, in fact, increase the antibody coverage. This can be observed in Figure 5-19. Figure 5-19 a shows the change in LPG transmission spectra after each deposition. Figure 5-19 b shows the sensitivity curve for streptavidin, and Figure 5-19 c illustrates the decrease in relative optical power after each deposition. In the previous experiment, there was only a 1.763 dB shift for the antibody which corresponds to a 33.4% decrease in the transmitted intensity. This time, however, there was a 3.252 dB shift, or a 52.7% decrease in intensity. Furthermore, increasing the

antibody coverage lead to a further factor of 10 increase in the sensitivity of the sensor. Previously, the lowest detectable concentration of PSA was 0.0001164 mg/ml (0.1164 μg/ml or 116.4 ng/ml). This time, the lowest detectable concentration was 0.00001164 mg/ml (0.01164 μg/ml or 11.64 ng/ml) PSA. For this concentration, there was a 0.42 dB shift, or a 9.2% decrease in the intensity. Last time, for the PSA concentration of 0.0001164 mg/ml there was only a 0.334 dB shift, which corresponds to a 7.4% intensity decrease. However, this time for 0.0001164 mg/ml there was a 0.935 dB shift, or a 19.4% decrease in intensity.

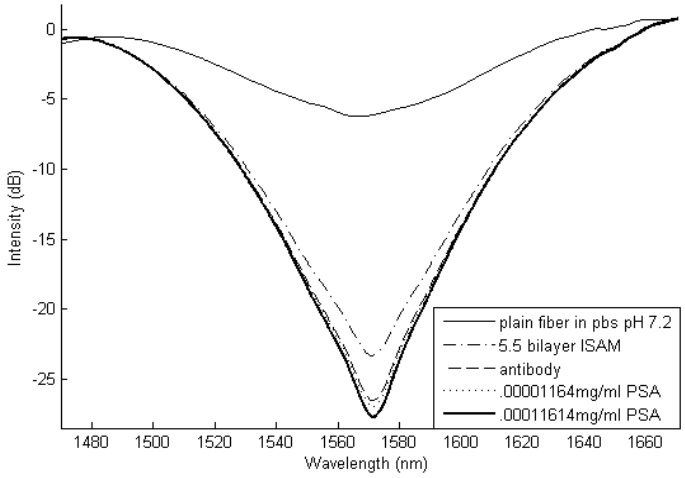

(a)

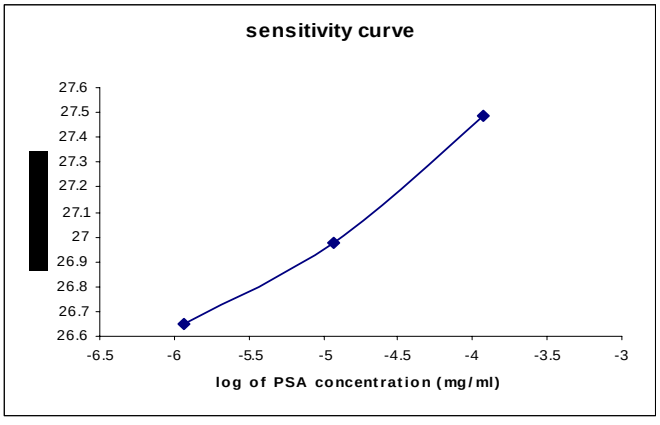

(b)

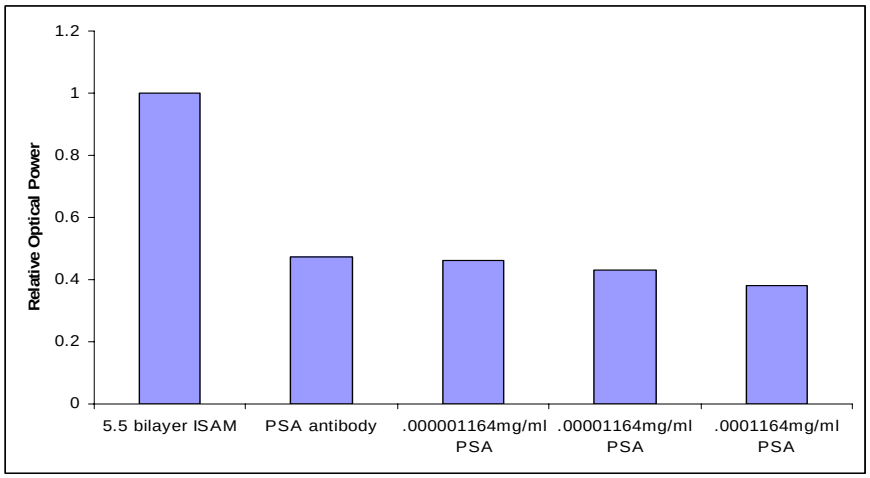

(c)

Figure 5-19: (a) Direct EDC cross-linking of carboxylates on antibody amines on ISAM-coated fiber. 18µl of 9.9 mg/ml antibody mixed with 34µl pbs, then mixed with EDC and NHS. Prostate specific antigen mixed with PBS and detected at concentrations of 0.000001164 mg/ml, 0.00001164 mg/ml, and 0.0001164 mg/ml; (b) sensitivity curve of log of PSA concentration in mg/ml; (c) decrease in relative optical power after each deposition of increasingly higher PSA concentrations.

Figure 5-20 displays the vast improvement between the prior experiment and the improved one. This is visible in the decrease in relative optical power for 0.0001164 mg/ml (116.4 ng/ml) PSA for the two experiments.

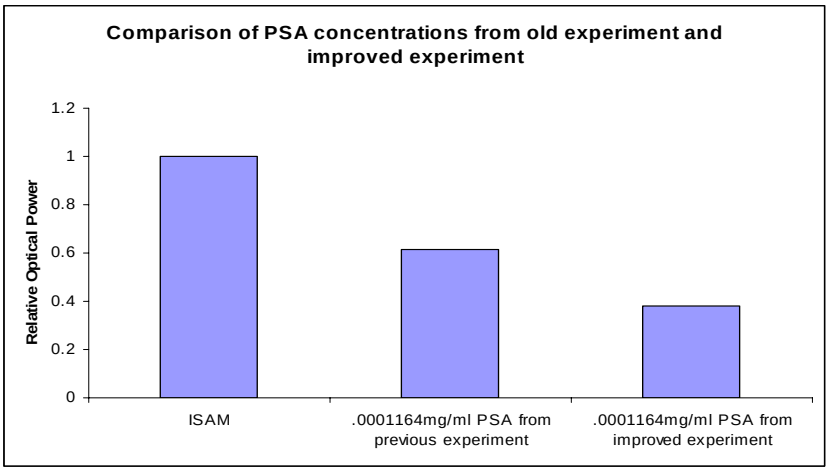

Figure 5-20: Comparison of decrease in relative optical power from the previous two experiments for the PSA concentration of 0.0001164 mg/ml.

With all of the improvements I made upon this PSA experiment, the smallest detectable PSA concentration was 11.64 ng/ml. Medical analysis requires a PSA detection threshold of about a factor of 3 lower than this. However, additional improvements on the PSA sensor can still be made. Several options to increase sensitivity would be: to work closer to the TAP because this is the most sensitive point in the grating, devise a way to get even more antibody binding, or use silica nanoparticles as the sensor platform instead of the PCBS to provide greater surface coverage, etc. Making these adjustments should lead to at least a factor a ten greater sensitivity, which would put this PSA sensor in the same ranks as (or higher than) the current clinical PSA sensors.

5.4 Summary

Preliminary results were obtained for the anthracis protective antigen-antibody biosensor. The smallest detectable antigen concentration was only 0.14 mg/ml. This experiment was performed very early on in the course of this work before the more sensitive TAP LPGs were obtained and before various aspects of the sensor platform were optimized. Hence, the results are not sufficient for environmental detection purposes. However, the experiment does verify the concept of the ISAM-coated TAP LPG biosensor.

The biotin-streptavidin system was next used as a model in order to develop approaches for optimization of the biosensor platform. Work done by another student prior to this thesis achieved a sensitivity of 0.0125 mg/ml streptavidin. Improvements were thus made on the biotin-streptavidin biosensor system to increase sensitivity. The first was to utilize the more sensitive TAP LPGs obtained from OFS Laboratories. The

second was to deposit a thicker ISAM film on the fiber to push the spectra closer to the TAP, which is the most sensitive point in the grating. Next, a more water-soluble biotin with a longer spacer arm was used to achieve better biotin coverage on the fiber, which led to more available binding sites for the streptavidin. All of these improvements yielded the detection of 12.0 ng/ml streptavidin.

One of the main projects in this thesis was to develop a biosensor for the early diagnosis of prostate cancer using ISAMs coated on TAP LPGs. The first experiment involved a complicated approach using biotin and streptavidin, and crosslinking the streptavidin to Protein A known for its ability to bind to the monoclonal antibody to prostate specific antigen. This method yielded a PSA detection limit of only 0.14 mg/ml PSA. It was decided that an easier, more direct approach to the PSA biosensor should be used. This involved directly crosslinking the Mab to the PSA to the ISAM film on the LPG. This method proved more successful than the previous one and was thus optimized further. Several improvements were made for this particular sensor design. First, a thicker ISAM film was again deposited on the fiber to push the spectra closer to the TAP to increase sensitivity. Then, both the concentration of the Mab to the PSA and the amount used were increased to obtain better antibody coverage on the fiber and increase the available binding sites for the PSA. These improvements yielded a PSA detection limit of 11.64 ng/ml. Although this is not quite at the 4 ng/ml level utilized in clinical diagnosis, a number of other improvements have been suggested that should allow at least another order of magnitude decrease in the lowest detectable concentration.

---

[1] http://en.wikipedia.org/wiki/Anthrax_toxin

[2] http://biology.kenyon.edu/BMB/Chime2/2001/anthrax/FRAMES/start.htm#STRUCTURE

[3] http://medarex.com/Development/Structure.htm

[4] http://www.vectorlabs.com/

[5] N. P. Huang, J. Voros, S. M. D. Paul, M. Textor and N. D. Spencer, "Biotin-Derivatized Poly(L-lysine)-g-poly(ethylene glycol): A Novel Polymeric Interface for Bioaffinity Sensing," *Langmuir* **18**, 220 (2002).

[6] http://www.vectorlabs.com/products.asp?catID=28&locID=0

[7] http://www.ofsoptics.com/

[8] Zhiyong Wang, Ph D Dissertation, (Virginia Tech, 2005).

[9] cells.http://www.cancer.gov/Common/PopUps/popDefinition.aspx?id=46066&version=Patient&language=English National Cancer Institute

[10] http://www.cancer.gov/cancertopics/factsheet/Detection/PSA

[11] K. W. K. Watt, P. J. Lee, T. M'Timkulu, W. P. Chan, R. Loor, "Human prostate-specific antigen: Structural and functional similarity with serine proteases," *Proc. Natl. Acad. Sci. USA*, **83**, 3166-3170, 1986.

[12] http://en.wikipedia.org/wiki/Prostate_specific_antigen

[13] http://www.cancer.gov/cancertopics/factsheet/Detection/PSA

[14] Brewer, M. K., "Prostate Specific Antigen," Marcel Dekker Inc., (2001).

[15] R. J. Babian, H. Miyashita, R. B. Evans, E. I. Ramirez. The distribution of PSA in men without clinical or pathological evidence of prostate cancer: Relationship to gland volume and age. J Urol **147**:837-840, 1992.

[16] J. E. Oesterling, S. J. Jacobsen, G. G. Klee, K. Petterson, T. Piironen, P. A. Abrahamsson, U. H. Stenman, B. Dowell, T. Lovgren, H. Lilja,. Free, complexed and total serum PSA: The establishment of appropriate reference ranges for their concentrations and ratios. J Urol **154**:1090-1095, 1995.

[17] http://www.piercenet.com/products/browse.cfm?fldID=02030378&WT.mc_id=keynum

[18] http://en.wikipedia.org/wiki/Amine

[19] http://en.wikipedia.org/wiki/Maleimide

[20] http://en.wikipedia.org/wiki/Thioether

[21] http://en.wikipedia.org/wiki/Protein_A

Chapter 6: Fiber Optic pH Sensor

In collaboration with Prime Photonics (Blacksburg, Va), we received funding to explore whether the ISAM LPG sensor platform could be used to sense pH. The basic concept is based on the sensitivity of ISAM films to pH. The thickness of each layer in an ISAM film depends on the pH at which it is deposited as a result of change in the charge density in the polyelectrolytes, as described previously in Section 3.1.3. More significantly here, ISAM films have also exhibited swelling behavior in response to pH or salts as described below. The swelling should, in principle, be detectable due to the resultant change in thickness and refractive index (caused by density changes).

6.1 Background

For several years now there has been much research regarding optical fibers for use as pH sensors. This type of sensor has some benefits such as safety for in vivo pH measurement[1,2], insensitivity to electromagnetic fields[1,2], and the ability to sense in remote areas[1]. Thus far, unfortunately, there have not been many designs for this type of sensor. Generally, the basis for the majority of the fiber-optic pH sensors is a coating adsorbed on the surface of the fiber that varies with respect to pH. The pH creates reversible effects within the sensing layer's optical properties (fluorescence, absorbance, refractive index).[1] These changes can be observed as changes in reflected or transmitted optical power. There are some optical pH sensors that rely on indicator dyes that are immobilized on the surface of the fiber. Other pH sensors use hydrogels to detect corrosion. This method needs polymers to be thermally cross-linked, which adds to

complexity. The sensors that rely on indicator dyes have several difficulties due to the difficulty in immobilizing the dyes and the necessity for optical sources with enough power, generally in the ultraviolet–visible (UV/VIS) spectral range.[1] The efficiency of semiconductor light sources decreases drastically with decreasing wavelength. Near-infrared indicators have been implemented in the creation of optical sensors. They are very efficient and readily available, but using indicators loaded on a polymeric matrix are prone to leaching and bleaching of the indicator.[1] This hinders the stability of the sensor. This issue can be fixed by covalently attaching dye molecules. However, this process is very difficult and results in decreased sensor sensitivity. The deposition method is also complex and it is difficult to control the thickness. Controlling the thickness is key because the overlay thickness affects the response time.

The ISAM deposition technique is most often used for creating organic or organic/inorganic hybrid thin films because the thickness can be controlled very precisely on the nano-scale level. This technique allows for the formation of uniform and smooth coatings on the optical fiber surface. The adsorption is based upon the interactions between polyelectrolyte solutions of opposite charges. When the polyelectrolytes used in the deposition are weak, the linear charge density is strongly dependent upon pH. Thus, the characteristics of the nanofilm are also pH dependent.[3] Shiratori and Rubner (2000) have examined poly(acrylic acid) (PAA)/poly-(allylamine hydrochloride) (PAH) multilayers in depth. They showed that the thickness and organization of the layers is sensitively dependent upon the pH.[4] This implies that the charge of the polyacid can be changed during its adsorption onto a polycation layer and after it has been deposited.[4] This alters the layer's thickness, which in turn changes its optical properties and the

LPGs transmission characteristics.

As we begin this project, Corres *et al.*[1,2] published two papers purporting pH detection using ISAM films on LPGs that was obtained because the thin films adsorbed on the LPG surface that are sensitive to the target parameter and the polymeric matrix adjusts its optical thickness when the pH is altered.[1,2]

Their sensor functions based on the idea that the sensitive layer swells when the pH is altered. Depositing the swellable ISAM film onto the LPGs surface leads to a shift in wavelength of the attenuation bands which can, in principle, be utilized to measure the pH. In their experiments they used an SMF-28 fiber with a LPG of 320 μm period. Their grating length was 25 mm. Their experimental set up was very similar to ours, with one end of the fiber connected to a broadband light source and the other end connected to an optical spectrum analyzer (OSA). They used PAH and PAA as their polyelectrolytes. The films were deposited onto the fiber using the ISAM deposition technique. Through experimentation, Corres *et al.*[1,2] found that the optimal sensitivity point occurred when the films were around 400 nm thick, which corresponded to 25 bilayers.[1]

Figure 6-1 shows the LPGs response to pH when using buffers in the pH range of 4.0-8.0. They limited the pH range so the film would not be degraded (which can occur at very low and very high pHs). The response they observed can be broken into two segments with respect to neutral pH. In the pH range 4.0-7.0, the response is monotonic. In this area, when the pH increased the resonant wavelength increased, and there was a higher attenuation of the resonance bands. In the second area, when the pH is higher than 7.0, there is a shift towards shorter wavelengths. They believe that this could be caused by an increase in the degree of ionization of the PAA as the pH increases. The maximum

ionization is achieved near neutral pH. As the charge density increases, highly ionically cross-linked films are created. This causes the film to contract. Thus, higher pHs lead to thinner films, while lower pHs lead to thicker films.

In the study of Corres *et. al.*[1,2], the pH's from which the PAH and PAA were fabricated were both 4.5, which is approximately the value that they found yields the maximum thickness per bilayer. They state that when the sensor is placed in a buffer of higher pH, the thickness of the layers should decrease, which can be seen in their results in Figure 6-1 below. Corres *et. al.*[1,2] also state that the changes in the spectra generated by the change of the polymer's ionization state are extremely reproducible and reversible.

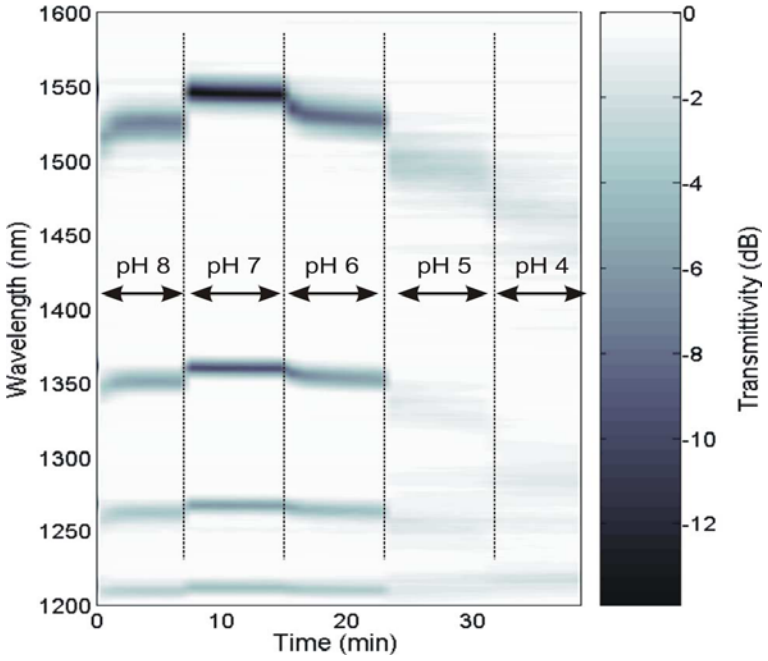

Figure 6-1: Response of PAH/PAA pH sensor of Corres *et al.*[1]

Corres *el al.*[1], performed a test where they alternated placing the sensor in buffers of pH 8.0 and pH 5.0 to measure the response time. The rise time was 120 s and the fall time was 270 s. They say that the rise and fall times are a result of the diffusion of the

buffer solutions in the polymeric matrix.[1] They also note that there is a slow drift in the response of the sensor, which may be caused by desorption of bilayers. They suggest that a thermal treatment would increase the sensor's stability, because this was done in Del Villar *et al.*[5] Corres *et al.*[1,2] used a conventional LPG rather than a TAP LPG. We therefore, decided to first try to duplicate their conditions, but using a TAP LPG, which should then provide us with higher sensitivity.

6.2 Experimental Results Using Colored Buffer Solutions

A great deal of time was spent trying to repeat the findings of Corres *et al.*[1,2], since they indicated PAH/PAA ISAM films at pH 4.5 could exhibit significant pH-induced swelling. The results of the first experiment can be seen in Figure 6-2. The materials used for this experiment are listed in Table 1.

Company	pH	Materials	Percentage of Material (%)
Jade Scientific	4	Water	97-98
		Potassium acid phthalate	1-2
		Propylene glycol	< 1
		FD & C red No. 40	< 1
LabChem Inc	5	Potassium hydrogen phthalate	1.02
		Sodium hydroxide	0.09
		formaldehyde	0.04
		Water	Balance
LabChem Inc	6	Potassium phosphate monobasic	0.68
		Sodium hydroxide	< 1
		Water	Balance
Jade Scientific	7	Potassium phosphate monobasic	0.72
		Sodium hydroxide	0.12
Jade Scientific	10	Water	>> 99

		Boric acid	< 1
		Potassium hydroxide	< 1
		FDC blue #1	< 1

Table 1: Detailed description of buffers used for experimentation.

The experimental procedure was as follows:

Day 1:

1. The LPG spectrum was taken at room temperature in PBS solution pH 7.2 prior to any film deposition.

2. PAH and PAA ISAM films were deposited onto the LPG. In this experiment, 15 bilayers of PAH/PAA were deposited onto the LPG. For the first 10 bilayers the pH of the PAH was 4.0 and the pH of the PAA was 6.0. For the last 5 bilayers the pH of the PAA was adjusted to 5.25 to create thicker layers.

3. The spectrum was taken at room temperature in PBS solution pH 7.2.

Day 2:

1. The LPG spectrum was taken at room temperature in PBS solution pH 7.2.

2. The fiber was annealed in an oven at 120 ^{0}C for 2 hours.

3. The fiber was removed from the oven and allowed to cool for 5 minutes.

4. The LPG spectrum was then taken at room temperature in DI water at pH 7.0.

5. The fiber was immersed in the pH 4.0 buffer.

6. The LPG spectrum was taken after 15 minutes of submersion in the buffer when the signal became stable.

7. The fiber was rinsed with DI water.

8. The fiber was immersed in the pH 5.0 buffer.

9. The LPG spectrum was taken after 5 minutes of submersion in the buffer when the signal became stable.

10. Steps 7, 8, and 9 were repeated for DI of pH 6.0 and 7.0.

11. The fiber was then re-immersed in pHs 6.0, 5.0, and 4.0 respectively following the same procedure as above.

The annealing step was done because it was suggested in a paper by Del Villar *et. al*.[5] that an ISAM-coated LPG baked at 100 ^{0}C for at least 2 hours exhibits more stable performance. Otherwise, an ongoing destruction of the ISAM films can occur when the fiber is immersed in buffer solutions of different pHs as discussed in [5].

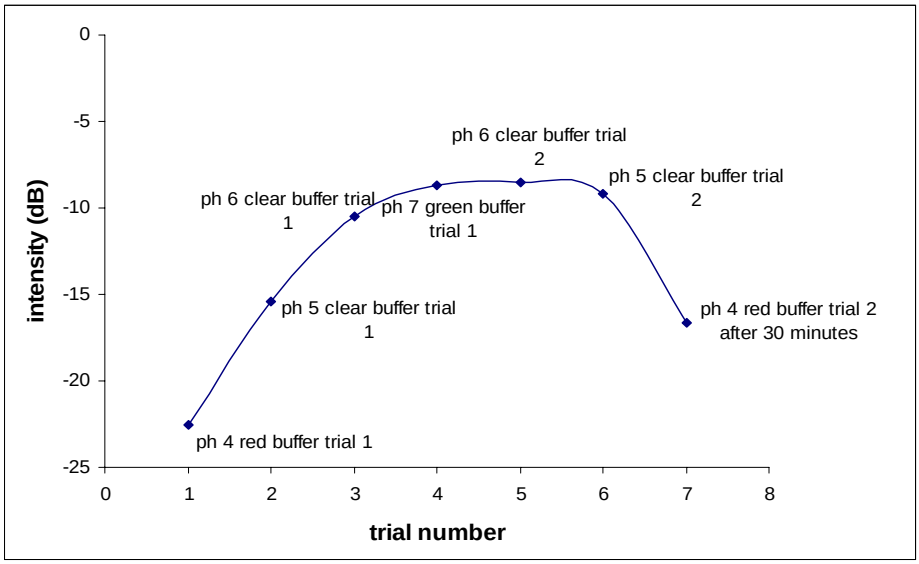

Figure 6-2: Changes in optical intensity at the TAP after soaking ISAM coated LPG in the various buffer solutions described in Table 1.

Figure 6-2 shows the light intensity at a wavelength of 1570 nm (which is the wavelength of strongest attenuation) during immersion in the various buffer solutions. It can be seen that pH 4.0, trial 1 begins at a very low intensity (~ -23 dB). This implies that the outer ISAM layer (PAA) is less charged and the cations in the pH buffer travel into the film and bind with the anion groups in the film to produce thicker layers. Consequently, the thicker layers lead to a decrease in intensity. As the pH is increased to 7.0, the outer ISAM layer (PAA) becomes more charged. Hence, the layers have a stronger attraction for one another, and consequently, are thinner. Another way of looking at it is the higher pH creates thinner films with fewer loops and trains due to electrostatic repulsion between the monomer units.[6] After pH 7.0 was reached, the fiber was immersed in pH 6.0 again. There was virtually no change in the intensity between pH 7.0 and pH 6.0 trial 2. Both were at about -9 dB. In principle, the films should have gotten thicker and the intensity should have decreased to that of pH 6.0 trial 1, which was around -10 dB. However, this was not the case. Then, the fiber was again immersed in pH 5.0. There was only a slight decrease in the intensity this time to a little over -10 dB, but not nearly as much of a decrease as pH 5.0 trial 1, which was recorded at about -15 dB. Lastly, the fiber was immersed in pH 4.0 again. As can be seen in Figure 6-2, the intensity did start to decrease, implying that the layers were getting thicker. However, the response time was extremely slow. The fiber was left in the pH 4.0 buffer for 30 minutes and the signal never stabilized. The intensity kept decreasing at a very slow rate and may have decreased to the same intensity as pH 4.0 trial 1, had the fiber been left to soak even longer. However, the time required for this was undesirably long.

These results follow the results of Corres *et. al.*[1,2] to some extent. They do show

that the films are thicker at lower pH and thinner at higher pH, which is what Corres *et. al.*[1,2] found as well. However, my results do not show repeatability, which is important. This may be due to the inordinately slow response time in going from higher pHs to lower pHs. Further investigation would be needed to verify this point.

In this next experiment, the procedure was essentially the same except for three changes. The first change was that the fiber was not annealed after the ISAM films were deposited this time. The annealing was not done because it was thought that it could potentially be causing a problem. The second difference was that the experiment was performed in one day instead of two. The third change was that the fiber was immersed in a DI water bath of pH 1.8 for 1 minute after the ph 7.0 trial 1. This was done in hopes of speeding up the slow response time that occurred in the previous experiment. The results can be seen in Figure 6-3.

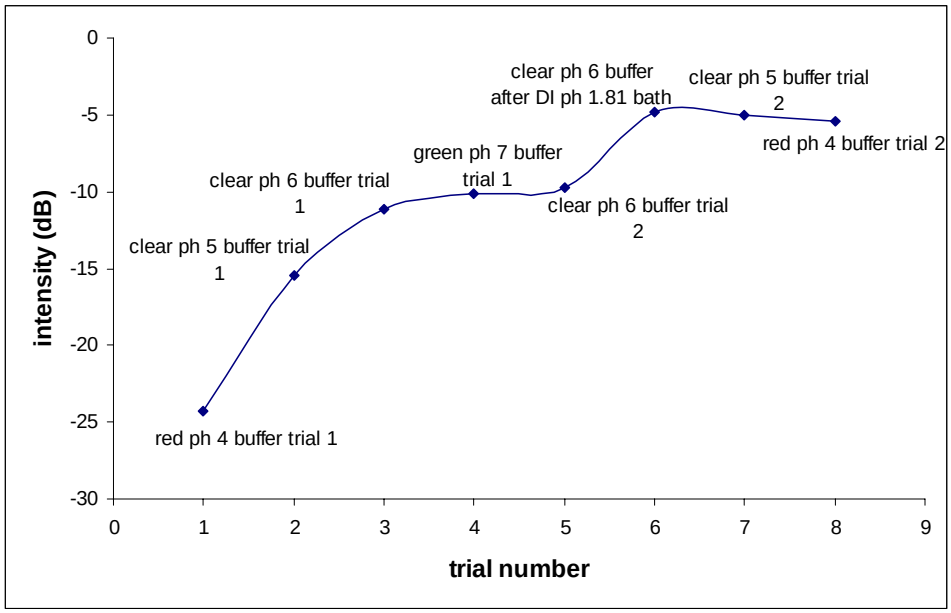

Figure 6-3: Changes in optical intensity at the TAP after soaking ISAM coated LPG in the various buffer solutions described in Table 1.

In this experiment, the first part of the results is similar to the previous experiment. Again, the intensity for pH 4.0 started at a low intensity, implying thicker layers. The layers became thinner as pH 7.0 was reached. Then, the fiber was immersed in pH 6.0 for the second time and the intensity was not much different than that of pH 7.0. This is the same problem that occurred in the prior trial. In attempt to correct this, the fiber was immersed in a DI bath of pH 1.8 for one minute. The idea here is that exposure to low pH would swell the film and "reset" it so that it could contract again when exposed to higher pH. This very acidic solution, however, appeared to remove all of the ISAM films. This can be observed from the increase in intensity after the acidic DI bath, to the intensity observed for the bare LPG implying that no films remained. Furthermore, when the fiber was re-immersed in pHs 5.0 and 4.0, virtually no change in intensity from the DI pH 1.8 reading was observed. Thus, the attempt to increase the response time when going from high pH to low pH was not successful. Upon further investigation, a paper was found that showed when the fiber is exposed to DI at pH of 1.75 or lower, the multilayers are dissolved/removed entirely from the substrate to reveal bare fiber.[7]

In the next experiment, the procedure was slightly different from the previous two. The PAH/PAA ISAM bilayers were deposited in the same manner as previously done. This time, however, the fiber was annealed in attempts to obtain more stable readings as done in the first experiment. This experiment was performed in one day, which is the same as the second experiment. The main difference between this experiment and the previous two was that in this experiment, the fiber was immersed in each pH twice in a row, rinsing with DI in between trials. Also, only buffers of pH 4.0

and 7.0 were used here. This is explained more clearly in the detailed procedure. In the previous two experiments, the fiber was immersed in the buffers in ascending order first, then descending order. Also, in this experiment, the fiber was left to soak in DI pH 7.0 overnight. The detailed procedure is:

1. The LPG spectrum was taken at room temperature in PBS solution pH 7.2 prior to any film deposition.

2. PAH and PAA ISAM films were deposited onto the LPG. In this experiment, 14 bilayers of PAH/PAA were deposited onto the LPG. For the first 8 bilayers the pH of the PAH was 4.0 and the pH of the PAA was 6.0. For the last 6 bilayers the pH of the PAA was adjusted to 5.25 to make thicker layers.

3. The spectrum was taken at room temperature in PBS pH 7.2.

4. The fiber was annealed in an oven at 120 ^{0}C for 2 hours.

5. The fiber was removed from the oven and allowed to cool for 5 minutes.

6. The LPG spectrum was then taken at room temperature in DI water at pH 7.0.

7. The fiber was immersed in the pH 4.0 buffer.

6. The LPG spectrum was taken after 10 minutes of submersion in the buffer when the signal became stable.

7. The fiber was rinsed with DI water.

8. The fiber was immersed in the pH 4.0 buffer again.

9. The LPG spectrum was taken after 10 minutes of submersion in the buffer when the signal became stable.

10. Steps 7, 8, and 9 were repeated for the pH 7.0 buffer.

11. Fiber was immersed in DI pH 7.0 overnight.

12. Rinsed fiber with DI.

13. Immersed fiber in DI pH 7.0 and took spectrum.

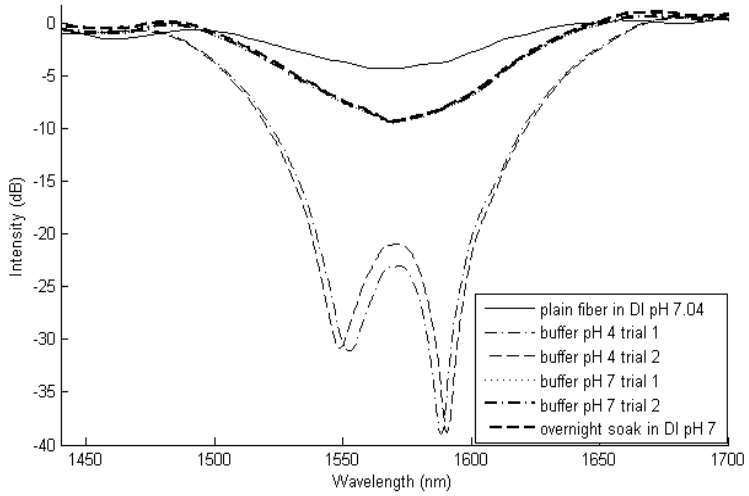

Figure 6-4: Changes in optical intensity after soaking ISAM coated LPG in the various buffer solutions described in Table 1.

The fiber was first immersed in the pH 4.0 buffer and the intensity decreased, indicating thicker layers were present. Then, the fiber was rinsed with DI water and a baseline reading was taken in the DI water. Next, the fiber was immersed in the pH 4.0 buffer again. By examining Figure 6-4 it can be seen that the spectra for both trials of pH 4.0 are very similar, indicating repeatability. Next, the same procedure was followed for the pH 7.0 buffer. There was an increase in intensity, indicating thinner layers. Furthermore, the spectra for both pH 7.0 trials are almost identical. Then, the fiber was allowed to soak in DI water of pH 7.0 overnight. When the spectrum was taken the next

day, it too was almost identical to the two pH 7.0 buffer trials. Thus, this experiment is consistent with those of Corres *et. al.*[1,2], and it also shows good repeatability. Stability is also shown due to the fact that the spectrum did not change when the fiber was allowed to soak in DI water for 24 hours.

6.3 Experimental Results Using pH Adjusted DI Water

The previous experiments were all performed using the colored buffer solutions described in Table 1. Corres *et. al.*[1,2] used buffers for their pH experiments as well. Thus, we initially tried to reproduce their results using buffers. However, we were only partially successful. More importantly, though, in order to be a true pH sensor, we should be able to detect changes in pH-adjusted DI water rather than buffer solutions. The experiment in Figure 6-5 is an attempt to do that. The procedure was as follows.

Day 1:

1. The LPG spectrum was taken at room temperature in PBS solution pH 7.2 prior to any film deposition.

2. PAH and PAA ISAM films were deposited onto the LPG. In this experiment, 9 bilayers of PAH/PAA were deposited onto the LPG. The pH of the PAH was 5.0 and the pH of the PAA was 6.0.

3. The spectrum was taken at room temperature in PBS solution pH 7.2.

Day 2:

1. The LPG spectrum was taken at room temperature in PBS solution pH 7.2.

2. The fiber was annealed in an oven at 120 ^{0}C for 2 hours.

3. The fiber was removed from the oven and allowed to cool for 5 minutes.

4. The LPG spectrum was then taken at room temperature in DI water at pH 7.0.

5. The fiber was immersed in DI pH 4.0.

6. The LPG spectrum was taken after 10 minutes of submersion in the DI when the signal became stable.

7. The fiber was rinsed with DI water.

8. Steps 5, 6, and 7 were repeated for DI of pH 5.0, 6.0, and 7.0.

9. Steps 5, 6, and 7 were repeated for DI of pH 6.0, 5.0, and 4.0.

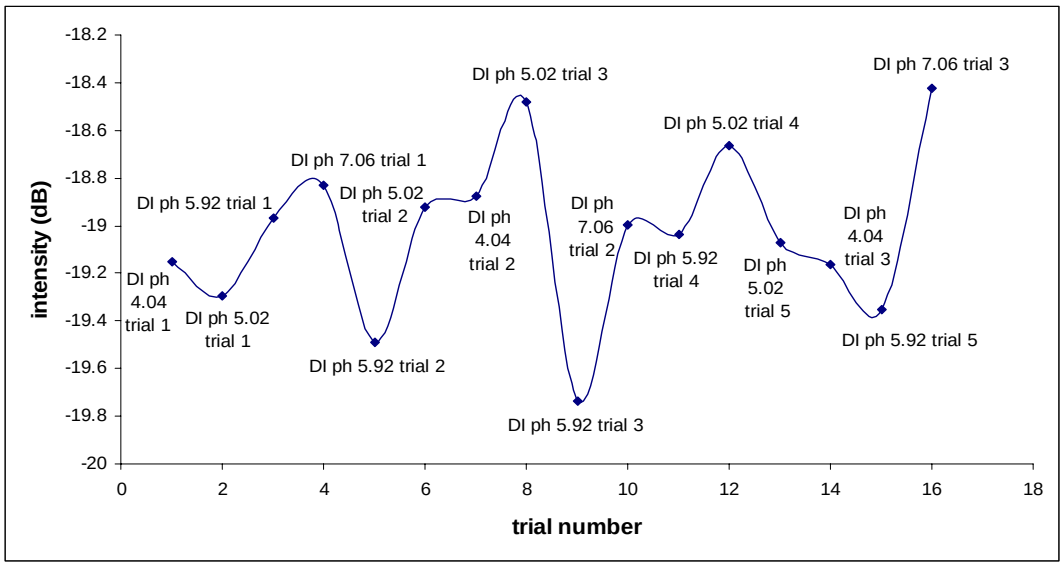

(a)

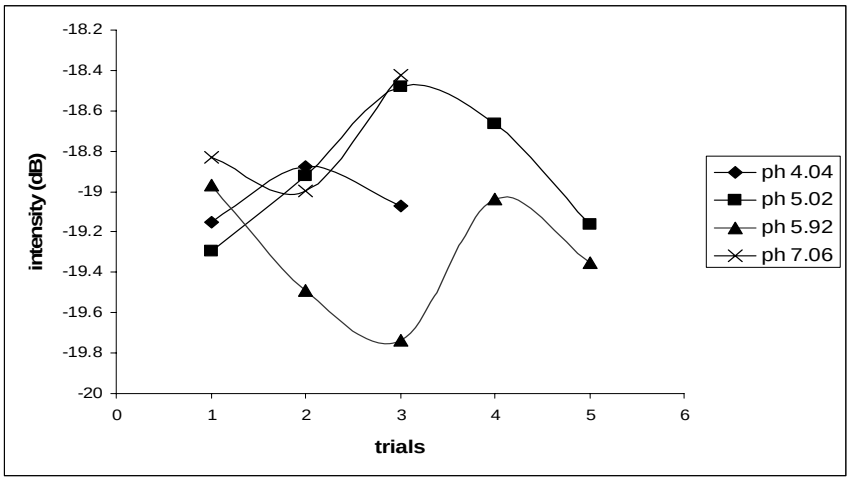

(b)

Figure 6-5: (a) Changes in optical intensity at the TAP after soaking ISAM coated LPG in pH adjusted DI water; (b) intensity values at the TAP at each pH for each trial.

As can be seen in Figure 6-5 a, there was no clear repeatability for this experiment. Furthermore, the changes in intensity are extremely small compared to the results for the buffer solutions. Figure 6-5 b shows the intensity values for all the trials at each pH. Ideally, these should be fairly straight lines with DI pH 4 having the lowest intensity and DI pH 7.0 having the highest intensity. Instead, the results appear to be simply small random variations.

The results depicted in Figure 6-6 are almost identical to the previous one in procedure except this time a different LPG was used in case something might have been wrong with the previous LPG. In this case, for the first 4 bilayers the pH of the PAH was 5.0 and the pH of the PAA was 6.0. For the remaining 5 bilayers, the pH of the PAA was adjusted to 5.26 to create thicker layers.

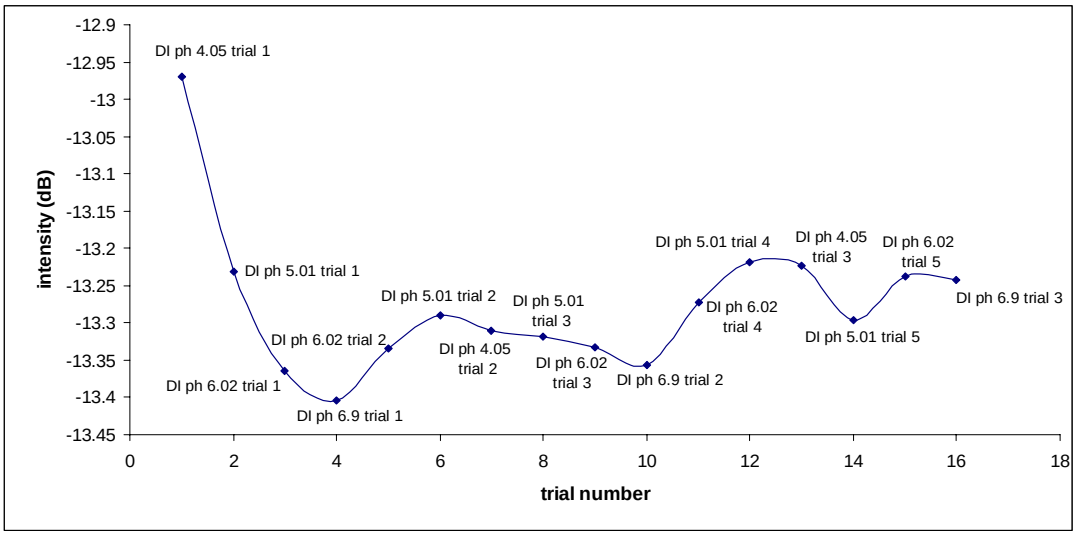

(a)

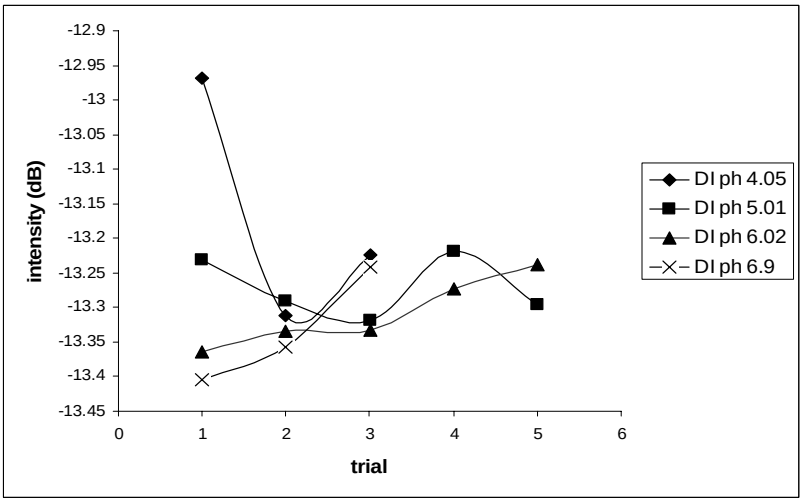

(b)

Figure 6-6: (a) Changes in optical intensity at the TAP after soaking ISAM coated LPG in pH adjusted DI water; (b) intensity values at the TAP at each pH for each trial.

Again, with this experiment the changes are small and there is no clear repeatability.

The next experiment was slightly different from the previous ones. The main differences in this experiment were that PCBS was used instead of PAA, the fiber was not heated, and the fiber was only left in each DI solution 5 minutes. The procedure was as follows.

Day 1:

1. The LPG spectrum was taken at room temperature in PBS solution pH 7.2 prior to any film deposition.

2. PAH and PCBS ISAM films were deposited onto the LPG. In this experiment, 7 bilayers of PAH/PCBS were deposited onto the LPG. The pHs of the PAH and PCBS were both 7.0. PCBS was used rather than PAA this time with the thought that its higher refractive index might lead to larger changes in the LPG spectra.

3. The spectrum was taken at room temperature in DI pH 7.0.

Day 2:

1. The LPG spectrum was taken at room temperature in DI pH 7.0.

5. The fiber was immersed in DI pH 4.0.

6. The LPG spectrum was taken after 5 minutes of submersion in the DI when the signal became stable.

7. The fiber was rinsed with DI water.

8. The fiber was immersed in DI pH 5.0.

9. The LPG spectrum was taken after 5 minutes of submersion in the DI when the signal became stable.

11. Steps 5, 6, and 7 were repeated for DI of pHs 6.0, 7.0, 8.0, 9.0.

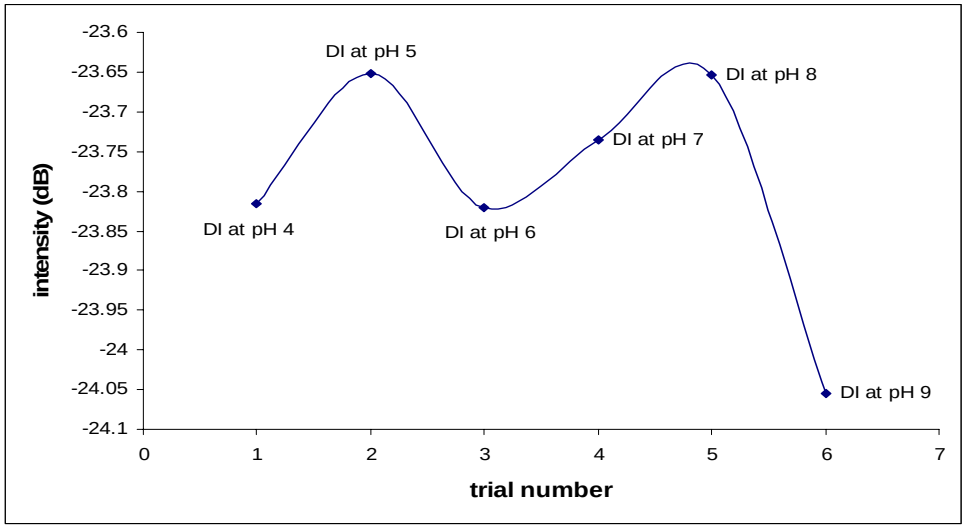

Figure 6-7: Changes in optical intensity at the TAP after soaking PAH/PCBS coated LPG in pH adjusted DI water.

Figure 6-7 displays the results of this experiment. Theoretically, the intensity should start out very low at pH 4.0, indicating thicker layers. Then, as pH 7.0 is reached, the intensity should monotonically increase, indicating thinner layers. Next, for pHs higher than 7.0, the intensity should start to decrease again according to Corres *et. al.*[1,2], implying thicker layers. However, as can be seen, there are again small and somewhat random variations.

In the next experiment, the procedure was, again, slightly different from the previous experiments. The main differences for this experiment were that the fiber was not heated, the pH of the PAH and PAA were both 5.0 to induce thicker layers, and the fiber soaked in each DI solution for 7 minutes. The procedure was as follows.

1. The LPG spectrum was taken at room temperature in DI water prior to any film deposition.

2. PAH and PAA ISAM films were deposited onto the LPG. In this experiment, 3 bilayers of PAH/PAA were deposited onto the LPG. The pHs of the PAH and PAA were both 5.0.

3. The spectrum was taken at room temperature in DI.

4. The fiber was immersed in DI pH 4.0.

5. The LPG spectrum was taken after 7 minutes of submersion in the DI when the signal became stable.

6. The fiber was rinsed with DI water.

7. The fiber was immersed in DI pH 4.0.

8. The LPG spectrum was taken after 7 minutes of submersion in the DI when the signal became stable.

9. Steps 4, 5, and 6 were repeated for DI of pHs 7.0 and 10.0.

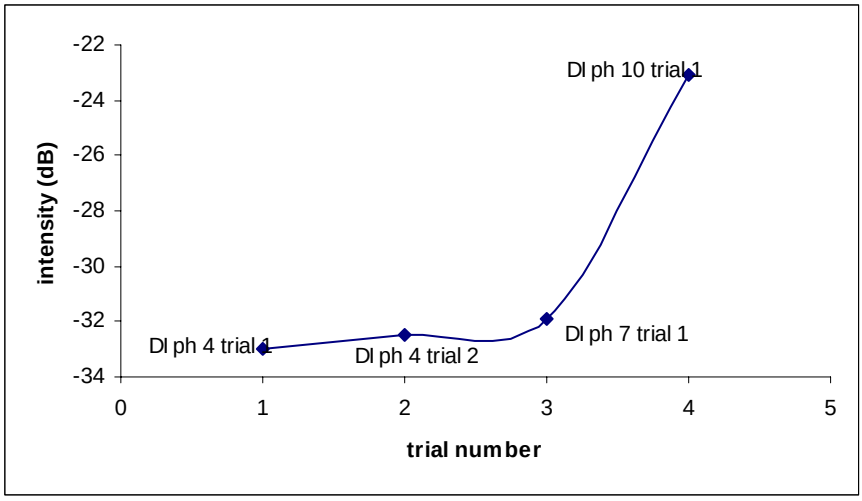

Figure 6-8: Changes in optical intensity at the TAP after soaking ISAM coated LPG in pH adjusted DI water.

As can be seen in Figure 6-8, the intensity for both trials of DI pH 4.0 was very low (~ -33 dB), which indicates thicker layers and repeatability. Then, for the DI pH 7.0, the intensity increased slightly to about -32 dB, indicating thinner layers. However, for DI pH 10.0, the intensity greatly increased to around -23 dB, indicating very thin layers. This does not agree with the results of Corres *et. al*.[1,2] who state that for pHs 8.0-10.0, the intensity should decrease, yielding thicker layers.

For the next experiment, the procedure was slightly different. The main differences in procedure were that the fiber was not heated, the pHs of the PAH and PAA started out at 4.0 and 6.0, respectively (then pH of PAA was adjusted to 5.27), and the fiber was left to soak in each DI solution for 10 minutes. The procedure is as follows.

1. The LPG spectrum was taken at room temperature in DI water prior to any film deposition.

2. PAH and PAA ISAM films were deposited onto the LPG. In this experiment, 10 bilayers of PAH/PAA were deposited onto the LPG. The pHs of the PAH and PAA were 4.0 and 6.0, respectively for the first 5 bilayers. The pH of the PAA was adjusted to 5.27 for the remaining 5 bilayers.

3. The spectrum was taken at room temperature in DI.

4. The fiber was immersed in DI pH 4.0.

5. The LPG spectrum was taken after 10 minutes of submersion in the DI when the signal became stable.

6. The fiber was rinsed with DI water.

7. The fiber was immersed in DI pH 4.0.

8. The LPG spectrum was taken after 10 minutes of submersion in the DI when the signal became stable.

9. Steps 4-8 were repeated for DI of pHs 5.5 and 7.0.

10. Let fiber soak overnight in DI pH 7.0.

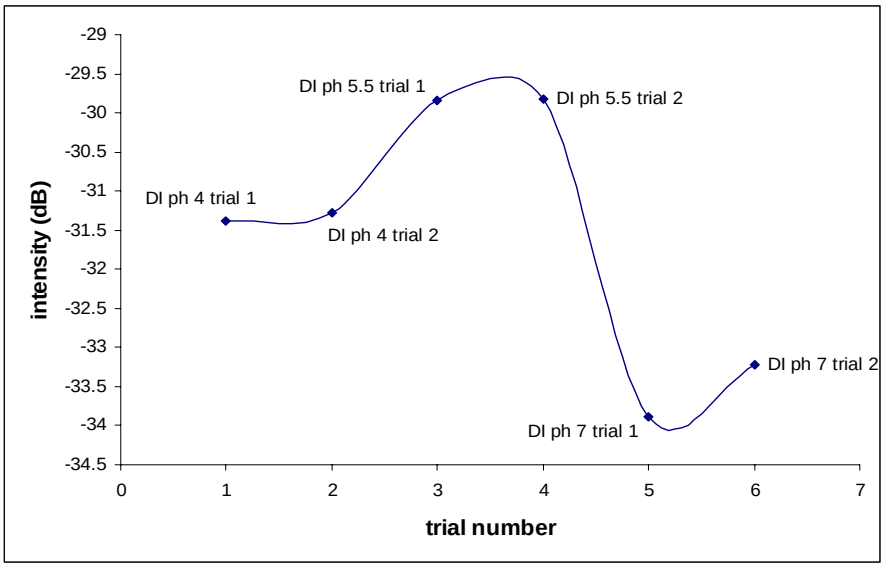

Figure 6-9: Changes in optical intensity at the TAP after soaking ISAM coated LPG in pH adjusted DI water.

As can be seen in Figure 6-9, the intensities for both DI pH 4.0 trials are very similar (~ -31 dB), as are the intensities for both DI pH 5.5 trials. The intensities for the two DI pH 7.0 trials are not as close. The results do not show the expected behavior in which the intensity should start low for pH 4.0 and monotonically increase as pH 7.0 is reached. In this experiment, the fiber was allowed to soak overnight in DI pH 7.0. However, the DI evaporated overnight. The next day, I performed another experiment using the fiber as it was from the previous day. The procedure for this second experiment is as follows.

1. The LPG spectrum was taken at room temperature in DI pH 7.0.

2. The fiber was annealed in an oven at 120 ^{0}C for 2 hours.

3. The fiber was removed from the oven and allowed to cool for 5 minutes.

4. The LPG spectrum was then taken at room temperature in DI water at pH 7.0.

5. The fiber was immersed in DI pH 4.0.

6. The LPG spectrum was taken after 7 minutes of submersion in the buffer when the signal became stable.

7. The fiber was rinsed with DI water.

8. The fiber was immersed in DI pH 4.0.

9. The LPG spectrum was taken after 7 minutes of submersion in the buffer when the signal became stable.

10. Steps 5, 6, and 7 were repeated for DI of pHs 5.5 and 7.0.

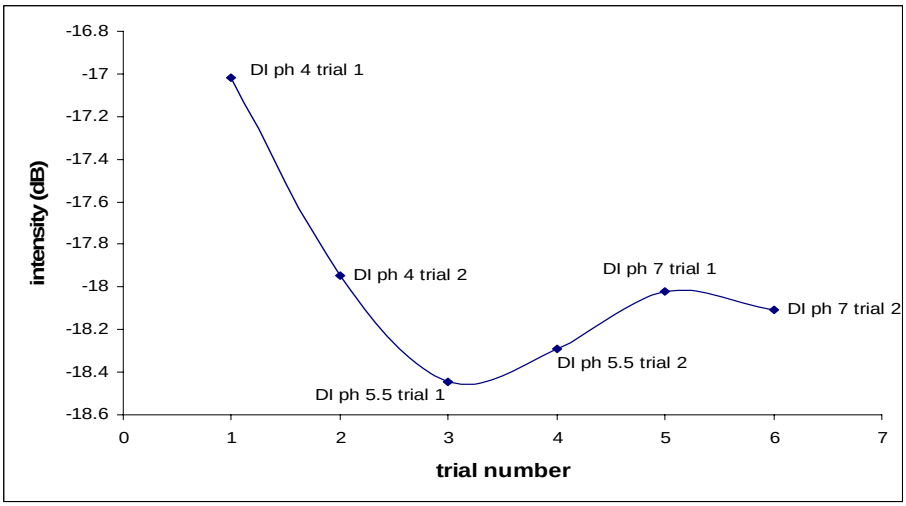

Figure 6-10: Changes in optical intensity at the TAP after soaking ISAM coated LPG in pH adjusted DI water.

As can be seen in Figure 6-10, there is again no monotonic increase in intensity in going from pH 4.0 to pH 7.0. Furthermore, there is no clear repeatability in the trials either.

6.4 Experimental Results Using Sodium Phosphate Buffers

Thus far, we have shown that we were only partially successful at reproducing the results of Corres *et al.*[1,2] using buffer solutions. Furthermore, we were unable to obtain any reproducible results using just pH adjusted DI. The buffer solutions we were using were all made from different materials, which is not very consistent. We then decided that we should make our own buffer solutions using the same materials for each pH. This would help address the question of whether we had a true pH sensor or just a sensor that detected ion concentrations. I made sodium phosphate buffers. The materials used were DI water, sodium phosphate monobasic (NaH_2PO_4) purchased from Sigma Aldrich, and sodium phosphate dibasic (Na_2HPO_4) purchased from Sigma Aldrich. I found a procedure online that described how to make a sodium phosphate buffer at any pH using different amounts of monobasic and dibasic sodium phosphate together. I made pHs 4.0, 5.0, 6.0, and 7.0 all at 10 mM concentrations. After making each buffer I tested its pH with a Denver Instruments pH meter. The pHs were not exact so I adjusted them using NaOH and HCl. The procedure for the sodium phosphate buffer experiment is outlined below.

Day 1:

1. The LPG spectrum was taken at room temperature in DI pH 7.0 prior to any film deposition.

2. PAH and PAA ISAM films were deposited onto the LPG. In this experiment, 16 bilayers of PAH/PAA were deposited onto the LPG. The pH of the PAH was 4.0 and the pH of the PAA was 6.0 for the first 9 bilayers. The pH of the PAA was adjusted to 5.26 for the remaining 7 bilayers.

3. The spectrum was taken at room temperature in DI pH 7.0.

Day 2:

1. The LPG spectrum was taken at room temperature in DI pH 7.0.

2. The fiber was annealed in an oven at 120 ^{0}C for 2 hours.

3. The fiber was removed from the oven and allowed to cool for 5 minutes.

4. The LPG spectrum was then taken at room temperature in DI water at pH 7.0.

5. The fiber was immersed in sodium phosphate buffer pH 4.0.

6. The LPG spectrum was taken after 10 minutes of submersion in the buffer when the signal became stable.

7. The fiber was rinsed with DI water.

8. Steps 5, 6, and 7 where repeated for sodium phosphate buffers of pH 5.0, 6.0, and 7.0.

9. Several trials were done with each pH.

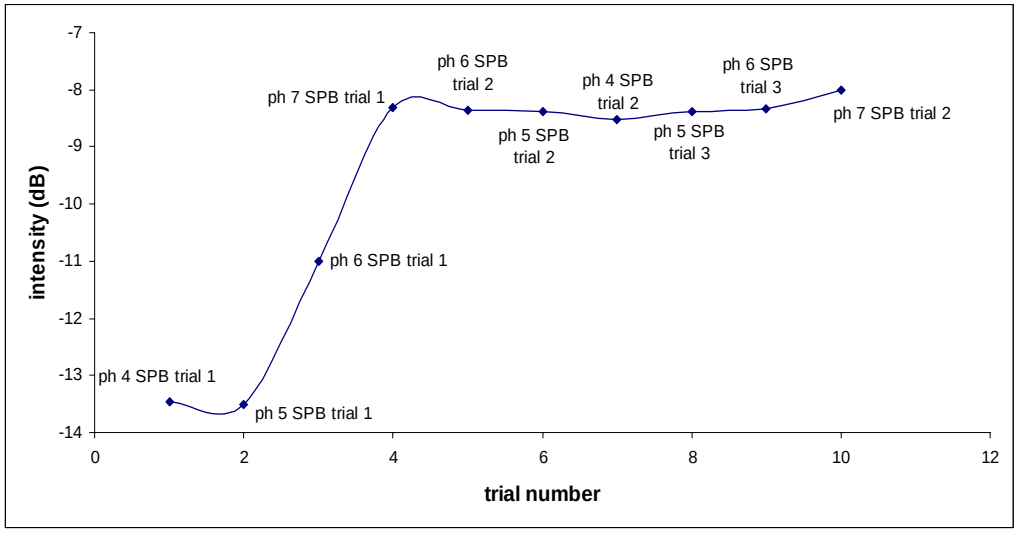

(a)

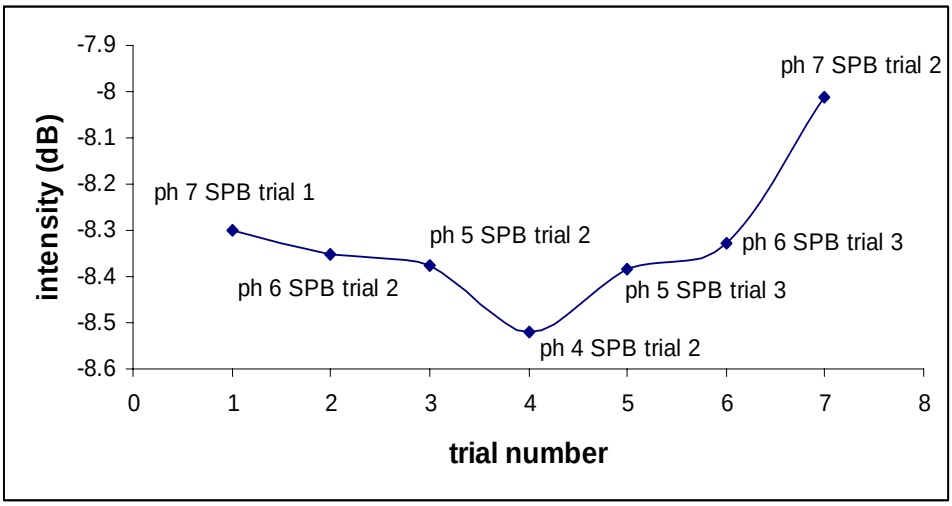

(b)

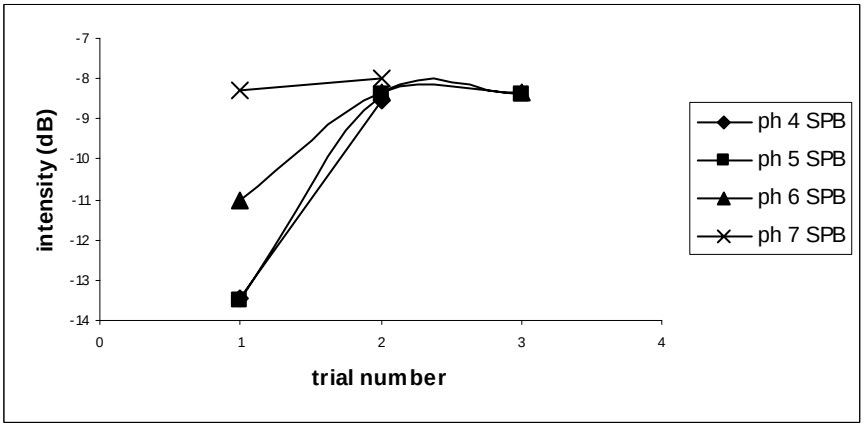

(c)

Figure 6-11: (a) Changes in optical intensity at the TAP after soaking ISAM coated LPG in sodium phosphate buffers of various pHs; (b) magnified view of a; (c) intensity values at the TAP at each pH for each trial.

The results from this experiment are displayed in Figure. As can be seen in Figure 6-11 a, there was an increase in intensity in going from the pH 4.0 sodium phosphate buffer to the pH 7.0 for the first trial (from around -13.5 to -8.5 dB). However, there was not much difference in the intensity for pH 4.0 and pH 5.0. They were both around -13.5 dB. Then, going from pH 7.0 buffer to pH 4.0 buffer there was a monotonic, but small, decrease in intensity (only from about -8.3 to -8.5 dB) Next, in going from pH 4.0 back to pH 7.0, there was again a small increase in intensity (from around -8.5 to -8.0 dB). These last two results can be seen more clearly in Figure 6-11 b. While there are some systematic changes, the repeatability is still not very good for a given pH. Also, it is worth noting that repeatability does appear to improve after the first trial. This is consistent with Itano *et al*.[8] where repeatability of pH-induced swelling of ISAM films was also not observed until after the first trial. Figure 6-11 c shows the intensities for each trial at each pH. These values should be fairly stable, but they do not appear to be so. However, they do clearly show the increase in intensity from pH 4.0 to pH 7.0, indicating that they layers get thicker as higher pHs are used. Thus, this experiment was somewhat successful.

For the following experiment, the procedure was the same as the previous experiment except for this one the fiber was not annealed and the pH 7.0 buffer was not used. In some of the experiments there was an issue that occurred when pH 7.0 was reached. That issue was that once pH 7.0 was reached the first time, the intensity would either not change or change very little when other pHs where deposited. In essence, the intensity seemed to get "stuck" at the intensity for pH 7.0. It was thought that if we eliminated the pH 7.0 buffer trial, perhaps we could avoid this problem.

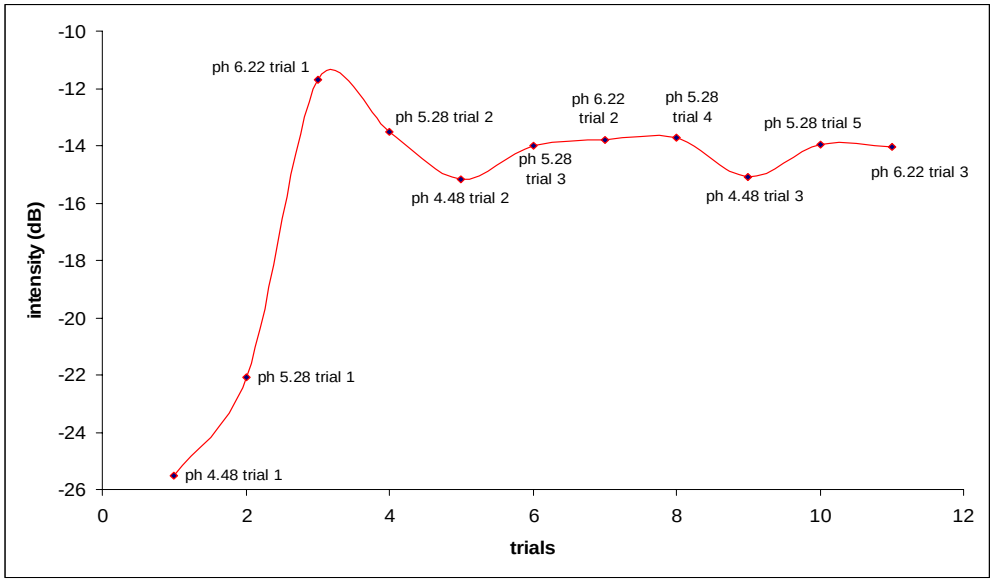

(a)

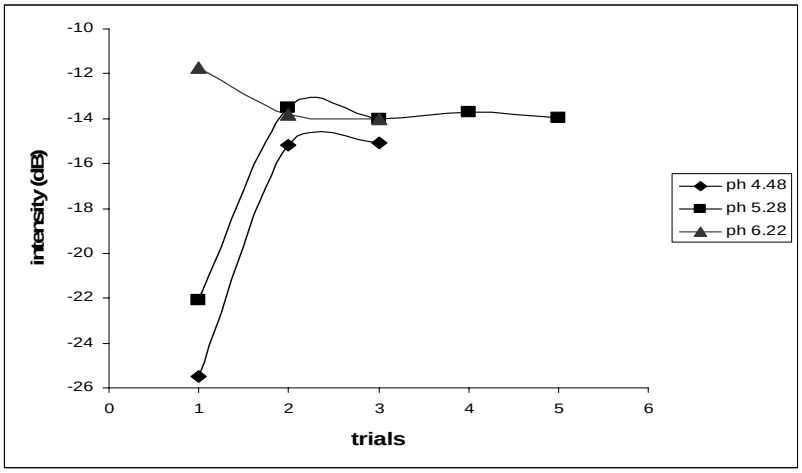

(b)

Figure 6-12: (a) Changes in optical intensity at the TAP after soaking ISAM coated LPG in sodium phosphate buffers of various pHs; (b) intensity values at the TAP at each pH for each trial.

As can be observed in Figure 6-12 a, there was a monotonic increase in intensity in going from the pH 4.0 sodium phosphate buffer to the pH 6.0 sodium phosphate buffer (from about -26 to -12 dB). However, we still do not start to see any type of repeatability until after the first trial. In looking at Figure 6-12 b, though, the intensities at each pH are still not very stable. However, it appears as though they might be had more trials been

performed.

For the following experiment, the procedure was the same as the previous experiment except this time the fiber was annealed. The results can be seen in Figure 6-13.

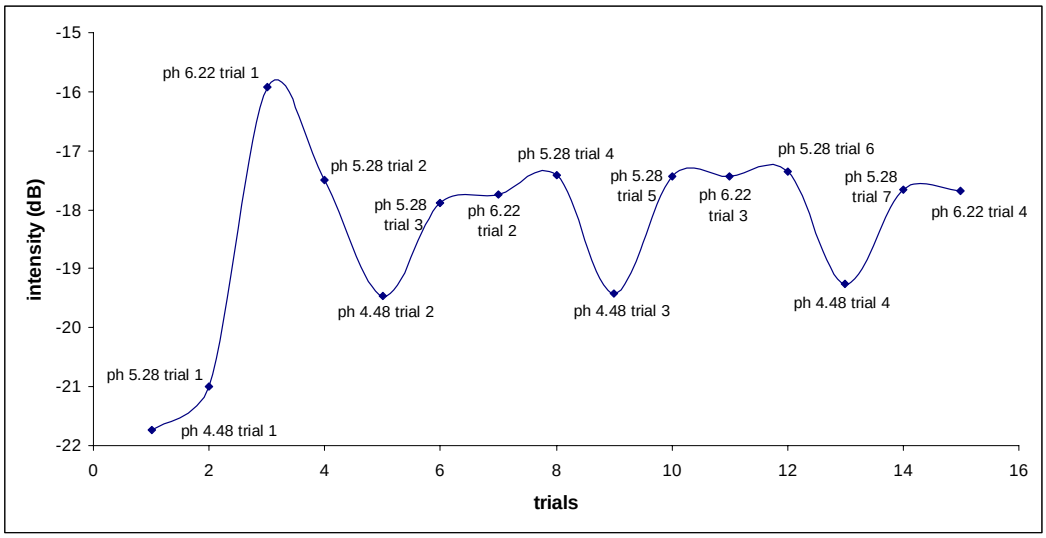

(a)

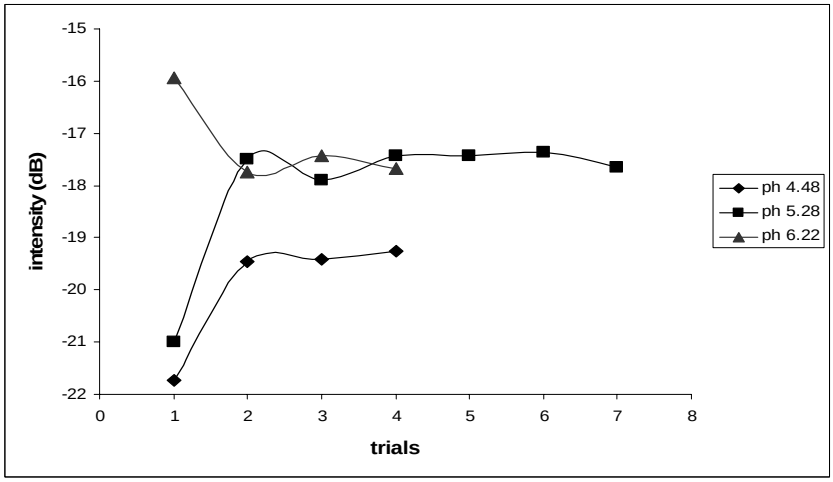

(b)

Figure 6-13: (a) Changes in optical intensity at the TAP after soaking ISAM coated LPG in sodium phosphate buffers of various pHs; (b) intensity values at the TAP at each pH for each trial.

Examining Figure 6-13 a it can be seen that there is, again, an initial monotonic increase in intensity when going from sodium phosphate buffer pH 4.0 to sodium

phosphate buffer pH 6.0 (about -22 to -16 dB). There is also a decrease in intensity when going from pH 6.0 to pH 4.0. There is some repeatability after the first trial. Observing Figure 6-13 b, it is noted that the intensities at each pH are still not completely stable even though more trials were performed. However, they seem to be more stable than the prior experiment. There also appears to be not much difference between the intensity values for pH 4.0 and 5.0 as more trials are done. However, this is consistent with Hiller and Rubner[9], Tanchak and Barret[10], Itano *et al*.[8] Thus, again, this experiment was somewhat successful.

6.5 pH Experiments Using a Different ISAM Chemistry

Because we were observing relatively large LPG spectrum changes with buffer solutions, but not with pH-adjusted DI water, it seems likely that the changes were due to the salt ions in the buffer solutions rather than hydrogen ion concentrations. There are a number of reports of salt-induced swelling of ISAM films[11,12], but far fewer indicating pH-induced swelling. Several papers by Rubner *et al*. indicate discontinuous pH-induced swelling of certain ISAM films.[8,9,10,13]

In the following experiment several important changes were made following the paper by Lee *et al,*[13] who used PAH and poly(sodium 4-styrenesulfonate) (PSS) at pHs greater than 9.0, with the outer ISAM layer being PAH. Thus, instead of using PAA as the polyanion, we used PSS. Instead of using the PAH at pH 4.0 and PAA at pH 6.0, we used both PAH and PSS at pH 9.3. Also, the fiber was not annealed. The experimental procedure is outlined below. Lee *et al*.[13] showed that these conditions exhibit discontinuous swelling/deswelling transitions as a function of pH conditions. They say

that these reversible discontinuous transitions are caused by discontinuous changes in the degree of ionization of free amine groups of PAH and a significant shift in the pK_a value of PAH because of its local environment (hydrophobic association of free amine groups) within the multilayers.[13] This effect causes a history-dependent swelling behavior of the multilayers.

1. The LPG spectrum was taken at room temperature in PBS pH 7.2.

2. 4.5 bilayers of PAH/PSS at pH 9.3 were deposited.

3. The fiber was immersed in DI water pH 2.0 for 3 minutes.

4. The LPG spectrum was taken after 3 minutes of submersion in the DI water when the signal became stable.

5. The fiber was rinsed with DI water.

6. The fiber was immersed in DI pH 10.5 for 3 minutes.

7. Steps 4 and 5 where repeated.

8. Several trials were done going back and forth between pH 2.0 and pH 10.5 each immersed for 3 minutes.

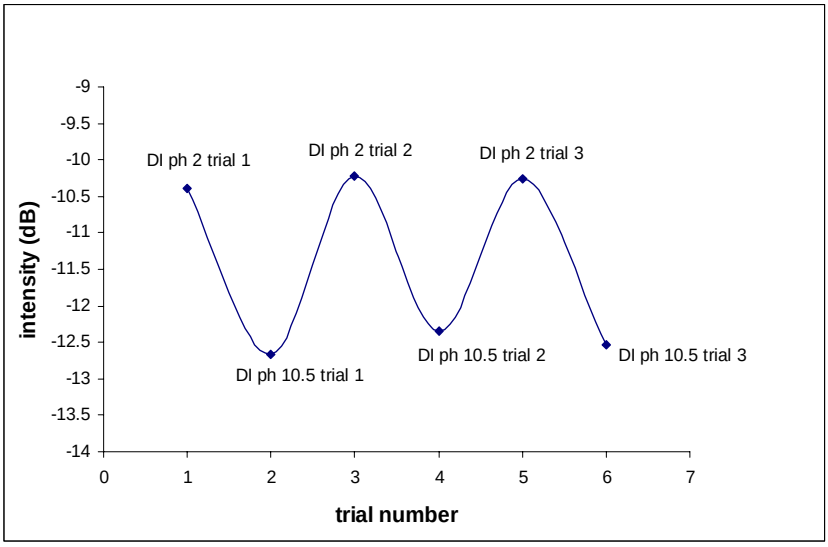

(a)

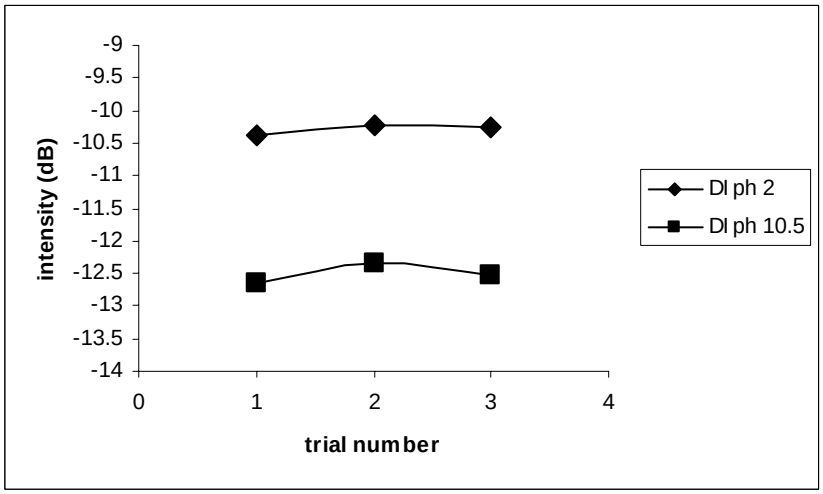

(b)

Figure 6-14: PAH/PSS ISAM chemistry. (a) Changes in optical intensity at the TAP after soaking ISAM coated LPG in pH adjusted DI water; (b) intensity values at the TAP at each pH for each trial.

The results from this experiment are shown in Figure 6-14. As can be seen in Figure 6-14 a there was a clear difference between pH values of 2.0 and 10.5 with very good repeatability. Figure 6-14 b shows that the pH values for DI of pH 2.0 and 10.5

where both fairly stable. These are significant improvements over all the previous pH experiments. Lee *et al.*[13] observed almost no swelling for exposure to pH 10.0 and about 800% swelling after exposure to pH 2.0. This would imply that the layers are very thin for pH 10.0 and very thick for pH 2.0. Itano *et al.*[8] also found a similar phenomenon when using PAH and PSS both at pH > 9.0. However, my results show that the intensity is higher for pH 2.0, indicating either thinner layers or lower refractive index. Lee *et al.*[13] indicate that the swelling they observe is due to the creation of 2 very porous materials, which would therefore have a significantly lower refractive index. It therefore appears that the effect of reduced refractive index is more important than the increased thickness in determining the LPG transmission spectrum. However, further studies would be required to confirm this.

In the following experiment, the same procedure was followed as the previous experiment, except here I have gone from pH 2.0 to pH 10.5. Then, from pH 10.5 back to pH 2.0. Then, from pH 2.0 to pH 4.0, 5.4, and 7.0. Then, from pH 7.0 to pH 5.4, 4.0, and 2.0. Each submersion in each pH was 3 minutes. The results are shown in Figure 6-15.

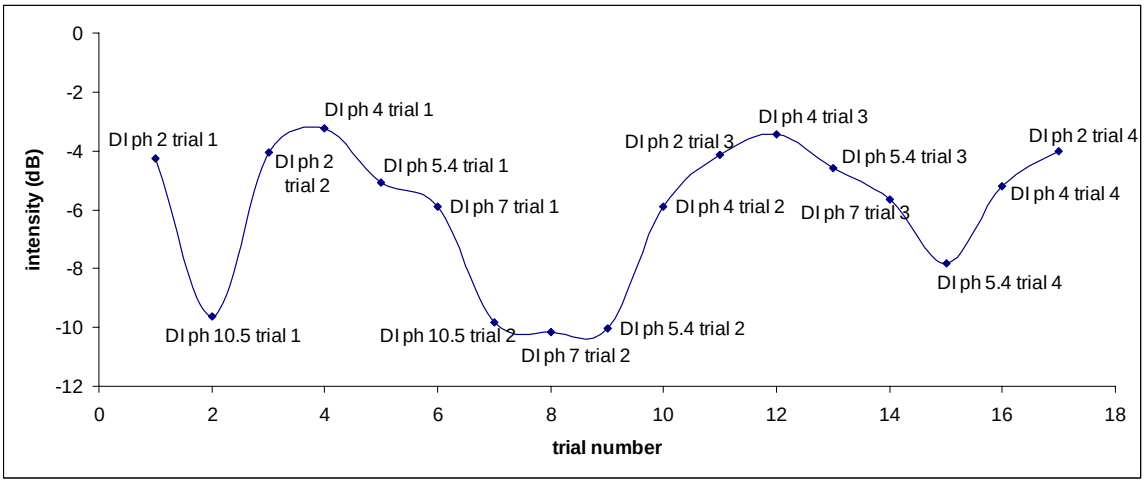

(a)

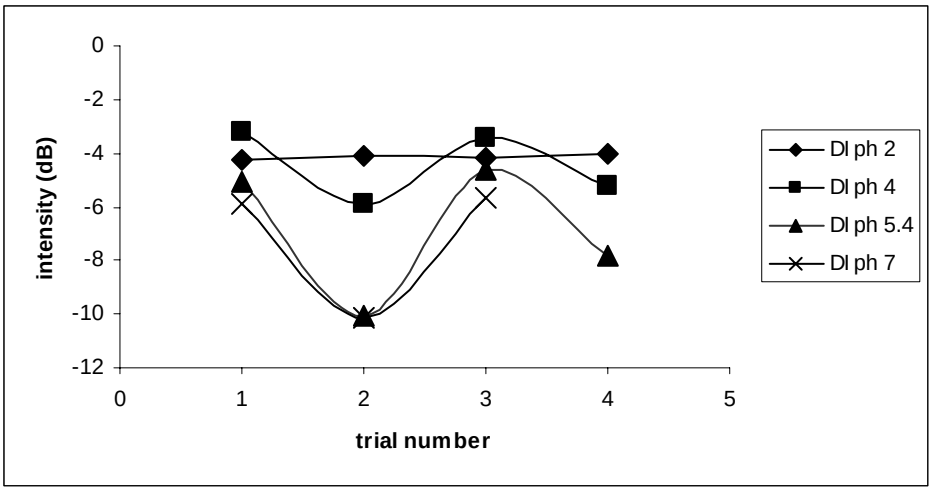

(b)

Figure 6-15: PAH/PSS ISAM chemistry. (a) Changes in optical intensity at the TAP after soaking ISAM coated LPG in pH adjusted DI water; (b) intensity values at the TAP at each pH for each trial.

By examining Figure 6-15 a it can be seen that there is a general trend of increased attenuation with increased pH, but there was no repeatability for a given pH value. Figure 6-15 b shows that the intensity values for the different pHs where not very constant for each trial, except for DI pH 2.0. However, it should be noted that for trials 1 and 3, both of which followed a soak in pH 2.0, the intensity values are quite similar.

A second experiment was performed the same day as the previous one. Here the same fiber with the same films on it was used. The procedure was also the same as before. The difference is that I first went back and forth between DI pH 2.0 and 4.0. Then, I alternated between DI pH 2.0 and 5.4, then DI pH 2.0 and 7.0. The idea here was that perhaps an immersion in pH 2.0 might "reset" the film to an initial swollen state that would increase repeatability for other pH value measurements. The results can be seen in Figure 6-16.

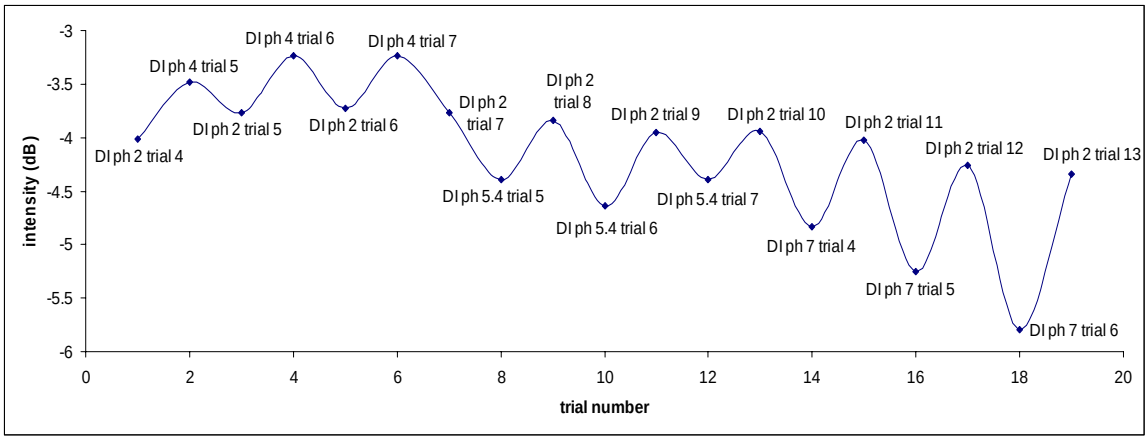

(a)

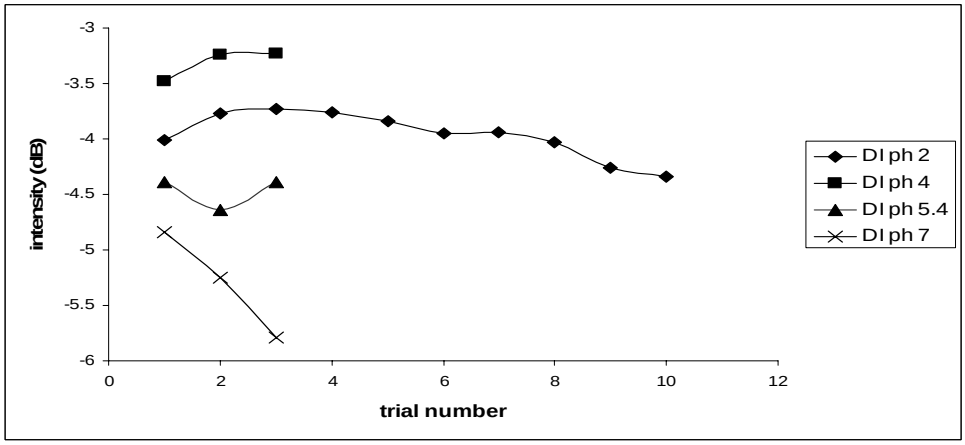

(b)

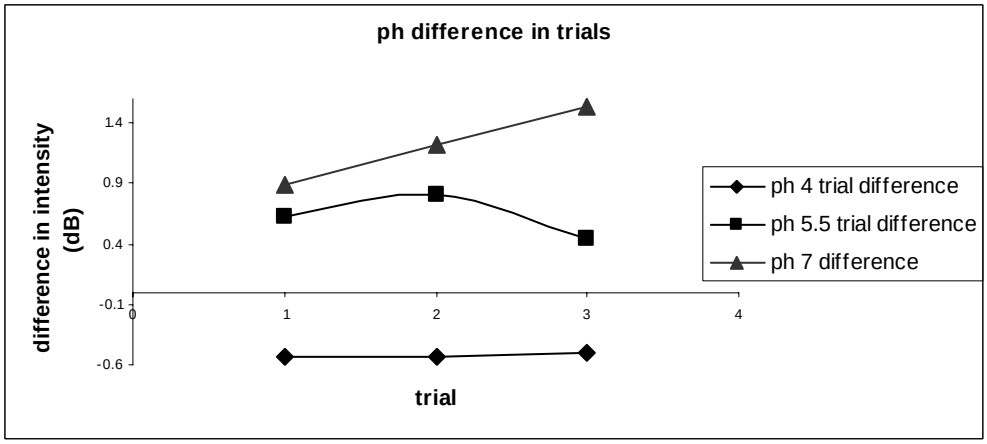

(c)

Figure 6-16: PAH/PSS ISAM chemistry. (a) Changes in optical intensity at the TAP after soaking ISAM coated LPG in pH adjusted DI water; (b) intensity values at the TAP at each pH for each trial; (c) difference in intensity value from the preceding pH 2.0 intensity for each pH.

As can be observed in Figure 6-16 a, there is repeatability to a certain degree in this experiment. However, there also appears to be an overall downward drift in the intensity values. The results suggest that that in order to observe any type of repeatability, the fiber should first be soaked in DI pH 2.0 for three minutes before putting water at any other pH on the fiber. This soak in DI pH 2.0 acted as a type of "reset" for the film and it seemed to increase the response time. This is somewhat consistent with Itano *et al*.[8] where prior to measurement, films were preconditioned in pH 2.0 water for 5 minutes. Although there is some repeatability in this experiment, it is still not very good. This can be seen in Figure 6-16 b where it is clear that the intensity values for each pH did not stay constant. Because of the drift in the measured values for pH 2.0, we examined whether that change in intensity relative to the preceding intensity at pH 2.0 would be somewhat constant. This is illustrated in Figure 6-16 c. However, the only pH that appeared to have a consistent intensity difference between trials was DI pH 4.0. It is also interesting to note that pH 4.0 has a higher transmitted intensity than pH 2.0 while pHs 5.5 and 7.0 are both lower.

For the next experiment a similar procedure to the previous experiment was followed. Here, however, instead of going in numerical order with the pH tests I tried them in random orders. I still did the 3 minute "reset" in DI pH 2.0 in between each trial. The results are illustrated in Figure 6-17.

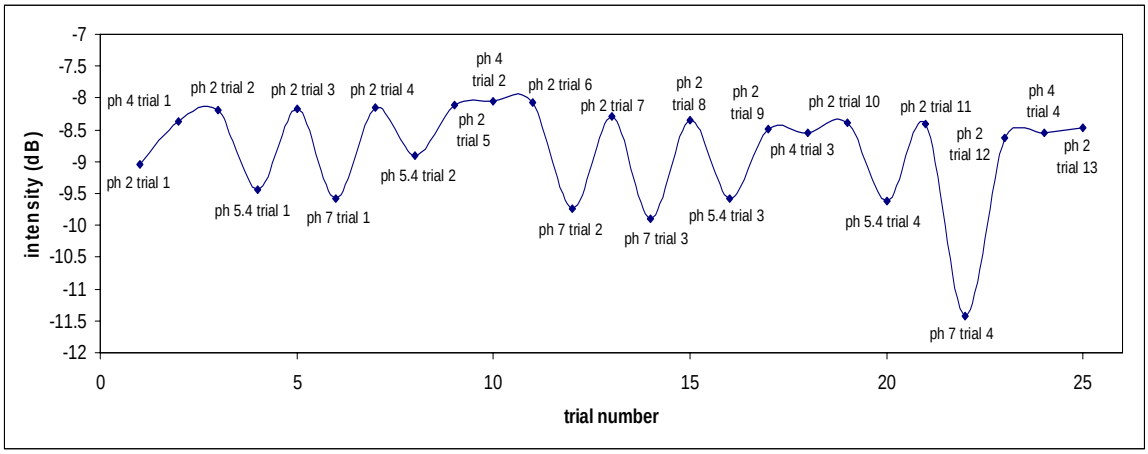

(a)

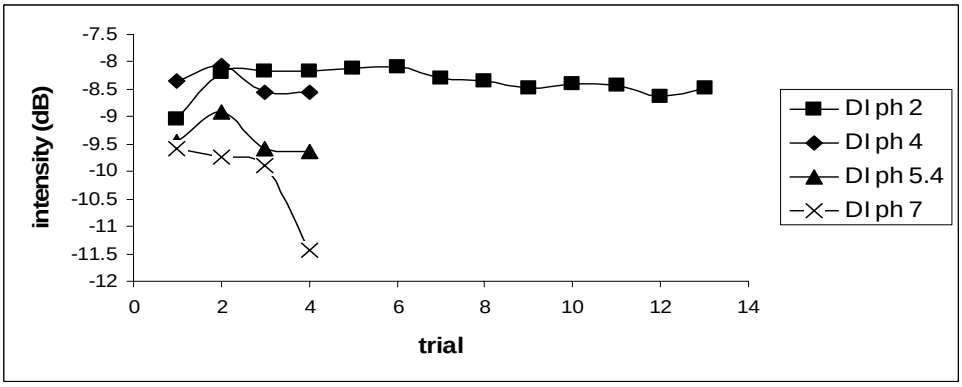

(b)

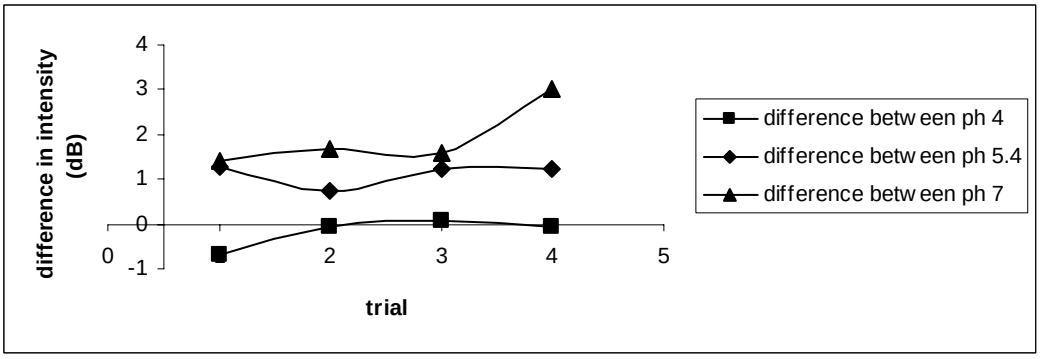

(c)

Figure 6-17: PAH/PSS ISAM chemistry. (a) Changes in optical intensity at the TAP after soaking ISAM coated LPG in pH adjusted DI water; (b) intensity values at the TAP at each pH for each trial; (c) difference in intensity value between each trial for each pH.

As can be seen in Figure 6-17 a, there is again some degree of repeatability, but

less than desired. This becomes more evident in Figure 6-17 b where, again, it is observed that the intensity values for each pH trial are still not quite constant, except for that of DI pH 2.0. The differences for each measurement with respect to the preceding measurement for pH 2.0 are shown in Figure 6-17 c. There is some degree of repeatability with the most notable exception being the final measurement for pH 7.0. There is a clear distinction between the pH 4.0 measurements and the other two pHs, but pHs 5.4 and 7.0 are not clearly separated.

It was believed that perhaps the soak time for each pH value was not long enough and therefore, a stable intensity value was not being reached. Thus, it was decided that the fiber would be soaked in each pH value for 10 minutes. However, there would still be a 3 minute soak in DI pH 2.0 in between each trial to "reset" the intensity value and increase the response speed. The results of this experiment can be seen in Figure 6-18.

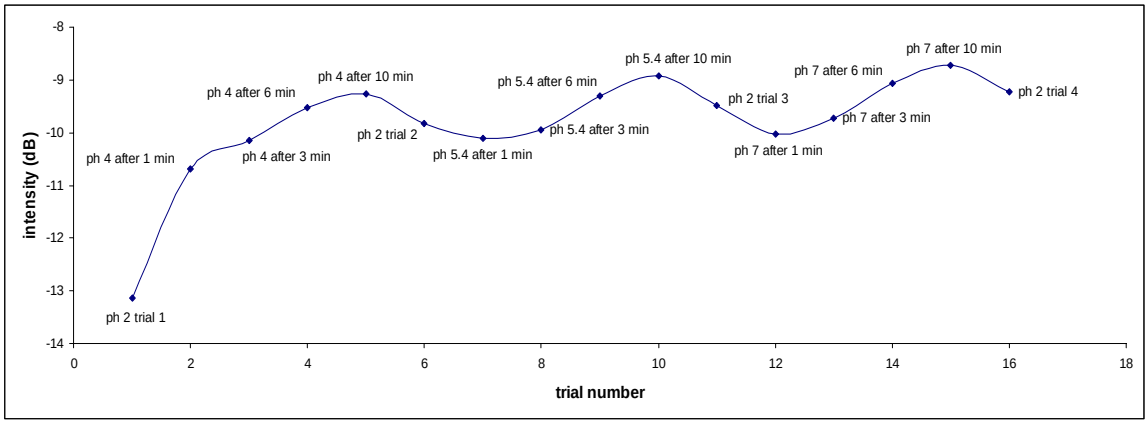

(a)

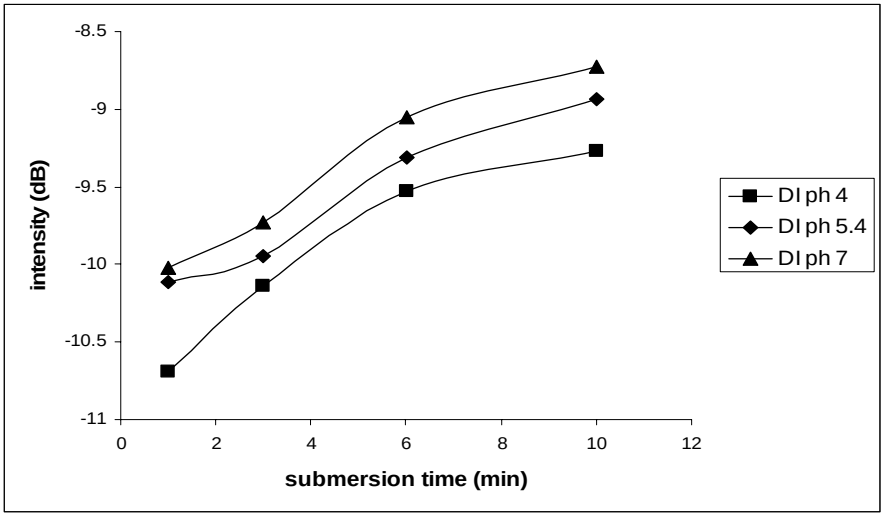

(b)

Figure 6-18: PAH/PSS ISAM chemistry. (a) Changes in optical intensity at the TAP after soaking ISAM coated LPG in pH adjusted DI water for increasing amounts of time; (b) intensity values at the TAP at each pH for each trial over the ten minute period.

Figure 6-18 a shows the intensity values at each pH after soaking 1, 3, 6, and 10 minutes. It can be seen more clearly in Figure 6-18 b that even after soaking the fiber in each pH for 10 minutes a stable intensity value was still not achieved. Thus, it was decided to retry the experiment, soaking the fiber in each pH for 30 minutes. There was a still a 3 minute soak in DI pH 2.0 in between each trial. These results can be observed in Figure 6-19.

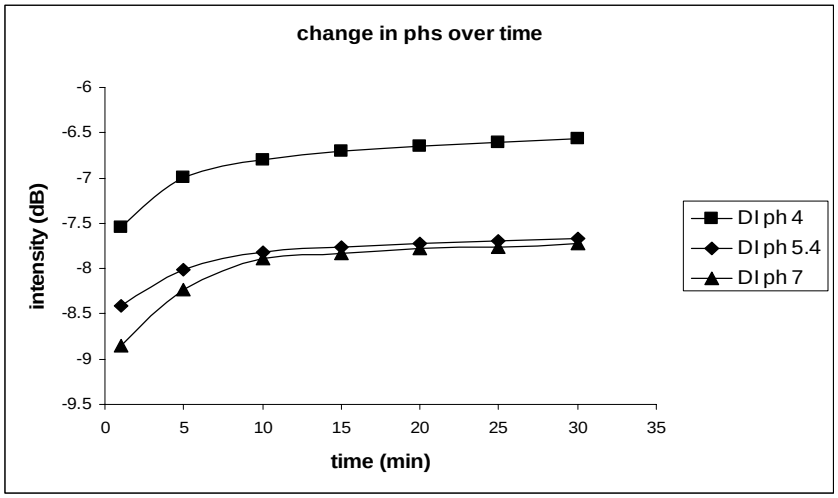

Figure 6-19: PAH/PSS ISAM chemistry. (a) Changes in optical intensity at the TAP after soaking ISAM coated LPG in pH adjusted DI water for increasing amounts of time; (b) intensity values at the TAP at each pH for each trial over the thirty minute period.

Upon examining Figure 6-19 it can be seen that an equilibrium appears to be reached after 15-20 minutes of soaking in each pH value. Furthermore, it can be seen that over time, there is not much difference in the intensity values for pH 5.4 and pH 7.0.

After quite a bit of time spent trying to reproduce the results of Corres *et al*.[1,2], who indicated that PAH/PAA ISAM films on LPGs exhibit clear and reproducible pH-dependent effects, we came to the conclusion that those effects are rather due to the salt ions in the buffer solutions. Following the work of Rubner *et al*. on pH-induced swelling in PAH/PSS films, we have seen indications of somewhat reproducible changes in TAP LPG transmission spectra at pHs of 4.0, 5.4, and 7.0. However, much work remains to be done with regards to obtaining reliable, stable measurements in light of the dynamical response of the ISAM film.

---

[1] J. M. Corres, I. R. Matias, I. del Villar, F. J. Arregui, "Design of pH Sensors in Long-Period Fiber Gratings Using Polymeric Nanocoatings," *IEEE Sensors Journal* **7**, 455-463, 2007.

[2] J. M. Corres, I. del Villar, I. R. Matias, F. J. Arregui, "Fiber-optic pH-sensors in long-

period fiber gratings using electrostatic self-assembly," *Optics Lett*. **32**, 29-31, 2007.
[3] N. Kato, P. Schuetz, A. Fery, and F. Caruso, "Thin multilayer films of weak polyelectrolytes on colloid particles," *Macromolecules* **35**, 9780-9787, 2002.
[4] S. S. Shiratori and M. F. Rubner, "pH-Dependent thickness behavior of sequentially adsorbed layers of weak polyelectrolytes," *Macromolecules* **33**, 4213-4219, 2000.
[5] I. Del Villar, I. R. Matias, F. J. Arregui, and R. O. Claus, "ESA-based in-fiber nanocavity for hydrogen-Peroxide detection," *IEEE Trans. Nanotechnol*. **4**, 187-193, 2005.
[6] D. Yoo, A. Wu, J. Lee, M. F. Rubner, *Synth. Metals* **85**, 1425-1426, 1997.
[7] J. D. Mendelsohn, C. J. Barrett, V. V. Chan, A. J. Pal, A. M. Mayes, and M. F. Rubner, "Fabrication of Microporous Thin Films from Polyeletrolyte Multilayers," *Langmuir* **16**, 5017-5023, 2000.
[8] K. Itano, J. Choi, M. F. Rubner, "Mechanism of the pH-Induced Discontinuous Swelling/Deswelling Transitions of Poly(allylamine hydrochloride)-Containing Polyelectrolyte Multilayer Films," *Macromolecules* **38**, 3450-3460, 2005.
[9] J. Hiller, M. F. Rubner, "Reversible Molecular Memory and pH-Switchable Swelling Transitions in Polyelectrolyte Multilayers," *Macromolecules* **36**, 4078-4083, 2003.
[10] O. M. Tanchak, C. J. Barret, "Swelling Dynamics of Multilayer Films of Weak Polyelectrolytes," *Chem. Mater*. **16**, 2734-2739, 2004.
[11] H. W. Jomaa, J. B. Schlenoff, "Salt-Induced Polyelectrolyte Interdiffusion in Multilayered Films: A Neutron Reflectivity Study," *Macromolecules* **38**, 8473-8480, 2005.
[12] S. T. Dubas, J. B. Schlenoff, "Swelling and Smoothing of Polyelectrolyte Multilayers By Salt," *Langmuir* **17**, 7725-7727, 2001.
[13] D. Lee, A. J. Nolte, A. L. Kunz, M. F. Rubner, R. E. Cohen, "pH-Induced Hysteretic Gating of Track-Etched Polycarbonate Membranes: Swelling/Deswelling Behavior of Polyelectrolyte Multilayers in Confined Geometry," *J. Am. Chem. Soc.* **128**, 8521-8529, 2006.

Chapter 7. Conclusion

The biosensor field is continuously growing with new, inventive and highly developed technologies. The estimated annual growth rate for the field is 60%. Biosensors have many areas of application including: environmental, medical, military, pharmaceutical, and food industry. In the environment, biosensors can be used to detect harmful and hazardous environmental pollutants. In the medical industry, they can be implemented for early diagnosis of disease or patient monitoring. In the military, biosensors can be utilized to detect harmful or deadly chemicals used in biological warfare. In the pharmaceutical industry, they can be used to help speed the progress of drug discovery. In the food industry, biosensors can be used to determine if harmful bacteria are growing in, or on, food items. These are just some of the many very useful applications for biosensors.

Specificity, sensitivity, and response time are the important features needed in all biosensor applications. Furthermore, in order to use a biosensor in the field it must be portable, rugged, and easy to operate. A biosensor that combines all of these qualities and characteristics is necessary to solve the real-world applications and issues in the medical industry, military, pharmacy, food industry, etc. Thus, the motivation for this work is to develop a biosensor that encompasses all of the aforementioned qualities and try to apply it to many of the pressing issues in today's world such as bioterrorism, deadly diseases, drug discovery, etc.

This thesis has focused on examining the potential of a new biosensor platform based on nanoscale self-assembled films on turnaround point long-period gratings. It

builds on prior work that demonstrated the exceptional sensitivity of optical fiber LPGs to nanoscale film with high refractive indices. The use of TAP LPGs is especially important because they yield even higher sensitivity than conventional LPGs and exhibit changes in the strength of the attenuation band, which are more easily measured than shifts in the attenuation wavelength. This thesis is concentrated on three primary areas: evaluation of approaches to increasing the sensitivity of the sensor platform; implementation of a biosensor for detection of the anthrax protective antigen, the biotin-streptavidin interaction, and prostate specific antigen; and preliminary evaluation of the potential for pH sensing.

Regarding the sensitivity of the sensor platform, studies were done on thickness and composition of the ISAM films. It was shown that as the number of bilayers deposited on the LPG is increased, the sensitivity of the LPG also increased. This is due to two effects. First, as previously shown theoretically, thicker films pull more of the optical field of the cladding mode towards the fiber/film outer surface where additional materials will bind. Second as the ISAM film thickness increases the LPG begins to operate closer to the TAP, which is the highest point of sensitivity in the fiber. It is also important to note that experiments performed in air produce the same results as experiments performed in aqueous solution. This is important because it demonstrates that the results are not compromised by performing an experiment in solution, and many of the real-world applications of biosensors will need to be made in solution. Furthermore, it shows that the sensitivity level is basically independent of the substance in which the readings are being taken.

It was also shown experimentally that when high refractive index materials are

used in the ISAM film the sensitivity of the LPG also increases. Prior calculations have shown that depositing a high refractive index film on the fiber increases the sensitivity to additional adsorbed materials even if those materials do not have a high refractive index themselves. Hence, experiments are not limited to high refractive index analytes. This is due to the fact that the high refractive index film also forces the mode profile of the cladding mode outwards toward the surface, consequently increasing the sensitivity to any surface material.

To further increase the sensitivity of the ISAM LPG sensor, incorporating silica nanoparticles into the ISAM film was examined. Nanoparticles provide increased film thickness and surface area for binding of probe and target molecules. This is due to the thickness of the nanoparticles bilayer, which is about 20 nm, while a bilayer of PAH/PCBS is only 1-2 nm. If larger silica nanoparticles were to be used, the sensitivity of the LPG is likely to increase even more. Thus, another way to make a more sensitive sensor would be to use larger silica nanoparticles in the platform. Furthermore, the shifts in attenuation with the underlying nanoparticle layer are also greater as more bilayers of PAH/PCBS are deposited. The silica nanoparticle ISAM films have a fairly low refractive index which may counteract the potential sensitivity increases as a result of increased surface area and thickness. Consequently, titania nanoparticles would be more likely to produce an even larger increase in LPG sensitivity. This is because the bulk refractive index of titania is about 2.5, which would generate a film refractive index of about 1.9 for 40% void space.

In the final year of this work, a different set of TAP-LPGs was obtained from OFS Laboratories. These LPGs were designed to dramatically increase dynamic range

and sensitivity over the previous LPGs that had been used. These LPGs have a 35 dB overall decrease in transmitted intensity at the TAP, whereas the older LPGs have only a 12 dB overall decrease in intensity at the TAP. More than four times as many bilayers of PAH/PCBS can be deposited on the new LPG before it gets to the TAP. Furthermore, near the TAP, the spectrum has a 7.159 dB decrease in intensity for one additional PAH/PCBS bilayer for the new LPG, whereas for the old LPG, there is only a 2.297 dB decrease near the TAP. These new LPGs allow for the construction of a sensor with drastically increased sensitivity and dynamic range, particularly considering the fact that dB corresponds to a logarithmic transmission scale.

Next, a series of studies were performed to investigate the implementation of an ISAM TAP LPG as a biosensor. Biosensors have important applications for homeland security. Hence, the first experiment was to try to develop a TAP-LPG biosensor that could detect the B. *Anthracis* (Anthrax) Protective Antigen (PA), which is released by the bacteria as the gateway of infecting host cells with Anthrax toxin. The protective antigen was detected at a concentration of 0.1 mg/ml, which showed up as a 41.6% decrease in the transmitted light intensity at the resonant wavelength. This, of course, is a very high antigen concentration. If this experiment were to be performed again with all of the improvements that will be mentioned later, the sensor would be able to detect a much lower antigen concentration.

Next, the biotin-streptavidin system was studied in detail as a model for evaluating approaches to enhanced sensitivity. Streptavidin has an extremely high affinity for biotin (on the order of $10^{15}/M^{-1}$). One major advantage of using biotin is that many biotin molecules can couple to a protein, and the biotinylated protein can bind to

multiple molecules of streptavidin. The biotin-streptavidin system can detect antigens, glycoconjugates, or nucleic acids by utilizing biotinylated antibodies, lectins, or nucleic acid probes, respectively. There are many benefits that the biotin-(strept)avidin mechanism has over direct coupling of the marker to a lectin, antibody, or nucleic acid probe.

In work done by a preceding student, for a streptavidin concentration of 0.0125 mg/ml, there was about a 1.7 dB decrease in intensity (i.e. ~ 32.4% decrease in transmitted light intensity). In my experiment work, I used one of the newer, more sensitive LPGs along with the more powerful broadband light source. I also did this experiment in PBS as opposed to in air. Furthermore, I made some initial slight changes in the experimental procedure to achieve improved results. In my first study, the lowest detectable signal was for 0.000125 mg/ml (125 ng/ml) streptavidin, which is 100 times more sensitive than that of the prior study. For the streptavidin concentration of 0.000125 mg/ml, there was a 0.645 dB shift, or a 14% decrease in the transmitted light intensity.

In the prior student's studies, the shift in transmission caused by the binding of the biotin layer was about 1.0 dB. For my first study, it was about 1.5 dB. To ensure the maximum amount of binding between biotin and streptavidin, it is necessary to have the largest amount of biotin absorbed onto the fiber, which creates the maximum number of binding sites for the streptavidin. After many, many trials and errors with different methods, it was found that EZ-link NHS-LC-LC-Biotin yielded the largest amount of biotin binding to the ISAM films. The longer spacer arm and increased water solubility of this biotin were responsible for the increased biotin binding. When the experiment

was performed again, the biotin layer created a 3.096 dB decrease in intensity, as opposed to the 1.0 or 1.5 dB decreases in intensity that were previously observed. Increased biotin binding sites for the streptavidin did indeed generate an overall increase in sensitivity for the sensor. One other factor that led to increased sensitivity was that the biotin and streptavidin were deposited at points much closer to the TAP of the LPG, which is the most sensitive point of the grating. Due to the aforementioned improvements, the lowest detectable streptavidin concentration was 0.000012 mg/ml (12.0 ng/ml). This is an additional factor of 10 more sensitive than the previous study, and a factor of 1000 more sensitive than the prior student's work. There was a 0.399 dB shift, or an 8.8% decrease in the transmitted light intensity for 0.000012 mg/ml streptavidin.

Next was an extensive study on the potential use of fiber optic biosensors for the early detection of prostate cancer. The concept for this system is the same as those previously applied, meaning that ISAM films on TAP LPGs are the basis for the biosensor platform. In clinical studies a cut-off level of 4.0 ng/ml of prostate specific antigen in a blood test is frequently used as an indicator of potential prostate cancer. The first PSA experiment involved a sensing layer of ISAM film/biotin/streptavidin/protein A/PSA antibody. The smallest detectable concentration of PSA was 0.14 mg/ml (140000 ng/ml). For this concentration, there was a 0.213 dB shift or a 5% decrease in the transmitted light intensity at the resonant wavelength. Obviously, this is not low enough for clinical detection.

Next, rather than the complex sequence of materials in the sensing layer, the monoclonal antibody to the PSA was directly cross-linked to the outer layer of the ISAM

film. For this experiment, the smallest detectable concentration of PSA was 0.014 mg/ml (14000 ng/ml). For 0.014 mg/ml PSA there was a 0.311 dB shift, or a 7% decrease in the transmitted light intensity. Further improvements were made by depositing more bilayers of ISAM film in order to get the spectrum closer to the TAP to increase the sensitivity of the sensor. Furthermore, the antibody concentration was 9 times higher than before, and each PSA concentration was incubated 2 hours instead of 1.5 hours to ensure maximum binding. In this experiment, the smallest detectable PSA concentration was 0.0001164 mg/ml (116.4 ng/ml). For 0.0001164 mg/ml PSA, there was a 0.334 dB shift, which corresponds to a 7.4% decrease in transmission. One final improvement was made to the direct-crosslink procedure in attempt to obtain better antibody coverage. This time I added 3 times as much antibody as before. Making this important change did, in fact, increase the antibody coverage. Previously, there was a 1.763 dB shift for the antibody which corresponds to a 33.4% decrease in the transmitted intensity. This time, however, there was a 3.252 dB shift, or a 52.7% decrease in intensity. Furthermore, increasing the antibody coverage led to a further factor of 10 increase in the sensitivity of the sensor. This time, the lowest detectable concentration was 0.00001164 mg/ml (11.64 ng/ml) PSA. For this concentration, there was a 0.42 dB shift, or a 9.2% decrease in the intensity. With all of the improvements I have made upon this PSA experiment, the smallest detectable PSA concentration was 11.64 ng/ml. Unfortunately, medical evaluation requires a PSA detection threshold of around a factor of 3 lower than this. However, additional improvements on the PSA sensor can still be made. Several options to increase sensitivity would be: to work closer to the TAP because this is the most sensitive point in the grating, devise a way to get even more antibody binding, and to use

silica nanoparticles as the sensor platform instead of the PCBS to provide greater surface coverage. Making these adjustments should lead to at least a factor a ten greater sensitivity, which would put this PSA sensor in the same ranges as (or better than) the current clinical sensors.

Finally, the development of the fiber optic sensor into a pH sensor was rigorously examined. In general, the platform for most of the fiber-optic pH sensors is a coating adsorbed on the fiber surface that changes with respect to pH. The pH induces reversible effects in the sensing layer's optical properties. These changes can be seen as changes in optical power that are either transmitted or reflected.

In prior work by Corres *et al.* (2007), pH detection was claimed based on LPGs that had PAH/PAA films adsorbed on their surface such that the polymeric matrix adjusted its optical thickness when the pH was altered. Their sensor worked based on the principle that the sensitive layer swelled when the pH was changed. In the study of Corres *et al*. (2007), the pH's of the PAH and PAA were both 4.5, which was approximately the value that they found that yielded the maximum thickness per bilayer. They stated that when the sensor was placed in buffer solutions of higher pH, the thickness of the layers should decrease giving shifts in the attenuation wavelength.

After many, many studies of PAH/PAA ISAM films on TAP LPGs, we came to the conclusion that Corres *et al*. were sensing the concentration of salt ions in the buffer rather than the hydrogen ion concentration. We thus switched our focus to work by Rubner *et al.* indicating discontinuous pH-induced swelling in PAH and PSS ISAM films fabricated from pHs greater than 9.0. Rubner *et al.* concluded that these reversible discontinuous transitions were caused by discontinuous changes in the degree of

ionization of free amine groups of PAH and a significant shift in the pK_a value of PAH because of its local environment within the multilayers. This caused a history-dependent swelling behavior of the multilayers.

In using PAH/PSS ISAM films fabricated from pH 9.3 on TAP LPGs, we did observe some systematic differences in the LPG spectrum when exposed to DI water with pHs of 4.0, 5.4, and 7.0. It was found that the spectra were more repeatable when each measurement was preceded by a three minute soak in DI pH 2.0 in order to "reset" the film to a swollen state. There are still significant improvements needed, however, in order to develop an approach with stable, reproducible measurements at any given pH.

7.1 Future Work

The goal of this research was to develop, test, and optimize the ISAM TAP LPG fiber optic biosensor system. Over the course of this thesis many great strides have been taken toward this goal. However, work still remains to be done to achieve the ultimate end of developing a commercially-competitive biosensor platform. Some future plans are:

7.1.1 Sensitivity Enhancements

- Implement silica nanoparticles into the ISAM films. Silica nanoparticles provide increased thickness and surface area for binding of target and probe molecules. This, in turn, will increase the sensitivity of the LPG.
- Work as close to the TAP as possible because this is the most sensitive point in the grading.

- Find a way to further increase antibody coverage on the LPG. The more antibody that is present on the LPG, the more binding sites there will be available for the antigen.

7.1.2 Further Studies of ISAM-LPG Biosensors

- Try to obtain at least a factor of 10 higher sensitivity for the PSA biosensor by implementing the above suggestions.
- Test the specificity of the PSA biosensor by determining if the system is effected by other proteins, enzymes, ligands, etc.
- Repeat the experiment for the Anthrax biosensor utilizing all the previously mentioned improvements and the more sensitive TAP LPGs.
- Extend the method to the detection of other targets, such as sensors to detect HIV, breast cancer, HPV, colon cancer, etc.